Cosmic Microwave Background anisotropies in the presence of a weak magnetic field.

A. Kahle*

November 23, 2003

Abstract

This paper presents a fully covariant and gauge invariant calculation of the evolution of Cosmic Microwave Background (CMB) anisotropies in the presence of a weak magnetic field.

*Department of Mathematics and Applied Mathematics, University of Cape Town, Rondebosch 7700, Cape Town, South Africa

Contents

[1]This section owes a great deal to the detailed review of Grasso and Rubenstein [35].

Chapter 1

Introduction

The past two decades have seen a remarkable change in the nature of cosmology, a shift from a predominately theoretical science to the new era of "precision cosmology", where predictions are measured against extremely accurate observations. In no small part, this change is due to our understanding of the Cosmic Microwave Background Radiation (CMB), and the new set of precise observations that have, and are still, being made of it.

So how did the CMB actually come to be? In order to understand this, it is important to realise that the further one looks out into the universe, the further back in time one is looking. This is easily understandable as soon as one realises that light, just like everything else, travels at finite velocity. Now, standard theories of the universe's past claim that it began very small and hot, and ever since has been cooling and expanding. Thus, the further back one looks, the hotter it is. At early enough times, it was hot enough to ionise hydrogen. In this epoch the universe was sufficiently dense for the coupling of the free electrons with the photons to render it opaque – the mean free path (average time until collision) of a photon was effectively zero. This all changed when the universe reached 3000 K, when atomic hydrogen formed, and significant interaction between the photons and the matter no longer took place. Thus the photon mean free path became effectively infinite, making the universe transparent to light. Now, if the universe was approximately isotropic and homogeneous this would have happened at roughly the same time in any direction we looked, creating an almost isotropic opaque shell surrounding us.

One of the first triumphs of precision cosmology was the detection of the black-body spectrum of the CMB by the COBE satellite. The theory governing the photon-baryon plasma predicts that the photon gas would have had a black-body spectrum at the time of decoupling, which is preserved as the light travels towards us. In fact, the universe acts as a giant gravitational lens, so that the further away light comes from, the more it is red-shifted by the universe. So instead of seeing a black-body spectrum centred at 3000 K (the ionisation temperature for Hydrogen), one would expect to see a black body spectrum at about 3 K. In 1989, the COBE satellite was launched to detect exactly this, and found, remarkably, that CMB was indeed black body with a radiation temperature of 2.736 ± 0.005 K. This observation is said to be the most accurate physical observation ever made.

While the CMB radiation is remarkably isotropic, possessing anisotropies of

the order of 10^{-5}, it is precisely the anisotropies that, with careful measurement, allow us to determine many of the fundamental parameters underlying our universe. These anisotropies are measured by first measuring the average temperature of the CMB (called the bolometric temperature), and then measuring the deviations from this in a particular direction. In fact, it is only the statistical properties of these deviations that is of interest – the map of the anisotropies that are observed is used to calculate the power at each angular scale using spherical harmonics. The resultant power spectrum, which is simply the graph of power versus angular scale, is an extremely powerful observational tool.

The theory of the CMB may be used to predict the power spectrum, given the values of the fundamental cosmological parameters. The spectrum is composed of a series of decreasing peaks. By measuring the position and height of these peaks, and doing a best fit to the theoretical power spectra, one may then determine the values of these constants. However, as is to be expected, there is some degeneracy in the fitting of the parameters, and other observations (such as supernova observations, red-shift surveys, etc.) should be used in conjunction with the CMB data in order to constrain the parameters. Nonetheless, the measurements of the CMB already performed (in particular, the COBE, BOOMerANG and WMAP measurements) have done a great deal to constrain the possible ranges of these parameters.

One of the questions cosmology still has not satisfactorily resolved is the origin of magnetic fields in the universe. These have been observed at all scales where man has devised means to observe them, from stellar scales, to intergalactic and intercluster scales. Indeed, there is no reason to believe that they are not present, at some level, at even larger scales. However, a satisfactory explanation for their origin is yet to be found.

The two most popular theories for the creation of these magnetic fields, namely the Galactic dynamo, and primordial field amplification, both rely on the presence of a seed field, which they then amplify. However, the galactic dynamo requires a far weaker seed field compared to primordial field amplification. It would thus be helpful, in trying to understand magnetogenesis, if one could discover some means to detect such a seed field.

One way to do so would be to search for a signature that such a magnetic field might leave on the CMB, and then look for the presence of this signature in CMB observations. This is the principal aim of this thesis.

The thesis is organised as follows:

- Chapter 2 introduces the theory required to calculate the CMB power spectrum taking into account the presence of a magnetic field. The chapter aims to be self contained, giving an overview of the calculation starting from first principles.

- Chapter 3 focuses on observations, giving a review of the current state of CMB observations, as well as observations of magnetic fields.

- Chapter 4 does a detailed theoretical calculation of the evolution of scalar perturbations in a magnetised radiation/dust universe, closely following a similar calculation by Padmanabhan [64], and comparing the results.

- Chapter 5 gives a careful overview of how one modifies the CAMB code

(which calculates the CMB power spectrum) to include the effects of a magnetic field. It then goes on to discuss the calculated power spectra.

- Chapter 6 presents a summary and discussion of the results.

Chapter 2

General Relativity and Cosmology

The Einstein Field Equations (EFEs),

$$G_{ab} + \Lambda g_{ab} = \kappa T_{ab}, \tag{2.1}$$

are the foundation stone of General Relativity. These equations link the matter content of the universe, represented by the energy-momentum tensor T_{ab}, with the universe's geometry, partly determined by the Einstein tensor:

$$G_{ab} \equiv R_{ab} - \frac{1}{2} R g_{ab}. \tag{2.2}$$

Here R_{ab} is the Ricci tensor, and R the Ricci scalar. g_{ab} is the metric tensor, and Λ is the cosmological constant[1]. The twice contracted Bianchi identities guarantee that energy-momentum is identically conserved.

The EFEs only determine ten of the twenty degrees of freedom of the Riemann tensor, defined by the Ricci identities,

$$R_{abcd} V^d = 2\nabla_{[a}\nabla_{b]} V_c. \tag{2.3}$$

Here V_a is any 4-vector, R_{abcd} is the Riemann tensor, and the square brackets denote antisymmetrisation on those indices. The remaining ten degrees of freedom are given by the Weyl tensor,

$$C_{abcd} = R_{abcd} - \frac{1}{2}(R_{ad} g_{bc} - R_{ac} g_{bd} + R_{bc} g_{ad} - R_{bd} g_{ac}) - \frac{1}{6} R (g_{ac} g_{bd} - g_{bc} g_{ad}), \tag{2.4}$$

which determines gravitational action at a distance, through tidal forces and gravitational waves. In analogy to Electromagnetism, the Weyl tensor is usually decomposed into an "Electric" and a "Magnetic" part, respectively:

$$E_{ab} \equiv C_{acbd} u^c u^d, \tag{2.5}$$

$$H_{ab} \equiv {}^*C_{acbd} u^c u^d. \tag{2.6}$$

We will later see that the "electric" part is involved in tidal forces, and the "magnetic" part in the propagation of gravitational waves.

[1] We use the sign conventions of [23] , and choose geometrised units such that $c = 1 = \kappa = 8\pi G/c^2$. Indices like $a, b, c \ldots$ range over $\{0, 1, 2, 3\}$, and indices like $i, j, k \ldots$ range over $\{1, 2, 3\}$.

2.1 The covariant approach to cosmology

In cosmology, we make the assumption that there exist a set of fundamental observers that moves along the paths given by x^a, having the corresponding 4-velocity

$$u^a = \frac{dx^a}{d\tau}, \tag{2.7}$$

with τ the proper time measured along the fundamental world lines[2]. There are generally a number of ways to choose the fundamental frame: most however involve the fundamental observers to be co-moving with one of the matter species, or, as in the case of the energy frame, with the "centre of mass" of all the matter.

With the definition of the fundamental 4-velocity, one may define the projection tensors:

$$h_{ab} \equiv g_{ab} + u_a u_b, \tag{2.8}$$
$$U_{ab} \equiv -u_a u_b, \tag{2.9}$$

which project respectively into 3-dimensional instantaneous rest space and 1-dimensional time-like sections.

It is easy to see that the U_{ab} and h_{ab} tensors are indeed (orthogonal) projection tensors, and are thus the metric tensors in the subspaces they project to:

$$h_{ab} = h_{(ab)}, \quad h_a{}^b h_b{}^c = h_a{}^c, \quad h_a{}^a = 3, \quad u^a h_{ab} = 0, \tag{2.10}$$
$$U_{ab} = U_{(ab)}, \quad U_a{}^b U_b{}^c = U_a, \quad U_a{}^a = 1, \quad h^{ab} U_{bc} = 0. \tag{2.11}$$

As is usual, the round brackets denote symmetrisation about these indices.

It is convenient now to introduce the spatial "derivative"[3] of a tensor:

$$\tilde{\nabla}^a T^{b\ldots c}{}_{d\ldots e} \equiv h_p{}^a h_r{}^b \ldots h_s{}^c h_d{}^t \ldots h_e{}^u \nabla^p T^{r\ldots s}{}_{t\ldots u}. \tag{2.12}$$

The usual time derivative can be similarly defined:

$$\dot{T}^{a\ldots b}{}_{c\ldots d} \equiv u_e \nabla^e T^{a\ldots b}{}_{c\ldots d}. \tag{2.13}$$

It is possible to find analogues of the usual divergence and curl of vector calculus in the instantaneous rest space of the fundamental observer; these are (for a vector, V_a, and a tensor, T_{ab}):

$$\mathrm{div} V = \tilde{\nabla}^a V_a, \quad \mathrm{div}(T)_a = \tilde{\nabla}^b T_{ab}, \tag{2.14}$$
$$\mathrm{curl} V_a = \varepsilon_{abc} \tilde{\nabla}^b V^c, \quad \mathrm{curl} T_{ab} = \varepsilon_{cd(a} \tilde{\nabla}^c T_{b)}{}^d. \tag{2.15}$$

Here $\varepsilon_{abc} = \eta_{abcd} u^d$ is the 3-dimensional volume element, which is simply the projection of the totally skew space-time volume element defined by $\eta_{0123} = \sqrt{|\det g^{ab}|}$.

[2]This may seem to be antithetical to the General Relativistic idea that any frame choice is valid. However, that validity of any particular frame does not have any bearing on its convenience, and it is primarily the convenience of calculations in the fundamental frame that lend it its importance. Many problems would be all but intractable without a convenient frame choice.

[3]The spatial derivative is in fact only a derivation in the instantaneous rest space at any point.

The projected symmetric trace-free (PSTF) part of a vector V^a and a tensor T^{ab} is defined as

$$V^{\langle a\rangle} \equiv h^a{}_b V^b, \quad T^{\langle ab\rangle} \equiv [h^{(a}{}_c h^{b)}{}_d - \frac{1}{3}h^{ab}h_{cd}]T^{cd}. \tag{2.16}$$

One may then inductively define the PSTF part of higher rank tensors.

With these operations, one may now split each index on tensor into its time-like and spatial parts, and further split the spatial part of the tensor into into its trace, its antisymmetric part, and its PSTF part. Applying this reduction systematically to General Relativity is the essence of the covariant approach to cosmology.

2.1.1 Kinematic variables

By performing a 1+3 splitting of the derivative of u^a, one obtains the fundamental equation:

$$\nabla_a u_b = -u_a a_b + \omega_{ba} + \sigma_{ab} + \frac{1}{3}\Theta h_{ab}. \tag{2.17}$$

Here a_a is the acceleration vector given by $a_a = u_b\nabla^b u_a$, Θ is the trace of the gradient ($\Theta = \nabla^a u_a$), and represents the volume expansion, σ_{ab} is the projected trace-free symmetric part of the gradient ($\sigma_{(ab)} = \nabla_{\langle a}u_{b\rangle}$, $\sigma_a{}^a = 0$, $\sigma_{ab}u^b = 0$), and represents the shear, or rate of distortion of the matter, ω_{ab} is the skew symmetric part of the gradient ($\omega_{[ab]} = \nabla_{[a}u_{b]}$, $\omega_{ab}u^b = 0$), and represents the vorticity, or rate of rotation of the matter. For later convenience we define the magnitudes

$$\sigma^2 \equiv \frac{1}{2}\sigma^{ab}\sigma_{ab}, \tag{2.18}$$

$$\omega^2 \equiv \frac{1}{2}\omega^{ab}\omega_{ab}. \tag{2.19}$$

One may gain further insight into the role of these variables by looking at the evolution of nearby observer[4].

If one adopts normalised co-moving coordinates $x^a = (s, y^i)$, so that

$$u^a = \delta^a_0, \quad \Leftrightarrow \quad \frac{ds}{d\tau} = 1, \frac{dy^i}{d\tau} = 0, \tag{2.20}$$

then the curves along the surfaces defined by $s = \text{const}$ are dragged along the world lines into other surfaces $s = \text{const}$. One such curve, $y^i = y^i(v)$ in a surface $s = s_0$, then links a set of fundamental observers throughout their evolution. Thus the vector $\eta^a = (d\eta^a/dv)\delta v$, which lies tangent to the this curve, and has co-moving coordinates

$$\eta^a = (0, \delta y^i), \quad \delta y^i = (dy^i/dv)dv, \tag{2.21}$$

links the worldlines of two nearby observers – $O : y^i = c^i$ and $G : y^i = c^i + \delta y^i$ (c^i and δy^i are constants). Thus the vector η^a is called the connecting vector, and is given in general coordinates $\{z^a\}$ by

$$\eta^a = \left(\frac{\partial z^a}{\partial y^i}\right)_{s=\text{const}} \delta y^i. \tag{2.22}$$

[4]This argument essentially follows Ellis in [30].

In general the connecting vector is not orthogonal to the fluid flow lines – it contains both a time-like and a spatial part. In order thus to get an analogue of the Newtonian relative position vector, we need to take its spatial projection:

$$\eta^a_\perp = h^a{}_b \eta^b. \tag{2.23}$$

This relative position vector can be decomposed into a relative distance δl, and direction e^a:

$$\eta^a_\perp = e^a \delta l, \quad e^a e_a = 1, e^a u_a = 0 \Rightarrow \eta^a_\perp \eta_{\perp a} = (\delta l)^2. \tag{2.24}$$

One may now find propagation equations for δl and e^a as follows:

With the definition of the relative position vector $\eta^a_\perp$, it is straightforward to define the relative velocity vector

$$v^a = (\eta^a_\perp)^{\cdot}{}_\perp = h^a{}_b (h^b{}_c \eta^c)_{;d} u^d. \tag{2.25}$$

As a consequence of η^a being a connecting vector, $[\boldsymbol{u}, \boldsymbol{\eta}]^a = 0$. One may then show

$$v^a = V^a{}_b \eta^b_\perp, \quad V_{ab} \equiv \tilde{\nabla}_b u_a. \tag{2.26}$$

Comparing with Eq. 2.20, we see that

$$V_{ab} = \omega_{ab} + \sigma_{ab} + \frac{1}{3}\Theta h_{ab}. \tag{2.27}$$

Using Eqs 2.24, 2.25, 2.26, one now finds the propagation equation for the relative separation (generalised Hubble's law)

$$\frac{\delta \dot{l}}{\delta l} = \frac{1}{3}\Theta + \sigma_{ab} e^a e^b, \tag{2.28}$$

and direction

$$\dot{e}^{\langle a \rangle} = \omega^a{}_b e^b + [\sigma^a{}_b - \delta^a{}_b (\sigma_{cd} e^c e^d)] e^b. \tag{2.29}$$

By setting the shear and the vorticity to zero, one may clearly see how Θ causes isotropic expansion. Similarly, setting Θ and ω^a to zero, we may see the effect of the shear. As its trace is zero, an non-zero shear will have three distinct (orthogonal) eigenvectors, with at least one of the eigenvalues negative (if the shear is non-zero). Choosing an orthonormal basis with these eigenvectors, we see that this leads to expansion in at least one direction, and contraction in at least one other. Turning to the vorticity (and setting Θ and σ_{ab} zero), we see that the vorticity causes pure rotation (the relative distances remain unchanged). We may find the axis of this rotation by defining the vorticity vector ω^a by

$$\omega^a = \frac{1}{2}\varepsilon^{abc}\omega_{bc} \Leftrightarrow \omega_{ab} = \varepsilon_{abc}\omega^c, \tag{2.30}$$

which shows the vorticity vector is a vector orthogonal to u^a (i.e. in the instantaneous rest space of u^a) and an eigenvector of ω_{ab} with a zero eigenvalue. Thus the vorticity vector is the axis about which the rotation takes place.

In general all of these quantities are nonzero. However, the only quantity that causes a change in the volume is Θ, as all the other variables are trace free.

The change of volume V is given by $\Theta : V \to V(1 + \delta t\Theta)$. It is then convenient to define the length scale $S(\tau)$ by

$$\frac{\dot{S}}{S} = \frac{1}{3}\Theta. \tag{2.31}$$

One then has that change in fluid volume is proportional to S^3. The Hubble parameter for the flow is defined by

$$\dot{S} \equiv HS. \tag{2.32}$$

We see that $\Theta = 3H$.

2.1.2 The energy-momentum tensor

The energy-momentum tensor of an imperfect fluid may be irreducibly split as

$$T_{ab} = \rho u_a u_b + 2q_{(a}u_{b)} + ph_{ab} + \pi_{ab}, \tag{2.33}$$

where $\rho = T_{ab}u^a u^l$ is the relativistic energy density, $q_a = -T^{bc}u_b h_{ca}$ is the relativistic momentum density (or, dually, the relativistic energy flux), $p = \frac{1}{3}T_{ab}h^{ab}$ is the isotropic pressure, and $\pi_{ab} = T_{cd}h^c{}_{\langle a}h^d{}_{b\rangle}$ is the anisotropic pressure.

The conservation of energy-momentum:

$$\nabla^a T_{ab} = 0, \tag{2.34}$$

which follows directly from the EFEs and the twice contracted Bianchi identities, gives rise to conservation equations for the energy

$$\dot{\rho} + (\rho + p)\Theta + \pi^{ab}\sigma_{ab} + q^a a_a + q^a{}_{;a} = 0, \tag{2.35}$$

and momentum

$$(\rho + p)a_a + h_a{}^c(p_{;c} + \pi_c{}^b{}_{;b} + \dot{q}_c) + \left(\omega_a{}^b + \sigma_a{}^b + \frac{4}{3}\Theta h_a{}^b\right) q_b = 0. \tag{2.36}$$

An important particular case is that of the perfect fluid. This is a fluid with only ρ and p non-zero. This greatly simplifies the equations for the conservation of energy and momentum:

$$\dot{\rho} + (\rho + p)\Theta = 0, \tag{2.37}$$

$$(\rho + p)a_a + h_a{}^c p_{;c} = 0. \tag{2.38}$$

The energy-momentum tensor is not sufficient for a complete description of the fluid; an equation of state linking ρ and p is also needed. This is often taken to be of the form:

$$p = w\rho, \tag{2.39}$$

with w a constant. The fluid is then known as barotropic. Some important fluids can be modelled in this way:

1. Dust (or pressure free matter) is a barotropic perfect fluid with $w = 0$.
2. Radiation is a barotropic fluid (often taken to be perfect) with $w = \frac{1}{3}$.

3. The cosmological constant can be seen as a barotropic perfect fluid with $w = -1$.

In reality the universe does not contain only one fluid species, but is in fact composed of various fluid components. Each component then has its own energy-momentum tensor $T^{(i)}_{ab}$, and only the total energy-momentum is conserved:

$$\sum_i \nabla^a T^{(i)}_{ab} = 0\,. \tag{2.40}$$

2.1.3 Dynamics

Propagation and constraint equations governing the variables need to be found in order to study their dynamics. We already have two such equations, Eqs 2.35 and 2.36, but more are needed in order to describe the dynamics completely. These will be found by considering the various identities involving the Riemann tensor (and its contractions) along with the Einstein Field Equations.

The Ricci identities

The Ricci Identities,

$$2\nabla_{[a}\nabla_{b]}u^c = R_{ab}{}^c{}_d u^d, \tag{2.41}$$

give rise to the first set of such equations. Substituting the expression for $u_{a;b}$ (Eq. 2.17), using the EFEs (Eq. 2.1), and reducing to trace, trace-free symmetric, and antisymmetric parts yields three propagation equations [31]:

$$\dot{\Theta} = -\frac{1}{3}\Theta^2 + a_a a^a + \tilde{\nabla}_a a^a - 2(\sigma^2 - \omega^2) - \frac{1}{2}\kappa(\rho + 3p) + \Lambda, \tag{2.42}$$

$$\dot{\omega}^{\langle a\rangle} = -\frac{2}{3}\Theta\omega^a + \sigma^a{}_b\omega^b + \frac{1}{2}\varepsilon^{abc}\tilde{\nabla}_b a_c, \tag{2.43}$$

$$\dot{\sigma}^{\langle ab\rangle} = -\frac{2}{3}\Theta\sigma^{ab} + a^{\langle a}a^{b\rangle} + \tilde{\nabla}^{\langle a}a^{b\rangle} - \sigma^{\langle a}{}_c\sigma^{b\rangle c} - \omega^{\langle a}{}_c\omega^{b\rangle c} - \left(E^{ab} - \frac{1}{2}\kappa\pi^{ab}\right), \tag{2.44}$$

and three constraint equations:

$$0 = \tilde{\nabla}_b\sigma^{ab} - \frac{2}{3}\tilde{\nabla}^a\Theta + \varepsilon^{abc}[\tilde{\nabla}_b\omega_c + 2a_b\omega_c] + \kappa q^a, \tag{2.45}$$

$$0 = \tilde{\nabla}_a\omega^a - a_a\omega^a, \tag{2.46}$$

$$0 = H^{ab} + 2a^{\langle a}\omega^{b\rangle} + \tilde{\nabla}^{\langle a}\omega^{b\rangle} - (\mathrm{curl}\sigma)^{ab}. \tag{2.47}$$

The propagation equations merit individual discussion:

1. The first equation, Eq. 2.42, is known as the Raychaudhuri equation, and is the basic equation of gravitational attraction. Recasting the equation as an equation for the scale factor,

$$3\frac{\ddot{S}}{S} = -2(\sigma^2 - \omega^2) + a^a{}_{;a} - \frac{1}{2}\kappa(\rho + 3p) + \Lambda, \tag{2.48}$$

and examining how each term affects the curve of S against time allows one to interpret the equation physically (see Fig 2.1). One may clearly see how,

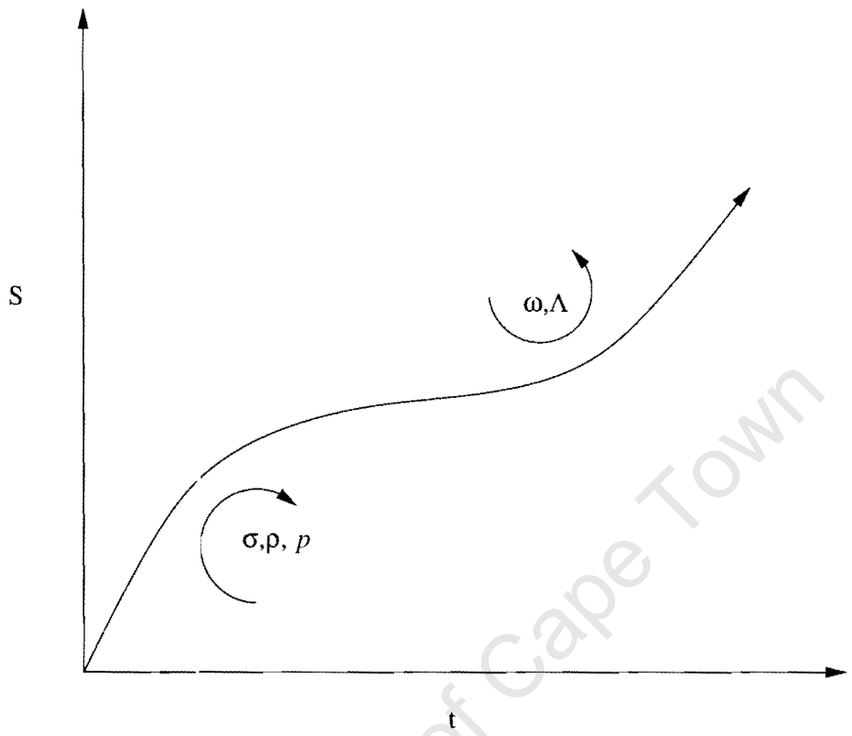

Figure 2.1: A schematic diagram showing the effect of the kinematic variables on the evolution of the scale factor.

in General Relativity, both ρ and p form part of the active gravitational mass, causing attraction if they are positive (unless the matter is extremely unusual, these quantities will be positive). In the Newtonian limit $(\rho + 3p) \to \rho$, so that, if one disregards Λ, the Raychaudhuri equation becomes the equation for Newtonian gravitation. We may see how the cosmological constant, Λ, can have both positive and negative effects on the curvature of the graph, depending on the sign on the constant. One may understand this by seeing that a positive cosmological can be interpreted as matter with negative pressure of magnitude equal to its density. The vorticity has a positive effect on the curvature of the graph. This is easy to understand – the centripetal forces of rotation work in the opposite direction to the centrifugal forces of gravity (with ordinary matter). The shear term has a negative effect on the curvature of the graph. One may understand this by remembering that in the case of non-vanishing shear, there is always at least one axis of inward motion.

2. Eq. 2.43 is the vorticity propagation equation. In the case of a barotropic perfect fluid, the equation becomes:

$$h^f{}_e(rS^3\omega^e)^{\cdot} = u^f{}_{;d}(rS^3\omega^d), \tag{2.49}$$

where r is an acceleration potential,

$$r(x^a) = \exp\left(\int_{p_0}^{p} \frac{dp}{\rho + p}\right). \tag{2.50}$$

This shows conservation of vorticity in barotropic perfect fluids, so that vorticity can only be generated by thermodynamically irreversible processes.

3. Eq. 2.44 is the shear propagation equation. This shows how the anisotropic pressure and the tidal forced (represented by E_{ab}) source shear.

The constraint equations (Eqs 2.45, 2.46, 2.47) are respectively named (0ν), vorticity divergence, and H_{ab} equations. The (0ν) equation shows how the momentum flux relates to the spatial inhomogeneity of the fluid. From Eq. 2.47 we see how the magnetic part of the Weyl tensor is made up of the curl of the shear and the "distortion" of the vorticity.

The Bianchi identities

The Bianchi identities,

$$\nabla_{[a}R_{bc]de} = 0, \tag{2.51}$$

may be used to obtain propagation and constraint equations for the Weyl tensor, which are similar to the Maxwell field equations in an expanding universe.

The propagation equations generated are the $\dot{E}_{ab}$ equation:

$$\begin{aligned}\left(\dot{E}^{\langle ab\rangle} + \frac{1}{2}\kappa\dot{\pi}^{\langle ab\rangle}\right) - (\mathrm{curl}H)^{ab} + \frac{1}{2}\kappa\tilde{\nabla}^{\langle a}q^{b\rangle} \\ = -\frac{1}{2}\kappa(\rho + p)\sigma^{ab} - \Theta\left(E^{ab} + \frac{1}{6}\kappa\pi^{ab}\right) + 3\sigma^{\langle a}{}_c\left(E^{b\rangle c} + \frac{1}{6}\kappa\pi^{b\rangle c}\right) \\ -\kappa a^{\langle a}q^{b\rangle} + \varepsilon^{cd\langle a}\left[2a_cH^{b\rangle}{}_d + \omega_c\left(E^{b\rangle}{}_d + \frac{1}{2}\kappa\pi^{b\rangle}{}_d\right)\right],\end{aligned} \tag{2.52}$$

and the $\dot{H}_{ab}$ equation:

$$\dot{H}^{\langle ab\rangle} - \frac{1}{2}\kappa(\mathrm{curl}\pi)^{ab} = -\Theta H^{ab} + 3\sigma^{\langle a}{}_{c}H^{b\rangle c} + \frac{3}{2}\kappa\omega^{\langle a}q^{b\rangle} - \varepsilon^{cd\langle a}\left[2a_{c}E^{b\rangle}{}_{d} - \frac{1}{2}\kappa\sigma^{b\rangle}{}_{c}q_{d} - \omega_{c}H^{b\rangle}{}_{d}\right], \quad (2.53)$$

and the constraints are:

$$0 = \tilde{\nabla}_{b}\left(E^{ab} + \frac{1}{2}\kappa\pi^{ab}\right) - \frac{1}{3}\kappa\tilde{\nabla}^{a}\rho + \frac{1}{3}\kappa\Theta q^{a} - \frac{1}{2}\kappa\sigma^{a}{}_{b}q^{b} - 3\omega_{b}H^{ab} - \varepsilon^{abc}\left[\sigma_{bd}H^{d}{}_{c} - \frac{3}{2}\kappa\omega_{b}q_{c}\right], \quad (2.54)$$

$$0 = \tilde{\nabla}_{b}H^{ab} + \kappa(\rho + p)\omega^{a} + 3\omega_{b}\left(E^{ab} - \frac{1}{6}\kappa\pi^{ab}\right) + \varepsilon^{abc}\left[\sigma_{bd}\left(E^{d}{}_{c} + \frac{1}{2}\kappa\pi^{d}{}_{c}\right) + \frac{1}{2}\kappa\tilde{\nabla}_{b}q_{c}\right], \quad (2.55)$$

known respectively as the $(\mathrm{div}E)_a$ and the $(\mathrm{div}H)_a$ equations. As with the Maxwell equations one may take the time derivative of either of the propagation equations, and use the other to generate a wave equation for either E_{ab} or H_{ab}. This then shows how gravitational radiation arises.

We have already seen how the twice contracted Bianchi identities give rise to Eqs 2.35 and 2.36.

2.2 Friedmann-Lemaître-Robertson-Walker universes

Although at small scales we observe marked inhomogeneities in the universe, when observed at a large enough scale, the universe appears remarkably homogeneous and isotropic. Now, it may be the case that we occupy a special place in the universe, and that from most other points the universe appears anisotropic. This is however philosophically unappealing, so it is usually assumed that there is nothing particularly special about our position in the universe. This assumption is usually referred to as the "cosmological principal". As an initial approximation we may then assume that the universe is perfectly isotropic about every point. This automatically leads to the universe being spatially homogeneous[5]. The Friedmann-Lemaître-Robertson-Walker (FLRW) family of solutions to the Einstein Field Equations are precisely those solutions which are spatially homogeneous and isotropic about every point.

We may gain a good understanding of these universes via the covariant approach outlined in the previous section.

The acceleration, $a_a = u_{a;b}u^b$, is orthogonal to u^a so is entirely spatial. By the isotropy of FLRW universes, this must then vanish (were it not to do so, one would have a unique spacelike direction). But then, by Eq. 2.17, $u_{a;b}$ is

[5]In fact this assumption is stronger than necessary for spatial homogeneity. One merely needs isotropy about two distinct world lines in order to prove that the universe is spatially homogeneous.

completely spatial, and is necessarily proportional to metric of the instantaneous rest spaces (for isotropy). So

$$u_{a;b} = \lambda h_{ab}. \tag{2.56}$$

Comparing with Eq. 2.17, we see that $\lambda = (1/3)\Theta$. Thus the shear and vorticity vanish, and $u_{a;b} = u_{(a;b)}$. But then there exists a "time function" $t(x^i)$ such that

$$u_a = -t_{;a}, \tag{2.57}$$

which represents proper time for each fundamental observer. For any "spatial" vector V^a, $V^a u_a = 0$ so that $V^a t_{;a} = 0$. In other words, spatial vectors lie in the surfaces of simultaneity $t = \text{const}$ and all clocks may be synchronised. It is usual to choose the time coordinate $x^0 = t$, and the spatial coordinates, x^i, to be co-moving, so that $x^i_{;a} u^a = 0$. The fundamental velocity then has components

$$u^a = \delta^a_0 = \{1, 0, 0, 0\}, \tag{2.58}$$

and the metric takes the form

$$ds^2 = -dt^2 + h_{ab} dx^a dx^b. \tag{2.59}$$

By the isotropy of FLRW universes, any physical or geometric function has to be a function of t alone. In particular, $\Theta = \Theta(t)$. But then,

$$u_{a;b} = \Gamma^0{}_{ab} = \frac{1}{2}\frac{\partial g_{ab}}{\partial t} \tag{2.60}$$

so that

$$\frac{1}{2}\frac{\partial h_{ab}}{\partial t} = \frac{1}{3}\Theta h_{ab} \tag{2.61}$$

which then gives

$$h_{ab}(x^\alpha) = S^2(t) f_{ab}(x^\alpha), \quad S(t) = A \exp \int_{t_0}^{t} \frac{1}{3}\Theta(t')dt'. \tag{2.62}$$

Then

$$\Theta(t) = 3\frac{\dot{S}(t)}{S(t)}. \tag{2.63}$$

In these coordinates,

$$\frac{\partial l}{\partial l} = \frac{1}{3}\Theta(t), \tag{2.64}$$

$$\dot{e}^{\langle a \rangle} = 0, \tag{2.65}$$

so that we may identify l with the scale factor, $S(t)$. The Hubble parameter is then only a function of t:

$$H(t) = \frac{1}{3}\Theta(t). \tag{2.66}$$

In order to get an expression for the metric we need to find f_{ab}. The three spaces with metric h_{ab} must be isotropic about every point. This requirement restricts the 3-Ricci tensor to be proportional to the 3-metric, so that

$${}^3R_{ab} = \frac{1}{3}{}^3R h_{ab}. \tag{2.67}$$

In three dimensions, the Ricci tensor has the same number of degrees of freedom as the full Riemann tensor, so that one may obtain the Riemann tensor from the Ricci tensor via

$$ {}^3R_{abcd} = {}^3R_{ac}h_{bd} - {}^3R_{ad}h_{bc} - {}^3R_{bc}h_{ad} + {}^3R_{bd}h_{ac} - \frac{1}{2}{}^3R_{ac}(h_{ac}h_{bd} - h_{ad}h_{bc}). \tag{2.68} $$

Combining Eqs 2.67 and 2.68 shows that the three spaces are spaces of constant curvature K^*:

$$ {}^3R_{abcd} = K^*(h_{ac}h_{bd} - h_{ad}h_{bc}), \quad K^* = {}^3R/6. \tag{2.69} $$

The contracted Bianchi identities show that the Ricci scalar is a function of t only:

$$ {}^3R(t) = \frac{A}{S^2(t)}, \tag{2.70} $$

where A is a constant. This then gives

$$ K^*(t) = \frac{k}{S^2(t)}, \tag{2.71} $$

with k a constant that can be rescaled arbitrarily by rescaling the scale function. We will agree to choose k to be one of -1, 0, or 1.

We will now choose specific coordinates in the 3-space at some time t to determine the final form of the metric. We denote by Σ_t the spatial section at time t. Now we choose some point p in Σ_t, and draw radial geodesics through p, with the parameter r the radial distance as measured my the spatial metric f_{ab} (f_{ab} is the metric at the time when $S(t) = 1$). The actual radial distance, as measured by h_{ab}, will then be $rS(t)$ that r is an affine parameter along the geodesic. Isotropy implies that the 2-surfaces given by r =const. are 2-spheres orthogonal to the geodesics. Thus the metric of Σ_t is given by:

$$ d\sigma^2 = h_{ij}dx^i dx^j = S^2(t)[dr^2 + f^2(r)(d\theta^2 + \sin^2\theta d\phi^2)]. \tag{2.72} $$

As $r \to 0$, the coordinates must approach those of a regular space-time point. Thus $f(r) \sim r$ for small r.

In order to find the explicit form of $f(r)$ we may use the geodesic deviation equation for radial geodesics with tangent vector $V^a = \delta^a{}_1$ and connecting vector $U^a = \delta^a{}_2$:

$$ \frac{\delta^2 U^a}{\delta r^2} + kU^a = 0. \tag{2.73} $$

Choosing a parallel propagated orthonormal basis gives us a second order ODE which may then be solved for the various values of k to give:

$$ f(r) = \begin{cases} \sin r, & k = 1, \\ r, & k = 0, \\ \sinh r, & r = -1\,. \end{cases} $$

We may now write down the metric explicitly:

$$ ds^2 = dt^2 + S^2(t)[dr^s + f^2(r)(d\theta^2 + \sin(\theta)d\phi^2)], \tag{2.74} $$

with $f(r)$ as above. The function $f(r)$ may be interpreted as the "corrected" radius of the 2-spheres of radius r, as the surface area of these spheres is not $4\pi r^2$, as would be the case in a Euclidean space, but $4\pi f(r)^2$.

One may easily see that if one were to choose a point p' instead of p as a starting point in the derivation of the metric, and obtained the same metric. Thus the FLRW universe is perfectly homogeneous, each point being equivalent to every other[6]. The homogeneity forces the value of each physical and geometric variable to be the same everywhere, so that they can only depend on time.

2.2.1 Matter in FLRW universes

The symmetries of FLRW universes impose restrictions on the matter allowed in these universes. The isotropy forces the anisotropic pressure, π_{ab} to vanish. We may see this by noting that by the isotropy, $\pi_{ab} = ch_{ab}$, where c is a constant. But $\pi^a{}_a = 0$, so that $c = 0$. Also, at a point about which the universe is perfectly isotropic, all vector quantities must vanish (if they failed to do so, there would be a preferred direction), so that q_a vanishes. We are thus forced to conclude that the only fluids allowed in FLRW universes are either baratropic perfect fluids or take perfect fluid form (e.g. have non-zero bulk viscosity). By the previous discussion, we see that the fluid variables may depend on t only.

In summary, FLRW universes are perfectly isotropic about every point, and are thus homogeneous. The only dynamical variable that remains is Θ, and the fluid takes on the perfect fluid form (so that only ρ and p remain). Isotropy implies that vectors vanish, so that all gradients of scalars vanish identically.

2.3 Gauge-invariant perturbations

The universe that we inhabit is of course not perfectly homogeneous. As cosmologists it is necessary to find some technique in dealing with this inconvenience, while still keeping the model of a manageable complexity. The closeness of the universe to perfect homogeneity and isotropy suggests that one may profitably adopt some perturbation scheme. However, there are serious gauge problems in attempting this. One may best see this by considering the obvious way to attempt such a scheme.

Suppose one had an FLRW universe with energy density $\rho(t)$. A more realistic universe will have an energy density $\rho^*(x,t) = \rho(t) + \delta\rho(x,t)$, the variable $\delta\rho$ being the density perturbation. One may similarly find a velocity perturbation δu. The gauge problems arise in the choice of background. It turns out that one may choose the background universe to give these variables arbitrary values. As an extreme case, one may imagine choosing a background universe so that density perturbations vanish completely, with the perturbations being absorbed into the velocity perturbation variable.

This unsatisfactory situation is saved by using the gauge-invariance lemma (Stewart and Walker [70]):

[6]This is of course evident from the fact that there are two points about which the universe is perfectly isotropic. However, this argument illustrates the homogeneity of FLRW universes nicely.

Lemma 2.3.1 (Gauge Invariance Lemma) *If a quantity $T^{\cdots}_{\cdots}$ vanishes in the background, then it is gauge invariant to all orders.*

This suggests an obvious approach:

1. Set all variables that do not vanish in the background (ρ, p, Θ and their time derivatives) to be zeroth order in the perturbation variable, ϵ.

2. Set all variables that vanish in the background, a_a, σ_{ab}, ω_{ab}, q_{ab}, π_{ab}, E_{ab} and H_{ab}, and their time and space derivatives, to be first order in ϵ.

One may now linearise the propagation and constraint equations described in Sec. 2.1.3 to obtain the propagation equations:

$$\begin{aligned}
\dot{E}_{ab} + \Theta E_{ab} - \mathrm{curl}H_{ab} + \frac{1}{6}\kappa[3(\rho+p)\sigma_{ab} & \\
+3\tilde{\nabla}_{\langle a}q_{b\rangle} + 3\dot{\pi}_{ab} + \Theta\pi_{ab}] &= 0, && (2.75)\\
\dot{H}_{ab} + \Theta H_{ab} + \mathrm{curl}(E_{ab} - \frac{1}{2}\kappa\pi_{ab}) &= 0, && (2.76)\\
\dot{\sigma}_{ab} + \frac{2}{3}\Theta\sigma_{ab} - \tilde{\nabla}_{\langle a}a_{b\rangle} + E_{ab} - \frac{1}{2}\kappa\pi_{ab} &= 0, && (2.77)\\
\dot{\omega}_{ab} - \tilde{\nabla}_{[a}a_{b]} + \frac{2}{3}\Theta\omega_{ab} &= 0, && (2.78)\\
\dot{q}_a + \frac{4}{3}\Theta q_a + (\rho+p)a_a + \mathrm{div}(\pi)_a + \tilde{\nabla}_a p &= 0, && (2.79)\\
\dot{\Theta} + \frac{1}{3}\Theta^2 - \mathrm{div}a + \frac{1}{2}\kappa(\rho+3p) &= 0, && (2.80)\\
\dot{\rho} + \Theta(\rho+p) + \mathrm{div}q &= 0, && (2.81)
\end{aligned}$$

and the constraint equations

$$\begin{aligned}
H_{ab} - \mathrm{curl}(\sigma_{ab} - \omega_{ab}) &= 0, && (2.82)\\
\mathrm{div}(H)_a - \frac{1}{2}\kappa[(\rho+p)\omega_a - \mathrm{curl}q_a] &= 0, && (2.83)\\
\mathrm{div}(E)_a - \frac{1}{6}\kappa(2\tilde{\nabla}_a\rho - 2\Theta q_a - 3\mathrm{div}(\pi)_a) &= 0, && (2.84)\\
\mathrm{div}(\omega)_a + \mathrm{div}(\sigma)_a - \frac{2}{3}\tilde{\nabla}_a\Theta + \kappa q_a &= 0, && (2.85)\\
\mathrm{div}\omega &= 0. && (2.86)
\end{aligned}$$

In order to describe density perturbations, we need to introduce two more variables:

$$\begin{aligned}
\mathcal{D}_a &\equiv S\frac{\tilde{\nabla}_a\rho}{\rho}, && (2.87)\\
\mathcal{Z}_a &\equiv S\tilde{\nabla}_a\Theta. && (2.88)
\end{aligned}$$

The first is the co-moving fractional density gradient, and may be considered analogous to $\delta\rho$, and the second is the co-moving spatial gradient of the expansion.

By taking the spatial gradients and commuting derivatives, one may obtain equations for $\mathcal{D}_a$ and $\mathcal{Z}_a$ from Eqs 2.81 and 2.80 resp. :

$$\begin{aligned}\rho\dot{\mathcal{D}}_a + (\rho+p)(\mathcal{Z}_a + S\Theta a_a) + S\tilde{\nabla}_a \mathrm{div} q & \\ +S\Theta\tilde{\nabla}_a p - \Theta p\mathcal{D}_a &= 0, \qquad (2.89)\\ \dot{\mathcal{Z}}_a + \frac{2}{3}\Theta\mathcal{Z}_a + S\left[\frac{1}{3}\Theta^2 + \frac{1}{2}\kappa(\rho+3p)\right]a_a & \\ +\frac{1}{2}\kappa S(\tilde{\nabla}_a\rho + 3\tilde{\nabla}_a p) & \\ -S\tilde{\nabla}_a \mathrm{div} a &= 0. \qquad (2.90)\end{aligned}$$

2.3.1 The gravitational instability

Given the equations for $\mathcal{D}_a$ and $\mathcal{Z}_a$, one may easily derive the gravitational instability for barotropic perfect fluids [16]. We are only interested in the "scalar" parts of these vectors, as these are the parts involved with the clumping of matter. We define the scalar variables as follows:

$$\mathcal{D} \equiv S\tilde{\nabla}^a\mathcal{D}_a, \qquad (2.91)$$

$$\mathcal{Z} \equiv S\tilde{\nabla}^a\mathcal{Z}_a. \qquad (2.92)$$

To linear order, these variables evolve via:

$$\dot{\mathcal{D}} = \Theta w\mathcal{D} - (1+w)\mathcal{Z}, \qquad (2.93)$$

$$\dot{\mathcal{Z}} = -\frac{2}{3}\Theta\mathcal{Z} - \frac{1}{2}\kappa\rho\mathcal{D} - \frac{c_s^2}{1+w}\left(\tilde{\nabla}^2 + \frac{3K}{S^2}\right)\mathcal{D}. \qquad (2.94)$$

One may eliminate $\mathcal{Z}$ and obtain the second-order equation for $\mathcal{D}$ (in a flat background):

$$\ddot{\mathcal{D}} + \frac{1}{3}\left(2 + 3c_s^2 - 6w\right)\Theta\dot{\mathcal{D}} - \left(\frac{1}{2} + 4w - \frac{3}{2}w^2 - 3c_s^2\right)\kappa\rho\mathcal{D} - c_s^2\tilde{\nabla}^2\mathcal{D} = 0. \qquad (2.95)$$

It is convenient to introduce the variable

$$\Phi \equiv \rho S^3\mathcal{D}. \qquad (2.96)$$

From Eq. 2.95 one may obtain the evolution equation for Φ. In conformal time, assuming a perfect fluid with a barotropic equation of state, and a flat background, this is:

$$\Phi'' + (1+3w)\frac{S'}{S}\Phi' - \frac{1}{2}(1+w)\rho S^2\Phi - w\tilde{\nabla}^2\Phi = 0. \qquad (2.97)$$

Here " $'$ " denotes differentiation with respect to the conformal time, η (defined via $d\eta/dt = 1/S$). Harmonically analysing the equation gives

$$\Phi_k'' + (1+3w)\Phi_k' + \left[wk^2 - (1+w)\rho S^2\right]\Phi_k = 0. \qquad (2.98)$$

In the background, the scale factor, energy density, and expansion are go like:

$$S \propto \eta^{\frac{2}{3w+1}}, \quad \rho \propto \eta^{-\frac{6(1+w)}{3w+1}}, \quad \Theta \propto \eta^{\frac{3(1+w)}{3w+1}}. \qquad (2.99)$$

Substituting into Eq. 2.98 gives us the general solutions:

$$\Phi_k = (k\eta)^{2-\nu}[C_+ J_\nu(wk\eta) + C_- G_\nu(wk\eta)], \quad w \neq 0, \tag{2.100}$$

$$\Phi_k = C_+\eta^2 + C_-\eta^{-3}, \quad w = 0, \tag{2.101}$$

with C_+ and C_- constants of integration, J_ν and G_ν Bessel functions of the first and second kind, of order ν, and k the wave-number. The growing mode when $w = 0$ (i.e. dust) represents the gravitational instability.

2.4 Magnetic fields in general relativity

Maxwell's theory of electromagnetic fields was one of the triumphs of nineteenth century physics, and its prediction that the speed of light was a constant invariant of the observer (at odds with Newtonian physics) was very important in Einstein's development of special relativity. Maxwell's theory is invariant under the Lorentz transformations, so can be used in Special Relativity without modification. In order to use it with curved space-time, the theory needs to be re-cast in terms of tensors, and then the principal of minimal coupling may be used to find a theory valid in general relativity. The resulting theory is extremely beautiful, showing clearly how electricity and magnetism are merely dual ways to view the same physical force.

We will now systematically develop the (general) relativistic theory of electromagnetism. The most important quantity in the theory is the Maxwell tensor, $F_{ab} = F_{[ab]}$, which is derived from a potential V_a, by

$$F_{ab} = -2V_{[a;b]}. \tag{2.102}$$

The aforementioned potential is a combination of the classical scalar and vector potentials (ϕ and A^i) of electromagnetism, i.e. $V_a = (\phi, A_i)$. This tensor combines the information contained in the classical electric and magnetic fields, E_a and B_a, which can be recovered from F_{ab} by

$$E_a = F_{ab}u^b, \tag{2.103}$$

$$B_a = {}^*F_{ab}u^b. \tag{2.104}$$

One can easily see why the electric and magnetic components of the Weyl tensor are so named, comparing this definition with Eq. 2.5 and Eq. 2.6. In fact, this analogy is far more than superficial, and a great deal of insight may be gained by exploring it carefully (see, for instance, Maartens and Bassett [59]). The two vectors completely represent the field – if one has E_a and B_a one may obtain F_{ab} by

$$F_{ab} = 2u_{[a}E_{b]} + \varepsilon_{abc}B^c. \tag{2.105}$$

Maxwell's equations take a particularly simple form in this formulation, being given by

$$F^{ab}{}_{;b} = j^a, \tag{2.106}$$

$$F_{[ab;c]} = 0, \tag{2.107}$$

where J_a is the divergence free 4-current generating the magnetic field, and is comprised of the charge $q = -J^a u_a$ and the projected current $j^a = J^{\langle a \rangle}$.

Decomposing these into temporal and spatial parts, one obtains:

$$\mathrm{div}E + 2\omega^a B_a = q, \tag{2.108}$$

$$\sigma^{ab}E_b + \varepsilon^{abc}\omega_c E_b - \frac{2}{3}\Theta E^a + \varepsilon^{abc}a_b B_c + \mathrm{curl}B^a = \dot{E}^{\langle a\rangle} + j^a, \tag{2.109}$$

$$\mathrm{div}B = 2\omega^a E_a, \tag{2.110}$$

$$\sigma^{ab}B_b - \varepsilon^{abc}\omega_b B_c - \frac{2}{3}\Theta B^a - \varepsilon^{abc}a_b E_c = \dot{B}^{\langle a\rangle}. \tag{2.111}$$

The electromagnetic field is most simply incorporated into the EFEs by writing it as a fluid with energy-momentum tensor:

$$T^{ab}_{\mathrm{em}} = F^{ca}F_c{}^b - \frac{1}{4}g^{ab}F_{cd}F^{cd}. \tag{2.112}$$

Performing the standard 1+3 decomposition of the tensor, one obtains

$$\begin{aligned} T^{ab}_{\mathrm{em}} &= \frac{1}{2}\left(E^2+B^2\right)u^a u^b + \frac{1}{6}\left(E^2+B^2\right)h^{ab} \\ &\quad +2u^{(a}\varepsilon^{b)cd}E_c B_d + \Pi^{ab}, \end{aligned} \tag{2.113}$$

$$\Pi^{ab} = \frac{1}{3}\left(E^2+B^2\right)h^{ab} - E^a E^b - B^a B^b, \tag{2.114}$$

where $E^2 = E_a E^a$, and $B^2 = B_a B^a$. Comparing this with the general form for an imperfect fluid in a fundamental observers frame (Eq. 2.33), one may make the identification

$$\rho_{\mathrm{em}} = \frac{1}{2}\left(E^2+B^2\right), \tag{2.115}$$

$$p_{\mathrm{em}} = \frac{1}{6}\left(E^2+B^2\right), \tag{2.116}$$

$$q^a_{\mathrm{em}} = \varepsilon^{abc}E_b B_c, \tag{2.117}$$

$$\pi^{ab}_{\mathrm{em}} = \Pi^{ab}. \tag{2.118}$$

We see that the electromagnetic fluid is radiation like (as one would expect), with an equation of state:

$$p_{\mathrm{em}} = \frac{1}{3}\rho_{\mathrm{em}}. \tag{2.119}$$

The energy-momentum tensor may then be added to the total energy-momentum tensor, and then used to generate the propagation and constraint equations in the presence of a magnetic field [80].

2.4.1 The pure magnetic field

Ohm's law may be stated in covariant form as [41]:

$$J_a - qu_a = \tilde{\sigma}E_a, \tag{2.120}$$

with $\tilde{\sigma}$ the conductivity of the medium. Taking the spatial projection of the equation gives

$$j_a = \tilde{\sigma}E_a, \tag{2.121}$$

so that one may have non-vanishing current with a vanishing electric field if the medium is infinitely conductive ($\tilde{\sigma} \to \infty$). Under this assumption, Maxwell's equations yield three constraints:

$$\omega^a B_a = \frac{1}{2}q, \tag{2.122}$$

$$\mathrm{curl}B^a = \varepsilon^{abc}B_b a_c + j^a, \tag{2.123}$$

$$\mathrm{div}B = 0, \tag{2.124}$$

and one evolution equation:

$$\dot{B}^{\langle a\rangle} = \sigma^{ab}B_b + \varepsilon^{abc}B_b\omega_c - \frac{2}{3}\Theta B^a. \tag{2.125}$$

With an infinitely conductive medium, the electro-magnetic fluid takes the form

$$T^{ab}_{\mathrm{em}} = \frac{1}{2}B^2 u^a u^b + \frac{1}{6}B^2 h^{ab} + \Pi^{ab}, \tag{2.126}$$

where

$$\Pi_{ab} = \frac{1}{3}B^2 h^{ab} - B^a B^b. \tag{2.127}$$

It is thus an imperfect fluid, with

$$\rho_{\mathrm{em}} = \frac{B^2}{2}, \tag{2.128}$$

$$p_{\mathrm{em}} = \frac{B^2}{6}, \tag{2.129}$$

$$q^a_{\mathrm{em}} = 0, \tag{2.130}$$

$$\pi^{ab}_{\mathrm{em}} = \Pi^{ab}. \tag{2.131}$$

It is customary to assume that the universe does indeed possess infinite conductivity (the standard argument for this may be found in Sec. 1.4 of [35]).

2.4.2 Gauge invariant perturbations with magnetic field

A large scale magnetic field naturally introduces a preferred direction in the universe. This naturally presents difficulties if one wants to work with magnetic fields in the FLRW context. In the papers by Tsagas and coworkers [80, 81, 83] it is assumed that there exists a large scale homogeneous magnetic field that is sufficiently weak so as not to disturb the overall isotropy of the universe. Zel'dovich [84] calculates that the magnetic field must be such that $B^2/\rho < 8 \times 10^{-5}$ if this assumption is to be consistent. As will be discussed in Ch. 3, the isotropy of the CMBR may be used to place strong limits on the magnitude of the magnetic field [1, 4, 5].

Alternatively, one may follow Battener et al. [6] and assume that there is no mean magnetic field on cosmological scales, or that $\langle B_a\rangle = 0$. They however allow the presence of magnetic field in smaller cells, with random field directions on larger scales. These models thus have a non-vanishing magnetic energy density $\langle B^2\rangle \neq 0$ even though the average magnetic field is zero. This approach is also followed by Kim et al. [47], who assume that the field directions are randomly oriented on scales smaller than the Hubble radius.

We use the same perturbation scheme as in Hobbs [39], where two perturbation variables are used. The first order variables introduced in Sec. 2.3 are all considered to be $O(\epsilon_1)$. The second perturbation variable, ϵ_2, is taken to be the Alfvén speed, $\frac{B^2}{\rho}$. The magnetic field is treated as a small test field propagating on the background, and is thus taken as zero order.

In order to preserve the closeness of the perturbed universe to an FLRW universe, we follow Tsagas [82] in requiring the magnetic anisotropic stress, Π_{ab}, and the co-moving gradient of the magnetic energy density,

$$\mathcal{B}_a \equiv \frac{S}{B^2}\tilde{\nabla}_a B^2, \tag{2.132}$$

to be $O(\epsilon_1)$. By demanding this, we ensure that even though the magnetic field is zero order, it does not disturb the isotropy of the background.

When linearising, then, we drop all terms higher than first order in ϵ_1 and ϵ_2, but retain terms like $O(\epsilon_1\epsilon_2)$. As a final step we may drop terms $O(\epsilon_2)$ relative to zero order terms in the coefficients of quantities that are $O(\epsilon_1)$. We may do this as the magnetic field is very weak. This may only be done as a final step, as doing this earlier in the calculations may lead to important terms being left out[7].

The magnetic field is frozen in with the baryons. Choosing any other frame will cause an electric field to be induced. When the relative velocity of the baryon fluid, $v_a^{(b)}$, to the chosen frame is $O(\epsilon_1)$, then the induced electric field is given by

$$E_a^{\rm ind} = \varepsilon^{abc} v_b^{(b)} B_c. \tag{2.133}$$

The magnetic fluid is then an imperfect fluid with

$$\rho^{\rm em} = \frac{1}{2}B^2, \tag{2.134}$$

$$p^{\rm em} = \frac{1}{3}\rho^{\rm em}, \tag{2.135}$$

$$q_a^{\rm em} = \frac{4}{3}\rho_{\rm em} v_a^{(b)}, \tag{2.136}$$

$$\Pi_{ab} = \frac{1}{3}B^2 h_{ab} - B_a B_b. \tag{2.137}$$

[7] From this point on all equations may be assumed to be derived using this system, including the effects of a magnetic field, unless it is otherwise noted.

We may now find the (linearised) propagation equations:

$$\dot{E}_{ab} + \Theta E_{ab} - \mathrm{curl}H_{ab} + \frac{1}{6}\Big[3\rho\Big(1+w+\frac{2B^2}{\rho}\Big)\sigma_{ab}$$
$$+3\tilde{\nabla}_{\langle a}q_{b\rangle} - 2B^2\tilde{\nabla}_{\langle a}v^{(b)}_{b\rangle} + 3\dot{\pi}_{ab} + \Theta\pi_{ab} + 3\dot{\Pi}_{ab} + \Theta\Pi_{ab}\Big] = 0, \quad (2.138)$$

$$\dot{H}_{ab} + \Theta H_{ab} + \mathrm{curl}\left[E_{ab} - \frac{1}{2}(\pi_{ab}+\Pi_{ab})\right] = 0, \quad (2.139)$$

$$\dot{\sigma}_{ab} + \frac{2}{3}\Theta\sigma_{ab} - \tilde{\nabla}_{\langle a}a_{b\rangle} + E_{ab} - \frac{1}{2}(\pi_{ab}+\Pi_{ab}) = 0, \quad (2.140)$$

$$\dot{\omega}_{ab} - \tilde{\nabla}_{[b}a_{a]} + \frac{2}{3}\Theta\omega_{ab} = 0, \quad (2.141)$$

$$\dot{q}^T_a + \frac{4}{3}\Theta q^T_a + \rho\left(1+w+\frac{2B^2}{3\rho}\right)a_a + \mathrm{div}(\pi)_a + \mathrm{div}(\Pi)_a$$
$$+\tilde{\nabla}_a p + \frac{1}{6}\frac{B^2}{S}\mathcal{B}_a = 0, \quad (2.142)$$

$$\dot{\Theta} + \frac{1}{3}\Theta^2 - A + \frac{1}{2}\rho\left(1+3w+\frac{B^2}{\rho}\right) = 0, \quad (2.143)$$

$$\dot{\rho} + \Theta\rho(1+w) + \mathrm{div}q = 0, \quad (2.144)$$

$$\dot{B}^2 + \frac{4}{3}\Theta B^2 + \frac{4}{3}B^2\mathrm{div}v^{(b)} = 0, \quad (2.145)$$

and constraint equations:

$$H_{ab} + \mathrm{curl}(\sigma_{ab} - \omega_{ab}) = 0, \quad (2.146)$$

$$\mathrm{div}(H)_a - \frac{1}{2}\left[\rho\left(1+w+\frac{2B^2}{3\rho}\right)\omega_a - \mathrm{curl}q_a\right] = 0, \quad (2.147)$$

$$\mathrm{div}(E)_a - \frac{1}{6}\Big[2\frac{\rho}{S}\mathcal{D}_a + \frac{B^2}{S}\mathcal{B}_a - 2\Theta q_a - \frac{4}{3}\Theta B^2 v^{(b)}_a$$
$$-3\mathrm{div}(\pi+\Pi)_a\Big] = 0, \quad (2.148)$$

$$\mathrm{div}(\omega)_a + \mathrm{div}(\sigma)_a - \frac{2}{3}\tilde{\nabla}_a\Theta + q_a + \frac{2}{3}B^2 v^{(b)}_a = 0, \quad (2.149)$$

$$\mathrm{div}\omega = 0, \quad (2.150)$$

for the variables. Here $A \equiv \mathrm{div}a$ and $q^T_a = q_a + \frac{2}{3}B^2 v^{(b)}_a$.

One may also obtain the propagation equations for $\mathcal{B}_a$ and Π_{ab}:

$$\dot{\mathcal{B}}_a = -\frac{4}{3}(\mathcal{Z}_a + S\Theta a_a) - \frac{4}{3}S\tilde{\nabla}_a\mathrm{div}v^{(b)}, \quad (2.151)$$

$$\dot{\Pi}_{ab} = -\frac{4}{3}\Theta\Pi_{ab} - \frac{2}{3}B^2\sigma_{ab} - \frac{2}{3}B^2\tilde{\nabla}_{\langle a}v^{(b)}_{b\rangle}. \quad (2.152)$$

Taking the spatial gradient of the conservation equation for energy density, one finds the propagation equation for the co-ming fractional density gradient:

$$\rho\dot{\mathcal{D}}_a + \rho(1+w)(\mathcal{Z}_a + S\Theta a_a) + S\tilde{\nabla}_a\mathrm{div}q + S\Theta\tilde{\nabla}_a p - \Theta p\mathcal{D}_a = 0. \quad (2.153)$$

Similarly, the spatial gradient of the Raychaudhuri equation yields the propagation equation for the the co-moving gradient of the expansion:

$$\dot{\mathcal{Z}}_a + \frac{2}{3}\Theta\mathcal{Z}_a + S\left[\frac{1}{3}\Theta^2 + \frac{1}{2}\rho\left(1+3w+\frac{B^2}{\rho}\right)\right]a_a \\ +\frac{1}{2}S\left(\tilde{\nabla}_a\rho + 3\tilde{\nabla}_a p + \frac{B^2}{S}\mathcal{B}_a\right) \\ -S\tilde{\nabla}_a A = 0. \quad (2.154)$$

2.5 Relativistic kinetic theory

While we have been describing the fluids that make up the universe in terms of bulk, or, average properties, we all realise that at a fundamental level a fluid is made up of interacting particles. How are we to relate the physics at this microscopic level to the bulk variables we use? Boltzmann's kinetic theory provides an elegant answer to this question, allowing us to take microscopic dynamics and transferring them to macroscopic laws which the fluid must obey. Boltzmann formulated his kinetic theory in the classical framework of his day. In order to make it relevant cosmologically, we must reformulate the theory in a general relativistic framework.

In the kinetic theory, the each fluid is described by means of a scalar valued distribution function $f(x,p)$ [63], defined so that an observer sees $f(x,p)dx^3dp^3$ particles of that species at space-time point x in the proper volume dx^3, with momentum p in the proper (momentum-space) volume dp^3. The 4-momentum, p^a, may be decomposed as

$$p^a = E(u^a + e^a), \quad e^a e_a = 1, \quad e^a u_a = 0, \quad (2.155)$$

where $E = -u_a p^a$ is the energy measured by an observer with velocity u^a, and e^a is a unit spacelike vector orthogonal to u^a describing the direction of propagation of the motion relative to the instantaneous rest space of the observer. One can now, when convenient, write $f^{(\gamma)}(E,e)$ for the distribution (the dependence on x is implicit).

If the fluid particle is at $x^a(\lambda)$ and the momentum $p^a(\lambda)$, then the path of the fluid particle in phase space is given by:

$$\frac{dx^a}{d\lambda} = p^a, \quad p^a\nabla_a p_b = 0, \quad (2.156)$$

with λ an affine parameter along the geodesic $x^a(\lambda)$.

The distribution function evolves according to the collisional Boltzmann equation:

$$\mathcal{L}f = \frac{d}{d\lambda}f[x^a(\lambda), p^a(\lambda)] = \mathcal{C}, \quad (2.157)$$

where $\mathcal{L}$ denotes the Liouville operator, and $\mathcal{C}$ the collisional operator. The collisional operator may be found by considering the microscopic nature of the fluid, and is how the two scales are linked. One may clearly see that in the absence of collisions, the distribution is conserved in phase space.

In order to recover the energy momentum tensor of the fluid, one must decompose the photon distribution function into angular harmonics:

$$f(e,E) = \sum_{l=0}^{\infty} F^{(l)}_{a_1\ldots a_l} e^{a_1} e^{a_2} \ldots e^{a_l}. \tag{2.158}$$

The covariant multipoles $F^{(l)}_{a_1\ldots a_l}$ have an implicit dependence on space-time position x and energy E. They are irreducible since they are Projected, Symmetric, and Trace Free (PSTF):

$$F^{(l)}_{a_1\ldots a_l} = F^{(l)}_{\langle a_1\ldots a_l\rangle}, \quad u^{a_1} F^{(l)}_{a_1\ldots a_l} = 0, \quad g^{a_1 a_2} F^{(l)}_{a_1\ldots a_l} = 0. \tag{2.159}$$

The l-multipole can be recovered from the distribution via

$$F^{(l)}_{a_1\ldots a_l} = \delta_l^{-1} \int d\Omega\, f^{(l)}(e,E) e^{a_1} e^{a_2} \ldots e^{a_l}, \quad \delta_l = 4\pi \frac{2^l (l!)^2}{(2l+1)!}, \tag{2.160}$$

with the measure $d\Omega$ being a solid angle in momentum space. The first three multipoles in fact determine the fluid (which is massless) energy-momentum tensor, with

$$\rho^{(\gamma)} = 4\pi \int_0^{\infty} dE\, E^3 F^{(0)}, \tag{2.161}$$

$$q_a^{(\gamma)} = \frac{4\pi}{3} \int_0^{\infty} dE\, E^3 F_a^{(1)}, \tag{2.162}$$

$$\pi_{ab}^{(\gamma)} = \frac{8\pi}{15} \int_0^{\infty} dE\, E^3 F_{ab}^{(2)}. \tag{2.163}$$

One may extend these dynamical quantities to higher orders by defining the higher moments:

$$I^{(l)}_{a_1\ldots a_l} = \frac{4\pi (2^l)(l!)^2}{(2l+1)!} \int_0^{\infty} dE\, E^3 F^{(l)}_{a_1\ldots a_l}. \tag{2.164}$$

Thus the energy-momentum tensor of the fluid is contained in the the distribution function. However, the distribution function contains far more information than merely the energy-momentum tensor, in the form of the higher angular moments. The energy-momentum tensor may be concisely written in terms of the distribution tensor via

$$T_{ab}^{(\gamma)} = \int dE\, d\Omega\, E f^{(\gamma)}(E,e) p_a p_b. \tag{2.165}$$

In many calculations spherical harmonics, $Y_l^m(\vec{e})$, are used in place of the $F^{(l)}_{a_1\ldots a_l}$, but the $F^{(l)}_{a_1\ldots a_l}$ are used here as they have have several advantages:

1. The $F^{(l)}_{a_1\ldots a_l}$ are covariant, so independent of the choice of momentum space coordinates.
2. $F^{(l)}_{a_1\ldots a_l}$ is a rank l tensor field on space-time for fixed E, and directly determines the l-multipole of radiation anisotropy after integration over energy.

2.5.1 Photon-Baryon fluids

We will now consider the important case where a photon fluid and a non-relativistic baryon fluid interact. In this case the photon fluid interacts with the thermal distribution of the baryons via Compton scattering off free electrons. We will assume the average energy of a photon is small compared to the electron mass, this interaction may be approximated by Thomson scattering. Furthermore, as the electrons are assumed to be moving slowly, the kinetic temperature of the electrons is small compared to the electron mass, and we may disregard the effect of their thermal motion on the scattering. By ignoring polarisation one may further simplify the system. However, it is important to note that Thomson scattering of an unpolarised but anisotropic distribution leads to the generation of polarisation, which in turn affects the collisional. Thus calculations performed without considering the effects of polarisation will lead to inaccuracies[8]. However, for simplicity of treatment, we will ignore polarisation here. One may consult Challinor's paper [13] for a treatment including the effects of polarisation.

With these assumptions, the collisional operator $\mathcal{C}$ takes the form[9][11]:

$$\mathcal{C} = n_e \sigma_T E^{(b)} [f_+^{(\gamma)}(x,p) - f^{(\gamma)}(x,p)], \tag{2.166}$$

where $E^{(b)} = -p^a u_a^{(b)}$ is the photon energy in the baryonic frame ($u_a^{(b)}$ is the baryonic 4-velocity), and $f_+^{(\gamma)}(x,p)$ describes the scattering into the phase space under consideration. $f_+^{(\gamma)}(x,p)$ is given by:[10]

$$f_+^{(\gamma)}(x,p) = \frac{3}{16\pi} \int f^{(\gamma)}(x,p')[1 + (g^{ab} e_a^{(b)} e'^{(b)}_b)^2] d\Omega_{e'^{(b)}}. \tag{2.167}$$

$e_a^{(b)}$ is the photon direction relative to $u_a^{(b)}$, so

$$p_a = E^{(b)}(u_a^{(b)} + e_a^{(b)}), \tag{2.168}$$

and $e'^{(b)}_a$ is the initial direction of the photon (relative to $u_a^{(b)}$) of the photon whose initial momentum is p'_a and final momentum is p_a. One may now multiply both sides of the Boltzmann equation (Eq. 2.157) by E^2 and integrate over all energies to obtain:

$$\begin{aligned} \int dE\, E^2 \mathcal{L} f^{(\gamma)}(E.e) \quad = \quad & \frac{3}{16\pi} n_e \sigma_T [\gamma^{(b)}(1 - e^f v_f^{(b)})]^{-3} \\ & \times g^{ab} g^{cd} T_{bd}^{(\gamma)} (u_a^{(b)} u_c^{(b)} + e_a^{(b)} e_c^{(b)}) \\ & - n_e \sigma_T \gamma^{(b)} (1 - e^a v_a^{(b)}) \int dE\, E^3 f^{(\gamma)}(E,e), \end{aligned} \tag{2.169}$$

where $v_a^{(b)}$ is the relative velocity of the baryons (satisfying $u^a v_a^{(b)} = 0$), and $\gamma^{(b)} = (1 - g^{ab} v_a^{(b)} v_b^{(b)})^{-1/2}$, allowing one to write:

$$u_a^{(b)} = \gamma^{(b)}(u_a + v_a^{(b)}), \tag{2.170}$$

[8] Hu et al. [40] demonstrated that the neglect of polarisation effects leads to errors of a few percent in the predicted temperature anisotropy.

[9] For the remainder of the paper the superscript "(γ)" refers to the photon fluid, "(b)" the baryon fluid, "(ν)" the neutrino fluid, and "(c)" to cold dark matter.

[10] Although the inclusion of a magnetic field changes the form of the collisional, the changes are small for a weak magnetic field and may be ignored to first order in the the field.

so, to first order in almost FRM universes,

$$u_a^{(b)} = u_a + v_a^{(b)}, \tag{2.171}$$

since the relative velocities of the matter components are first order in FLRW universes. Linearising Eq. 2.169 about a FLRW background then gives:

$$\begin{aligned}\int dE\, E^2 \mathcal{L} f^{(\gamma)}(E,e) &= \frac{3}{16\pi} n_e \sigma_T \left[\frac{4}{3}(1+4e^a v_a^{(b)})\rho^{(\gamma)} + \pi_{ab}^{(\gamma)} e^a e^b\right] \\ &\quad - n_e \sigma_T \int dE\, E^3 f^{(\gamma)}(E,e). \end{aligned} \tag{2.172}$$

Expanding this equation now into angular harmonics and separating out the components now yields the (linearised) propagation equations[11]

$$\begin{aligned}\dot{I}_{A_l}^{(l)} + \frac{4}{3}\Theta I_{A_l}^{(l)} + \frac{l}{2l+1}\tilde{\nabla}_{\langle a_l} I_{A_{l-1}\rangle}^{(l-1)} + \tilde{\nabla}^b I_{bA_l}^{(l+1)} + \frac{4}{3}\delta_l^1 I a_a \\ = -n_e \sigma_T (I_{A_l}^{(l)} - \delta_l^0 I - \frac{4}{3}\delta_l^1 I v_{a_1}^{(b)} - \frac{1}{10}\delta_l^2 I_{a_1 a_2}). \end{aligned} \tag{2.173}$$

Note, these equations only link the $l-1$, l, $l+1$ angular multipoles. If one were working with the full nonlinear set of equations the equations would link five successive harmonics [28].

One may now take the spatial derivative of zeroth moment equation and commute derivatives to obtain the propagation equation:

$$\mathcal{D}_a^{(\gamma)} + \frac{4}{3}\mathcal{Z}_a + \frac{S}{\rho^{(\gamma)}}\tilde{\nabla}_a \mathrm{div} q^{(\gamma)} - \frac{4}{3} S\Theta a_a = 0. \tag{2.174}$$

The magnetised baryon fluid is non-relativistic, so may be described as an ideal gas coupled to the magnetic field, and strongly coupled to the photon gas (via Thomson scattering) so that its energy-momentum tensor takes the form

$$T_{ab}^{(b)} = \rho^{(b)} u_a u_b + p^{(b)} h_{ab} + 2(\rho^{(b)} + p^{(b)}) u_{(a} v_{b)}^{(b)} \tag{2.175}$$

in the linear theory.

The photon, magnetic, and baryon fluids are coupled, so exchange energy. Thus neither energy-momentum tensor is conserved alone, only total energy-momentum is conserved:

$$\nabla^a T_{ab}^{(\gamma)} + \nabla^a T_{ab}^{(b)} + \nabla^a T_{ab}^{(\mathrm{em})} = 0. \tag{2.176}$$

This now allows us to find propagation equations for the baryon fluid's kinematic

[11] Unless otherwise stated, I_{A_l} always refers to photon angular harmonics. Here the subscript refers to the lumped index $a_1 \ldots a_l$.

variables[12]:

$$\dot{\rho}^{(b)} + (\rho^{(b)} + p^{(b)})\Theta + (\rho^{(b)} + p^{(b)})\mathrm{div}v^{(b)} = 0, \tag{2.177}$$

$$\rho^{(b)}\left(1 + w^{(b)} + \frac{2B^2}{3\rho^{(b)}}\right)(\dot{v}_a^{(b)} + a_a) + \frac{1}{3}\rho^{(b)}\left(1 + w^{(b)} + \frac{2B^2}{3\rho^{(b)}}\right)\Theta v_a^{(b)} + \mathrm{div}(\Pi)_a + \dot{p}^{(b)}v_a^{(b)} + \frac{1}{6}(B^2)\dot{v}_a^{(b)} + \tilde{\nabla}_a p^{(b)} + \frac{1}{3}\frac{B^2}{S}\mathcal{B}_a + n_e\sigma_T\left(\frac{4}{3}\rho^{(\gamma)}v_a^{(b)} - q_a^{(\gamma)}\right) = 0. \tag{2.178}$$

One must naturally complement these equations with an equation of state linking the baryon energy density and pressure. From Eq. 2.177 we may find the linearised propagation equation for the co-moving fractional spatial gradient of the baryon energy density:

$$\rho^{(b)}\dot{\mathcal{D}}_a^{(b)} + (\rho^{(b)} + p^{(b)})(\mathcal{Z}_a + S\tilde{\nabla}_a\mathrm{div}v^{(b)} + S\Theta a_a) + S\Theta\tilde{\nabla}_a p^{(b)} - \Theta p^{(b)}\mathcal{D}_a^{(b)} = 0. \tag{2.179}$$

2.5.2 Neutrinos

The massless neutrinos form a non-interacting relativistic fluid. They may thus be modelled using a zero collisional. Following much the same process as in the previous section, we may find propagation equations for the neutrino fluid components[13]:

$$\dot{G}_{A_l}^{(l)} + \frac{4}{3}\Theta G_{A_l}^{(l)} + \frac{l}{2l+1}\tilde{\nabla}_{\langle a_l}G_{A_{l-1}\rangle}^{(l-1)} + \tilde{\nabla}^b G_{bA_l}^{(l+1)} + \frac{4}{3}\delta_l^1 G a_a = 0. \tag{2.180}$$

The equation for the fractional co-moving spatial gradient is given by:

$$\dot{\mathcal{D}}_a^{(\nu)} + \frac{4}{3}\mathcal{Z}_a + \frac{S}{\rho^{(\nu)}}\tilde{\nabla}_a\mathrm{div}q^{(\nu)} - \frac{4}{3}S\Theta a_a = 0. \tag{2.181}$$

2.5.3 The Sachs-Wolfe effect

The temperature fluctuation, $\tau(x,e)$, is defined in terms of the directional bolometric brightness:

$$T(x,e) = T(x)[1 + \tau(x,e)] = \left[\frac{4}{\pi}\int E^3 f(x,E,e)dE\right]^{1/4}, \tag{2.182}$$

where $T(x)$ is the bolometric temperature. Its variation can be obtained from the linearised integrated Boltzmann equation:

$$\int E^2 dE\left[\nabla_a f p^a + \frac{dE}{d\lambda}\frac{\partial f}{\partial E}\right] \approx \int E^2 \mathcal{C}[f]dE. \tag{2.183}$$

[12] It should be recalled that the magnetic energy density is identically conserved.
[13] Unless otherwise stated, G_{A_l} refers to the higher neutrino angular moments.

Substituting the identity

$$\frac{dE}{d\lambda} = -E^2\left[\frac{1}{3}\Theta + a_a e^a + \sigma_{ab}e^a e^b\right], \tag{2.184}$$

into the integrated Boltzmann equation and integrating by parts, one obtains

$$\tau(x,e)' + \frac{\rho^{(\gamma)'}}{4\rho^{(\gamma)}}(1+4\tau(x,e)) + \frac{1}{3}(1+4\tau(x,e)) + a_a e^a + \sigma_{ab}e^a e^b \approx \frac{\pi}{\rho^{(\gamma)}}\int E^2\mathcal{C}[f]dE. \tag{2.185}$$

To linear order, the collisional term is given by:

$$\int E^2\mathcal{C}[f]dE \approx \frac{n_e\sigma_T}{\pi}\rho^{(\gamma)}v_a^{(b)}e^a + \frac{3n_E\sigma_T}{16\pi}\pi_{ab}^{(\gamma)}e^a e^b - \frac{n_E\sigma_T}{\pi}\rho^{(\gamma)}\tau(x,e). \tag{2.186}$$

Substituting into Eq. 2.185 one obtains the result

$$\begin{aligned}\tau(x,e)' \quad &+ \quad n_e\sigma_T\tau(x,e) + \left(\frac{1}{3}\Theta + \frac{\rho^{(\gamma)'}}{4\rho^{(\gamma)}}\right)(1+4\tau(x,e)) \\ &\approx \quad -\sigma_{ab}e^a e^b - a_a e^a + n_E\sigma_T\left[v_a^{(b)}e^a + \frac{3}{16\rho^{(\gamma)}}\pi_{ab}^{(\gamma)}e^a e^b\right],\end{aligned} \tag{2.187}$$

where " $'$ " denotes differentiation with respect to the parameter ν along a null geodesic, so that $d\nu/d\lambda = E$. This equation includes contributions from all perturbation types, and is valid in open, flat, and closed universes. It, however, does not include polarisation effects.

In order to obtain an expression for the temperature anisotropy in a given direction, one may integrate this equation along a null geodesic whose tangent vector projects to that direction, through the observation point x_R. It is convenient to substitute for the expansion in terms of known variables. This is done via the energy conservation equation for radiation written using the spatial gradient of the energy density, $X_a^{(\gamma)} = \tilde{\nabla}_a\rho^{(\gamma)}$ along the null vector $p_a = E(e^a + u^a)$:

$$e^a X_a^{(\gamma)} = \rho^{(\gamma)'} + \frac{4}{3}\Theta\rho^{(\gamma)} + \tilde{\nabla}^a q_a^{(\gamma)}. \tag{2.188}$$

This gives:

$$\frac{1}{3}\Theta + \frac{\rho^{(\gamma)'}}{4\rho^{(\gamma)}} = \frac{1}{4\rho^{(\gamma)}}\left(e^a X_a^{(\gamma)} - \tilde{\nabla}^a q_a^{(\gamma)}\right), \tag{2.189}$$

which then gives (writing $q_a^{(\gamma)} = 4/3\rho^{(\gamma)}v_a^{(\gamma)}$):

$$\begin{aligned}\tau(x,e)' + n_E\sigma_T\tau(x,e) \quad &\approx \quad -\left(\frac{1}{4S}e^a\mathcal{D}_a^{(\gamma)} - \frac{1}{3}\tilde{\nabla}^a v_a^{(\gamma)}\right) - \sigma_{ab}e^a e^b - a_a e^a \\ &+ \quad n_e\sigma_T\left(v_a^{(b)}e^a + \frac{3}{16\rho^{(\gamma)}}\pi_{ab}^{(\gamma)}e^a e^b\right).\end{aligned} \tag{2.190}$$

One may now integrate this equation along the null geodesic connecting the reception point x_R to a point in the past, x_A, to obtain an integral solution on scales where instantaneous recombination is valid. In the case where one assumes the photons are collision free, $n_e\sigma_T \to 0$, we obtain the Sachs-Wolfe formula:

$$\tau(x,e) = -\int_A^R\left(\frac{1}{4S}\mathcal{D}_a^{(\gamma)}e^a - \frac{1}{3}\tilde{\nabla}^a v_a^{(\gamma)} + \sigma_{ab}e^a e^b + a_a e^a\right)d\nu. \tag{2.191}$$

2.6 Decomposition into harmonic modes

The decomposition of partial differential equations into harmonic modes has been an extremely successful technique to render otherwise intractable problems tractable. The technique relies on splitting the spatial and time dependencies of the PDEs, by decomposing the functions (at each time) relative to some basis and then finding evolution equations for the coefficients (for instance, in Fourier analysis this decomposition is done with respect to the sine and cosine functions). These evolution equations then turn out to be ODEs, which one may then solve with the standard methods.

In order to follow this procedure in our covariant approach, one must find a relevant set of basis functions with which one may perform such a decomposition. As we are dealing with tensor perturbation equations, we may decompose the perturbation types into the scalar, vector, rank-2 tensor, etc. parts. It turns out that these different rank perturbations decouple, and that, furthermore, we may ignore perturbations of rank higher than a rank-2 tensor[14] (which will henceforth simply be known as tensor perturbations). In addition, it may be shown that vector perturbations decay [29], so that we may ignore these too. These separate perturbation types will now be dealt with separately.

2.6.1 Scalar modes

In the covariant approach, scalar modes are characterised by asking the requirement that the magnetic part of the Weyl tensor, as well as the vorticity, be second order. Making $H_{ab} = 0 + O(2)$ forces gravitational waves to be negligible. By choosing $\omega_{ab} = 0 + O(2)$ one makes sure that density gradients seen by the observer in the u^a frame are due to clumping, and not from kinematic effects due to the vorticity.

This requirement generates a set of constraints [11] which may be satisfied by constructing the covariant and gauge invariant variables from tensors derived from scalar potentials. One may separate the temporal and spatial aspects of the problem by expanding the scalar potentials in terms of the eigenfunctions, $Q^{(k)}$, of the generalised Helmholtz equation

$$\tilde{\nabla}^2 Q^{(k)} = -\frac{k^2}{S^2} Q^{(k)}, \tag{2.192}$$

$$\dot{Q}^{(k)} = 0, \tag{2.193}$$

where these equations hold to zeroth order only. In general one cannot constrain $\dot{Q}^{(k)} = 0$ to higher order. The allowed eigenvalues depend on the curvature of the background model: for $K = 0$, k is any positive real number, for $K > 0$, $k^2 = \gamma(\gamma + 2)K$, $\gamma \in \mathbb{N}^+$, and for $K < 0$, k is any real satisfying $k^2 \geq |K|$.

From the $Q^{(k)}$, one may construct a vector eigenfunctions

$$Q_a^{(k)} \equiv \frac{S}{k} \tilde{\nabla}_a Q(k), \tag{2.194}$$

satisfying

$$u^a Q_a^{(k)} = 0, \quad \dot{Q}_a^{(k)} = 0, \tag{2.195}$$

[14] These higher rank perturbations do not contribute to the CMB, which is the focus of this paper.

and higher order tensors via the recursion formula:

$$Q^{(k)}_{a_1\ldots a_l} = \frac{S}{k}\left(\tilde{\nabla}_{(a_1}Q^{(k)}_{a_2\ldots a_l)} - \frac{l-1}{2l-1}\tilde{\nabla}^b Q^{(k)}_{b(a_1\ldots a_{l-2}}h_{a_{l-1}a_l)}\right), \tag{2.196}$$

satisfying

$$u^{a_1}Q^{(k)}_{a_1\ldots a_l} = 0, \quad h^{a_1a_2}Q^{(k)}_{a_1a_2\ldots a_l} = 0, \quad \dot{Q}^{(k)}_{a_1\ldots a_l} = 0. \tag{2.197}$$

One may now construct the gauge invariant variables as follows:

$$\mathcal{D}^{(i)}_a = \sum_k k\mathcal{D}^{(i)}_k Q^{(k)}_a, \tag{2.198}$$

$$\mathcal{B}_a = \sum_k k\mathcal{B}_k Q^{(k)}_a, \tag{2.199}$$

$$q^{(i)}_a = \rho^{(i)}\sum_k q^{(i)}_k Q^{(k)}_a, \tag{2.200}$$

$$v^{(i)}_a = \sum_k v^{(i)}_k Q^{(k)}_a, \tag{2.201}$$

$$\pi^{(i)}_{ab} = \rho^{(i)}\sum_k \pi^{(i)}_k Q^{(k)}_{ab}, \tag{2.202}$$

$$\Pi_{ab} = \frac{B^2}{2}\sum_k \Pi_k Q^{(k)}_{ab}, \tag{2.203}$$

$$\mathcal{Z}_a = \sum_k \frac{k^2}{S}\mathcal{Z}_k Q^{(k)}_a, \tag{2.204}$$

$$E_{ab} = \sum_k \frac{k^2}{S^2}\Phi_k Q^{(k)}_{ab}, \tag{2.205}$$

$$\sigma_{ab} = \sum_k \frac{k}{S}\sigma_k Q^{(k)}_{ab}, \tag{2.206}$$

$$a_a = \sum_k \frac{k}{S}a_k Q^{(k)}_a, \tag{2.207}$$

where the particle species is labelled by i. We further assume that the higher order moments may be expanded in terms of $Q^{(k)}_{a_1\ldots a_l}$ harmonics. One may then define:

$$I^{(l)}_{A_l} = \rho^{(\gamma)}\sum_k I^{(l)}_k Q^{(k)}_{A_l}, \tag{2.208}$$

$$G^{(l)}_{A_l} = \rho^{(\nu)}\sum_k G^{(l)}_k Q^{(k)}_{A_l}. \tag{2.209}$$

The expansion coefficients, like $\mathcal{D}^{(i)}_k$ are themselves first order, and satisfy

$$\tilde{\nabla}^a\mathcal{D}^{(i)}_k = 0 + O(2). \tag{2.210}$$

In terms of these variables, the total matter variables[15] $\mathcal{D}_k$, q_k and π_k are defined

[15]Unless otherwise specified, "total" excludes the magnetic fluid. This is done in order to isolate the effects of that fluid.

as

$$\rho\mathcal{D}_k = \rho^{(\gamma)}\mathcal{D}_k^{(\gamma)} + \rho^{(\nu)}\mathcal{D}_k^{(\nu)} + \rho^{(c)}\mathcal{D}_k^{(c)} + \rho^{(b)}\mathcal{D}_k^{(b)}, \quad (2.211)$$

$$\rho q_k = \rho^{(\gamma)}q_k^{(\gamma)} + \rho^{(\nu)}q_k^{(\nu)} + \rho^{(c)}v_k^{(c)} + (\rho^{(b)} + p^{(b)})v_k^{(b)}, \quad (2.212)$$

$$\rho\pi_k = \rho^{(\gamma)}\pi_k^{(\gamma)} + \rho^{(\nu)}\pi_k^{(\nu)}. \quad (2.213)$$

In addition it is convenient to define a total flux which *includes* the magnetic flux:

$$\rho^T q_k^T = \rho^{(\gamma)}q_k^{(\gamma)} + \rho^{(\nu)}q_k^{(\nu)} + \rho^{(c)}v_k^{(c)} + \rho^b b\left(1 + w^{(b)} + \frac{2B^2}{3\rho^{(b)}}\right)v_k^{(b)}, \quad (2.214)$$

where $\rho^T = \rho + B^2/6$ is the total energy density (including that of the magnetic fluid). One may now derive propagation and constraint equations for these coefficients. In the pure GR case, with photons, baryons, cold dark matter and neutrinos, these equations are [11]:

- The density perturbation variables:

$$\dot{\mathcal{D}}_k^{(\gamma)} + \frac{k}{S}\left(\frac{4}{3}\mathcal{Z}_k - q_k^{(\gamma)}\right) + \frac{4}{3}\Theta a_k = 0, \quad (2.215)$$

$$\dot{\mathcal{D}}_k^{(\nu)} + \frac{k}{S}\left(\frac{4}{3}\mathcal{Z}_k - q_k^{(\nu)}\right) + \frac{4}{3}\Theta a_k = 0, \quad (2.216)$$

$$\dot{\mathcal{D}}_k^{(c)} + \frac{k}{S}\left(\mathcal{Z}_k - v_k^{(c)}\right) + \Theta a_k = 0, \quad (2.217)$$

$$\dot{\mathcal{D}}_k^{(b)} + \left(1 + \frac{p^{(b)}}{\rho^{(b)}}\right)\left[\frac{k}{S}\left(\mathcal{Z}_k - v_k^{(b)}\right) + \Theta a_k\right] - \left(\frac{p^{(b)}}{\rho^{(b)}} - c_s^2\right)\Theta\mathcal{D}_k^{(b)} = 0, \quad (2.218)$$

$$\dot{\mathcal{B}}_k + \frac{k}{S}\left(\frac{4}{3}\mathcal{Z}_k - v_k^{(b)}\right) + \frac{4}{3}\Theta a_k = 0. \quad (2.219)$$

- The spatial gradient of the expansion:

$$\dot{\mathcal{Z}}_k = -\frac{1}{3}\Theta\mathcal{Z}_k - \frac{1}{2}\frac{S}{k}\kappa[B^2\mathcal{B}_k + 2(\rho^{(\gamma)}\mathcal{D}_k^{(\gamma)} + \rho^{(\nu)}\mathcal{D}_k^{(\nu)}) + \rho^{(c)}\mathcal{D}_k^{(c)} + (1 + 3c_s^2)\rho^{(b)}\mathcal{D}_k^{(b)}] - \frac{S}{k}a_k\left[\frac{3}{2}\kappa\rho\left(1 + w + \frac{2B^2}{3\rho}\right) - \frac{3K}{S^2}\right]. \quad (2.220)$$

- The heat fluxes:

$$\dot{q}_k^{(\gamma)} + \frac{1}{3}\frac{k}{S}\left[2\pi_k^{(\gamma)}(3K/k^2 - 1) + \mathcal{D}_k^{(\gamma)} + 4a_k\right] = n_e\sigma_T\left(\frac{4}{3}v_k^{(b)} - q_k^{(\gamma)}\right), \quad (2.221)$$

$$\dot{q}_k^{(\nu)} + \frac{1}{3}\frac{k}{S}\left[2\pi_k^{(\nu)}(3K/k^2 - 1) + \mathcal{D}_k^{(\nu)} + 4a_k\right] = 0, \quad (2.222)$$

- The peculiar velocities:

$$\dot{v}_k^{(c)} + \frac{1}{3}\theta v_k^{(c)} + \frac{k}{S}a_k = 0, \tag{2.223}$$

$$\left(1+w^{(b)}\right)\left[\dot{v}_k^{(b)} + \frac{1}{3}(1-3c_s^2)\theta v_k^{(b)} + \frac{k}{S}a_k\right] + \frac{1}{6}\frac{k}{S}\frac{B^2}{\rho^{(b)}}\mathcal{B}_k$$
$$+\frac{k}{S}c_s^2\mathcal{D}_k^{(b)} + \frac{2B^2}{3\rho^{(b)}}\left(\dot{v}_k^{(b)} + \frac{k}{S}a_k\right) + \frac{1}{3}\frac{k}{S}\frac{B^2}{\rho^{(b)}}\left(\frac{3k}{K^2}-1\right)\Pi_k$$
$$= -n_e\sigma_T\frac{\rho^{(\gamma)}}{\rho^{(b)}}\left(\frac{4}{3}v_k^{(b)} - q_k^{(\gamma)}\right). \tag{2.224}$$

- The anisotropic stresses:

$$\dot{\pi}_k^{(\gamma)} + \frac{3}{5}\frac{k}{S}\left(\frac{8K}{k^2}-1\right)J_k^{(3)} + \frac{2}{5}\frac{k}{S}q_k^{(\gamma)} + \frac{8}{15}\frac{k}{S}\sigma_k = -\frac{9}{10}n_e\sigma_T\pi_k^{(\gamma)}, \tag{2.225}$$

$$\dot{\pi}_k^{(\nu)} + \frac{3}{5}\frac{k}{S}\left(\frac{8K}{k^2}-1\right)J_k^{(3)} + \frac{2}{5}\frac{k}{S}q_k^{(\nu)} + \frac{8}{15}\frac{k}{S}\sigma_k = 0, \tag{2.226}$$

$$\dot{\Pi}_k + \frac{4}{3}\frac{k}{S}\sigma_k + \frac{4}{3}v_k^{(b)} = 0, \tag{2.227}$$

- The higher moments by

$$\dot{J}_k^{(l)} - \frac{k}{S}\left\{\frac{l+1}{2l+1}\left[1-l(l+2)\frac{K}{k^2}\right]J_k^{(l+1)} - \frac{l}{2l+1}J_k^{(l-1)}\right\} = -n_e\sigma_T J_k^{(l)}, \tag{2.228}$$

$$\dot{G}_k^{(l)} - \frac{k}{S}\left\{\frac{l+1}{2l+1}\left[1-l(l+2)\frac{K}{k^2}\right]G_k^{(l+1)} - \frac{l}{2l+1}G_k^{(l-1)}\right\} = 0. \tag{2.229}$$

- The electric part of the Weyl tensor and the shear:

$$\left(\frac{k}{S}\right)^2\left(\dot{\Phi}_k + \frac{1}{3}\Theta\Phi_k\right) + \frac{1}{2}\frac{k}{S}\kappa\rho\left[\left(1+w+\frac{2B^2}{3\rho}\right)\sigma_k + q_k^T\right]$$
$$-\frac{1}{6}\rho\Theta(3w+2)\pi_k + \frac{1}{2}\rho\dot{\pi}_k - \frac{B^2}{2}\Theta\Pi_k + \frac{B^2}{4}\dot{\Pi}_k = 0, \tag{2.230}$$

$$\left(\frac{k}{S}\right)\left(\dot{\sigma}_k + \frac{1}{3}\Theta\sigma_k\right) + \left(\frac{k}{S}\right)^2(\Phi_k - a_k) - \frac{1}{2}\kappa\rho\pi_k - \frac{B^2}{4}\Pi_k = 0. \tag{2.231}$$

- The constraints:

$$2\left(\frac{k}{S}\right)^3\left(1-\frac{3K}{k^2}\right)\Phi_k+\frac{k}{S}\kappa\rho\left[\mathcal{D}_k+\left(1-\frac{3K}{k^2}\right)\pi_k\right]$$
$$+\frac{k}{S}\frac{B^2}{2}\left[B_k+\left(1-\frac{3K}{k^2}\right)\Pi_k\right]-\kappa\rho\Theta q_k^T=0, \quad (2.232)$$
$$\frac{2}{3}\left(\frac{k}{S}\right)^2\left[\mathcal{Z}_k+\left(1-\frac{3K}{k^2}\right)\sigma_k\right]-\kappa\rho\Theta q_k^T=0. \quad (2.233)$$

2.6.2 Tensor modes

The tensor modes in covariant analysis are characterised by the vanishing of the vorticity and all vectors to first order [12, 14, 38]. This means that all fluids share effectively the same 4-velocity when one considers tensor modes. Also, only the transverse parts of the tensorial variables (the electric and magnetic parts of the Weyl tensor as well as the shear and the anisotropic stresses) are important, as

$$\tilde{\nabla}^a E_{ab}=0, \quad \tilde{\nabla}^a H_{ab}=0, \quad \tilde{\nabla}^a\sigma_{ab}=0, \quad \tilde{\nabla}^a\pi_{ab}^{(i)}=0. \quad (2.234)$$

With this restriction, the propagation equations for the dynamic variables reduce to

$$\dot{E}_{ab}+\Theta E_{ab}-\mathrm{curl}H_{ab}+\frac{1}{6}\left[3\rho\left(1+w+\frac{2B^2}{3\rho}\right)\sigma_{ab}\right.$$
$$\left.+3(\pi_{ab}+\Pi_{ab})^{\cdot}+\Theta(\pi_{ab}+\Pi_{ab})\right] = 0, \quad (2.235)$$
$$\dot{H}_{ab}+\Theta H_{ab}+\mathrm{curl}\left[E_{ab}-\frac{1}{2}(\pi_{ab}+\Pi_{ab})\right] = 0, \quad (2.236)$$
$$\dot{\sigma}_{ab}+\frac{2}{3}\Theta\sigma_{ab}+E_{ab}-\frac{1}{2}(\pi_{ab}+\Pi_{ab}) = 0, \quad (2.237)$$
$$\dot{\Theta}+\frac{1}{3}\Theta^2+\frac{\rho}{2}\left(1+3w+\frac{B^2}{\rho}\right) = 0, \quad (2.238)$$
$$\dot{\rho}+\Theta(\rho+p) = 0, \quad (2.239)$$
$$\dot{B}^2+\frac{4}{3}\Theta B^2 = 0. \quad (2.240)$$

Only one constraint equation remains:

$$H_{ab}-\mathrm{curl}\sigma_{ab} = 0. \quad (2.241)$$

The tensor harmonics must satisfy

$$\tilde{\nabla}^2 Q_{ab}^{(k)}=-\frac{k^2}{S^2}Q_{ab}^{(k)}, \quad (2.242)$$

at zero-order. By construction they satisfy the zero-order relations

$$\tilde{\nabla}^a Q_{ab}^{(k)}=0, \quad \dot{Q}_{ab}^{(k)}=0. \quad (2.243)$$

As with scalar harmonics, their spectrum changes depending on the choice of background. We define $\nu\equiv[(k^2+K)/|K|]^{1/2}$, which then leads to the spectrum

the spectrum of regular, normalisable solutions for open and flat backgrounds having $\nu \geq 0$, and closed models having the integral values $\nu \geq 3$. The mode label k is understood to distinguish degenerate solutions of the defining equation.

With scalar modes one may do much of ones analysis without actually choosing a specific representation for the harmonics. In the case of the tensors, however, it convenient to choose the representation early on. We follow Challinor [12] in our choice of representation. With this choice, there are two distinct parities in the harmonics, the electric and the magnetic. Label the magnetic parity with an overbar, one may decompose the tensor variables via:

$$E_{ab} = S^{-2}\sum_k k^2(E_k Q_{ab}^{(k)} + \bar{E}_k \bar{Q}_{ab}^{(k)}), \tag{2.244}$$

$$H_{ab} = S^{-2}\sum_k k^2(H_k Q_{ab}^{(k)} + \bar{H}_k \bar{Q}_{ab}^{(k)}), \tag{2.245}$$

$$\sigma_{ab} = S\sum_k k(\sigma_k Q_{ab}^{(k)} + \bar{\sigma}_k \bar{Q}_{ab}^{(k)}), \tag{2.246}$$

$$\pi_{ab}^{(i)} = \rho^{(i)}\sum_k (\pi_k^{(i)} Q_{ab}^{(k)} + \bar{\pi}_k^{(i)} \bar{Q}_{ab}^{(k)}). \tag{2.247}$$

$$\tag{2.248}$$

The specific representation has the identity

$$\mathrm{curl} Q_{ab}^{(k)} = \frac{k}{S}\left(1 + \frac{3K}{S^2}\right)^{1/2} \bar{Q}_{ab}^{(k)}. \tag{2.249}$$

relating the electric and magnetic parities.

With the above definitions and Eq. 2.249, the constraint reduces to

$$H_k = \left(1 + \frac{3K}{S^2}\right)^{1/2} \bar{\sigma}_k, \tag{2.250}$$

with a similar result for the magnetic parity. This allows one to decouple the electric and the magnetic parities, and allows one to eliminate H_{ab} from the discussion.

One now may obtain the propagation equations for the various mode expanded variables,

$$\frac{k^2}{S^2}\left(\dot{E}_k + \frac{1}{3}\Theta E_k\right) - \frac{k}{S}\left[\frac{k^2}{S^2} + \frac{3K}{S^2} - \frac{1}{2}\left(1 + w + \frac{2B^2}{3\rho}\right)\rho\right]\sigma_k = \frac{1}{6}\rho(3w+2)\Theta\pi_k - \frac{1}{2}\rho\dot{\pi}_k + \frac{B^2}{2}\Theta\Pi_k - \frac{1}{4}B^2\dot{\Pi}_k, \tag{2.251}$$

$$\frac{k}{S}\left(\dot{\sigma}_k + \frac{1}{3}\Theta\sigma_k\right) + \frac{k^2}{S^2}E_k = \frac{1}{2}\rho\pi_k + \frac{1}{4}B^2\Pi_k, \tag{2.252}$$

with similar results for the barred variables. The moments for the relativistic fluids obey:

$$\dot{I}_k^{(l)} + \frac{k}{S}\left[\frac{l}{2l+1}\kappa_l I_k^{(l-1)} - \frac{(l+3)(l-1)}{(l+1)(2l+1)}\kappa_{(l+1)} I_k^{(l+1)}\right] - \frac{8}{15}\frac{k}{S}\delta_{2k}\kappa_2\sigma_k = -n_e\sigma_T I_k^{(l)}, \tag{2.253}$$

where, of course, the collisional term is zero for the neutrino moments. The κ_l are constants defined by

$$\kappa_l \equiv \left[1 - (l^3 - 3)K/k^2\right]^{1/2}, \qquad l \geq 2. \tag{2.254}$$

The magnetic anisotropic stress evolves via:

$$\dot{\Pi}_k + \frac{4}{3}\frac{k}{S}\sigma_k = 0. \tag{2.255}$$

This then, along with the choice of an equation of state, gives a closed system for the evolution of tensor variables.

Chapter 3

Observations

Observations underpin the whole of Science. Without observation, there would be no check on the validity of scientific theory, and no clues as to how the theory should evolve. Cosmology is no exception in this regard. It is an "historical" science, in that one may not meaningfully talk about doing experiments – there is only one Universe wherefrom we may gather our results. In fact, it is only in the last twenty years that it has been possible to make observations of the principal cosmological variables with any real precision. In fact, perhaps the most precise physical measurement ever made, the measurement of the CMB black-body spectrum, is cosmological. The recent release of the WMAP results has provided estimates for the fundamental cosmological parameters to extraordinary precision [7]: the age of the universe is estimated at 13.7 $\pm$0.2 Gyr old, with the total mass-energy of the universe estimated at $\Omega_{\text{tot}} = 1.02 \pm 0.02$, suggesting that the universe is marginally closed. The data gives strong evidence for the existence of a cosmological constant, $\Omega_\Lambda = 0.70^{+0.07}_{-0.05}$. Assuming a flat universe, one finds the composition to be 4.4% baryons, 22% dark matter and 73% dark energy. The Hubble parameter is estimated at $h = 0.69 \pm 0.07$. This data is truly remarkable – until quit recently the Hubble parameter was only known to 20% accuracy!

3.1 The Cosmic Microwave Background Radiation

The Cosmic Microwave Background Radiation is perhaps the cleanest cosmological observable. Indeed, the observation of its blackbody spectrum by COBE in 1990 ushered in the era of "precision cosmology". The CMBR is extremely rich, allowing us to deduce many of the fundamentally important cosmological variables by measuring it. In order to understand how this may be done, we need to understand how the CMBR came about, and where its anisotropies come from.

3.1.1 The origin of the CMBR

As we look out into the universe, we are also looking back in time. This is because light travels at a finite constant speed in vacuum. We know that the

universe is expanding, and was originally much smaller and hotter. At some point in the past, then, it was hot enough to ionise hydrogen, which would then render the universe opaque. Due to the homogeneity and isotropy of the universe, this time would be roughly the same, no matter in which direction you look. Thus, at some redshift, we have an opaque sphere of ionised Hydrogen surrounding us. This is the CMBR.

It is not the CMBR itself that provides the most important information, but rather the small anisotropies present in it. One may divide the cause of these anisotropies into three main classes [55]:

- **Sachs-Wolfe effect**
  This is caused by photons climbing out of an overdensity in the universe (a gravitational well) which causes a change of temperature of

$$\frac{\delta T}{T} = \frac{\delta \Phi}{c^2}, \tag{3.1}$$

  where Φ is the change in the Newtonian potential. However, due to time-dilation, one is looking at a younger, and hence hotter, universe in the region of overdensity, correcting the effect to:

$$\frac{\delta T}{T} = \frac{\delta \Phi}{3c^2}. \tag{3.2}$$

  This effects dominates on angular scales larger than about 2°.

- **Doppler effect**
  The photon-baryon fluid undergoes acoustic oscillations during and shortly before recombination. This motion of the bulk plasma means that photons scattered off it suffer a Doppler effect leading to a change of

$$\frac{\delta T}{T} = \frac{\mathbf{v} \cdot \hat{\mathbf{r}}}{c}, \tag{3.3}$$

  with $\mathbf{v}$ the plasma velocity, and $\hat{\mathbf{r}}$ the photon direction.

- **Adiabatic effect**
  The compression and rarefaction undergone by the oscillating plasma resp. heats and cools the oscillating plasma. This leads to the temperature change:

$$\frac{\delta T}{T} = \frac{1}{3}\frac{\delta \rho^{(b)}}{\rho^{(b)}}. \tag{3.4}$$

The last two effects (Doppler and adiabatic) dominate at scales less than 2° and are clearly linked to the acoustic oscillations. The wavelength of these oscillations is determined by the sound speed,

$$c_s^2 = c^2 \left(3 + \frac{9\rho^{(b)}}{4\rho^{(\gamma)}}\right). \tag{3.5}$$

Working in Fourier space, and changing to conformal time, one may show that

$$\left.\frac{\delta \rho^{(\gamma)}}{\rho^{(\gamma)}}\right|_{\text{scale } k} \sim \cos(k c_s \eta_{rec}), \tag{3.6}$$

where η_{rec} is the conformal time of recombination. We see that this is periodic in k.

Inflation only produces fluctuations in the growing mode, eventually leading to the fluctuations at a given k being coherent, giving a set of oscillations in the power spectrum.

In order to obtain the power spectrum, we measure the CMB over the whole sky (in principle), and decompose it into spherical harmonics:

$$\frac{\delta T}{T}(\theta, \phi) = \sum_{l,m} a_{lm} Y_{lm}(\theta, \phi), \tag{3.7}$$

from which one obtains the power spectrum:

$$C_l = \langle |a_{lm}|^2 \rangle. \tag{3.8}$$

In fact, one usually plots $l(l+1)C_l$ which is the power per unit log interval in l.

Lengths at recombination get translated to an angle on the sky vial the angular diameter distance formula, which is mainly a function of Ω_{total}. Thus the position of the peaks (which come from the physical distance $\cos(kc_s\eta_{rec})$) as a function of l are a sensitive indicator of the total energy in the universe.

Two further parameters are important for observation: n, the slope of the primordial power-law power spectrum, defined via

$$\langle |\delta_k|^2 \rangle \propto k^n, \tag{3.9}$$

and the ratio of tensor to scalar perturbations (inflation predicts that vector perturbations will be very small). Inflation usually predicts $n \approx 1$.

One may do a detailed fitting of the major parameters to the observations given a particular model. These measurements usually need to be complemented with secondary measurements (for instance, supernova measurements), as there is degeneracy in some of the parameters. None the less, the CMB measurements allow us to deduce the values of the cosmological parameters to unprecedented accuracy.

3.1.2 Contaminants

The detection of CMB anisotropies to the order of $\Delta T/T \sim 10^{-5}$ is beset with a wide range of difficulties. A major problem is contamination by foregrounds. The components of the contamination that are most interesting are:

- **Galactic dust emission**
  This is important at high frequencies (typically larger than 100 GHz).
- **Galactic thermal (free-free) emission**
  Thermal emission and non-thermal (synchrotron) radiation are important at frequencies lower than $\sim$ 30 GHz.
- **Atmospheric emission**
  This is the dominant contribution in ground and balloon based experiments.
- **"Spinning dust"**
  This is important in the range 10-100 GHz.

The most obvious method of avoiding these contaminants is running the experiment at a frequency where the contaminants are kept low. In the window of frequencies between ~ 10 and ~ 40 GHz both atmospheric and Galactic emissions should be dominated by CMB emission. However, in order reach sufficient accuracy it is necessary to perform spectral discrimination of foregrounds using multi-frequency data. This takes the form of either closely spaced samples for accurate discrimination of the foreground, or a wide set of samples to give a good 'lever-arm' in spectral discrimination.

There are three principal methods to avoid atmospheric contamination (apart from moving the detector out of the atmosphere):

- **The switched beam method**
  Here the telescope switches rapidly between two or more beams so that a differential measurement may be made between two different parts of the sky, allowing one to filter out atmospheric variation.

- **Scanned beam methods**
  Here the telescope has a single receiver with a continuously moving mirror allowing different parts of the sky to be scanned. A computer may re-synthesise the motion of the mirror. This method provides greater flexibility at angular scale measurements.

- **Interferometric measurements**
  Here, output measurements of each baseline horn are cross-correlated so that the Fourier components of the sky can be measured. In this fashion the atmospheric component can be efficiently removed, allowing a clean CMB map to be re-constructed. Furthermore, the beams are electronically synthesised, so that they have lower levels of sidelobe pickup, and better rejection of systematics.

3.2 Magnetic fields in the universe[1]

Magnetic fields are ubiquitous. They have been observed from the very small scales to the very large. We see magnetic fields in stars, galaxies, clusters of galaxies and in high redshift objects.

3.2.1 Observing magnetic fields in a cosmological setting

The principal means by which magnetic fields are observed at astronomical scales are:

- The Zeeman effect, whereby spectral lines emitted are split into a number of closely spaced lines by a strong magnetic field.

- The intensity and polarisation of synchrotron emission from free relativistic electrons, whereby the electrons emit radiation while being forced to move in curved paths due to the presence of a magnetic field.

- Faraday rotation measurements (RMs) of polarised electromagnetic radiation passing through an ionised medium. The magnetic field in the

[1] This section owes a great deal to the detailed review of Grasso and Rubenstein [35].

direction of propagating of the radiation causes a rotation in its plane of vibration.

Though a direct measurement of the strength of a magnetic field, Zeeman splitting is typically too small to be useful outside our galaxy. The other techniques, unfortunately, suffer from the necessity to determine n_e, the local electron density, independently. This is often extremely difficult, especially for very rarefied media. This makes measurements of the intergalactic medium very difficult. With synchrotron emission, the intensity is proportional to $n_e B^2$. This leads researchers sometimes to estimate B by assuming equipartition of energy between the magnetic field and plasma energy densities.

Faraday rotation is always used for observation of distant objects. The agreement between RMs and those inferred from synchrotron emission for nearby sources give confidence to the measurements of distance objects using the former method. However RM requires knowledge of the electron column and possible field reversals, which, while obtainable for nearby objects through pulsar frequency and their delays, are difficult to determine for distant measurements. This makes determining the magnetic field of the intergalactic medium via RMs quite hard, so that only model upper limits are available.

3.2.2 Current observations

Galaxies

The magnetic field in the interstellar medium of the Milky Way has been determined using several methods. The average field strength is $3 - 4\mu$G, which corresponds to an approximate equipartition of energy between the magnetic field, the small-scale turbulent motion, and the cosmic rays confined to the Galaxy – $\rho_m \approx \rho_{CR} \approx \rho_t$. This energy density almost coincides with that of the CMBR. The orientation of the field is maintained on scales of the order of a few kiloparsecs (comparable to the size of the galaxy) and two reversals have been observed between the galactic arms. This suggests a symmetric configuration of the field morphology.

Similar strength fields have been observed in other spiral galaxies, but while some (like M33) seem to share the property of equipartition of energy, others seem to have a field that is too strong for this. The field morphology also seems to vary from galaxy to galaxy, with some showing axially symmetric geometry, others symmetric geometry, and some with no discernible field structure [35, 86].

Galaxy clusters

The observations on a large number of Abel clusters [46], some of which are known to be x-ray sources (which allow independent determination of n_e), give insight to the strength of magnetic fields in galaxy clusters. The phenomenological equation:

$$B_{ICM} \sim 2\,\mu G \left(\frac{L}{10kpc}\right)^{-\frac{1}{2}} (h_{50})^{-1}, \tag{3.10}$$

with L the reversal field length and h_{50} the reduced Hubble constant, describes the magnetic field strength of the intercluster medium (ICM) well. Typical values for L are $10 - 100$ kpc, to give corresponding field strengths of $1 - 10$

μG. The Coma cluster [33] provides a concrete example, with a core magnetic field of $B \sim 8.3 h_{100}^{\frac{1}{2}}$G tangled at scales of about 1 kpc. Some clusters can have quite strong magnetic fields; RMs show the Hydra A cluster to have a 6μG field coherent over 100 kpc, superimposed with a tangled field with a strength of approximately 6μG [78].

The magnetic field strength at the centre of these clusters can be far higher. High resolution images of radio sources embedded in galaxy clusters show that the central regions have a typical field strength $\sim 10 - 30$ μG with peak values of ~ 70 μG[21]. For such large fields the magnetic pressure exceeds the gas pressure derived form X-ray data. Indeed, the discrepancy between the estimate of the mass of the Abel cluster 2218 derived from gravitational lensing and that derived from X-ray measurements [57] may be well explained by magnetic field strengths ~ 50 μG [35].

The cause of the apparent decrease in the field strength away from the centre of the clusters is still not clear; whilst it may be due to the intrinsic field structure, it is also possible that it is merely due to the decrease of gas density. Observations show that the field may have a filamentary structure, where the filaments, according to [21], should be structured as a flux rope – the field lies along the central axis, becoming helical as it moves away.

These observations make it plausible that magnetic fields exist in all galactic clusters, which then raises severe problems for the theories of magnetogenesis.

High redshift objects

The most significant measurements of high redshift objects are high resolution RMs of very far quasars by Kronberg *et al.* [51]. These allow one to probe magnetic fields in the early past. The magnetic field strength of a relatively young spiral galaxy at redshift $z = 0.395$ was determined by RMs of the quasar PKS 1229-021, which lies behind the galaxy at redshift $z = 1.038$, to be in the range $1 - 4$ μG. Interestingly, the galaxy was determined to field reversals were observed at a scale roughly consistent with the spiral arm separation, as our Milky Way has.

RMs of the radio emissions of the quasar 3C191, at a redshift of $z = 1.945$, thought to be due to a magnetised gas at the same distance, are consistent with a field strength of $0.4 - 4$ μG.

Intergalactic magnetic fields

The rarefied nature of the intergalactic medium (IGM) makes it difficult to make any meaningful RMs. However, using reasonable assumptions on the value of the magnetic coherence length and well known estimates of the Universe ionisation fraction allows one to limit this field. For instance, if one takes the unlikely case of a field aligned on cosmological scales, with the additional assumptions of $\Lambda = 0$, $\Omega = 1$, and $H = 0.75$, RMs of distant quasars limit $B_{IGM} \lesssim 10^{-11}$G [51]. Adopting the more realistic reversal scale of 1 Mpc (the largest scale at which reversals are observed in galaxy clusters) allows Kronberg to give the less stringent limit of $B_{IGM} \lesssim 10^{-9}$ at the present time.

3.2.3 Magnetogenesis

The ubiquity of magnetic fields raises natural questions as to their origin, which have yet to be settled. Two main theories purport to explain the origin of these magnetic fields in galaxies:

The galactic dynamo This is the oldest theory of magnetogenesis, whereby a rotating galaxy is seen as a giant dynamo generating the field. The dynamo mechanism takes place when the first term in the propagation equation for the magnetic field:

$$\frac{\partial \mathbf{B}}{\partial t} = \nabla \times (\mathbf{v} \times \mathbf{B}) + \frac{1}{4\pi\sigma}\nabla^2 \mathbf{B}, \tag{3.11}$$

where σ is the electric conductivity, dominates the second term (called the frozen-in limit). This equation clearly shows that the existence of an initial seed field is crucial to the process. Three other elements are crucial to the process: hydrodynamic turbulence, differential rotation and fast recombination of field lines. The turbulent motion stretches and distorts the magnetic field lines in the frozen-in limit. It can be shown that this stretching of the field lines results in the increase of B. However, this effect alone is not sufficient to explain the exponential amplification required for the dynamo theory to be successful. This exponential amplification is obtained by noting that the turbulent motion can cause twisting of closed flux tube, and then put the ends together, resulting in the original single-loop configuration but with double the flux. This process may be repeated n times, to give a 2^n-fold strengthening of the field. The gluing together of the ends requires a change in the field line topology, which may only happen in the presence of a small finite resistivity. This doubling is a small-scale process (in regions of small extension the field is more tangled and the diffusion times smaller) causing the magnetic configuration to evolve local tangled structures to a mean ordered structure. In fact, one of the main predictions of the galactic dynamo model is the generation of an axially symmetric mean field.

A general prediction of the theory is that the dynamo amplification will stop when an approximate equipartition of energy between the magnetic field and small scale turbulence is reached, corresponding to magnetic energy densities of $2 - 8\ \mu$G. The time to reach this equipartition, starting from seed fields with intensities as low as 10^{-20}G, may be $10^8 - 10^9$ years. This estimation holds under the assumption of a CDM dominated universe with vanishing cosmological constant. In the presence of a cosmological constant the dynamo has more time available for amplification, and the seed field intensity may be as small as 10^{-30} G.

Primordial field amplification The main alternative to the galactic dynamo is the assumption that galactic fields result from a primordial field which gets adiabatically compressed with the collapse of the protogalactic cloud. Due to the high conductivity of the intergalactic medium magnetic flux is conserved, implying that the magnetic field strength increases with the square of the size of the system so that

$$B_{prim} = B_{gal}\left(\frac{\rho_{cosmic}}{\rho_{gal}}\right)^{2/3}. \tag{3.12}$$

Since, at present, $\rho_{IGM}/\rho_{gal} \simeq 10^{-6}$, and $B_{gal} = 10^{-6}$ G, the required strength of the primordial magnetic field at the time of galaxy formation, $z \sim 5$, adiabatically rescaled to the present time, is

$$B_{prim} \simeq 10^{-10} \text{ G}. \tag{3.13}$$

The theory predicts that the field should be wrapped into a symmetric spiral with a field reversal along the galactic disk diameter, and no reversal across the galactic plane.

The galactic dynamo has become unfashionable due to criticism levelled at it resulting from improved theoretical work. Its detractors point out that the theory ignores the strong amplification of small-scale magnetic fields which might reach equipartition long before a coherent field is developed.

Observationally, there are three main ways to decide between the theories:

- the observation of intensity and spatial distribution of galactic magnetic fields,
- the observation of intensity and spatial distribution of intergalactic magnetic fields,
- the observation of magnetic fields at high redshifts.

As noted, observations of the intensity of the magnetic fields of some galaxies show evidence of equipartition of energy between the magnetic field and the small scale turbulent motion supporting dynamo theories. However, other galaxies, such as the M82 galaxy in the Magellanic Clouds, have magnetic fields that are far stronger than the equipartition field. Some spiral galaxies, like our own, have been seen to have field reversals, supporting primordial field theories. However other galaxies, like M31 and IC342, show no field reversal. At present the number of observations is so small that any statistical inferences would be premature [86].

The origin of the magnetic fields in the intercluster medium is even more mysterious. They are far to strong to explain simply by means of ejection of galactic magnetic fields. Some theorists postulate some kind of dynamo mechanism produced by the turbulent wakes of galaxies, but this has been criticised by others. Kronberg [51] asserts that the independence of field strength from the local matter density suggests that the galactic systems evolved in an environment with $B \gtrsim 1\mu$G.

All of these theories require a seed field prior to galaxy formation. While there are several mechanisms where this field might have been generated pre-recombination, one may also envision scenarios where they might have been generated afterwards. One such alternative is the Biermann battery effect [8] which may produce seed fields which are amplified at a galactic scale by a dynamo powered by turbulence in the protogalactic cloud [52, 54]. However, this mechanism fails to account for the observed fields in galaxy clusters.

If magnetic fields existed prior to recombination, it would be reasonable to expect some imprint of them in the CMB power-spectrum. Indeed, one might hope to place bounds on such a primordial field via measurements of the power spectrum. The next section deals with possible imprints of primordial magnetic fields on the CMB power spectrum.

3.2.4 Magnetic imprints in the CMB power spectrum

The presence of magnetic fields prior to photon/baryon decoupling may be expected to leave an imprint on the CMB. This the CMB power might allow one constrain early time magnetic fields. Here the known effects of magnetic fields on the CMB are described, along with such constraints as current observations of the CMB have placed on magnetic field strengths prior to decoupling.

Homogeneous magnetic fields

Large scale homogeneous magnetic fields break the isotropy of the universe, inducing a preferred direction. Indeed, as we have seen in earlier sections, the magnetic field acts like an imperfect fluid with "negative" pressure along the field direction. Zeldovich and Novikov [85] calculated such a field having a strength today of $10^{-9} \pm 10^{-10}$ Gauss would induce a temperature anisotropy $\delta T/T \lesssim 10^{-6}$. This analysis was updated by Barrow, Ferreira and Silk [5] to place an upper limit on the field strength on the basis of the COBE microwave background anisotropy measurements. The limit

$$B(t_0) < 3.5 \times 10^{-9} f^{1/2} (\Omega_0 h_{50}^2)^{1/2} \, \mathrm{G} \tag{3.14}$$

was thus obtained. Here f is an $O(1)$ shape factor accounting for possible non-Gaussian characteristics of the COBE data set. This shows that even without dynamo amplification COBE data is not inconsistent with magnetic fields observed today.

Magnetic field effects at small angular scales

While the anisotropy resulting in the above discussion is essentially acausal in nature, at small angular scales ($< 1°$) the anisotropies are caused by causal physical mechanisms. As described in the section on the origin of CMB anisotropies, primordial density fluctuations give rise to acoustic oscillations in the plasma when they enter the horizon some time before last scattering. These then produce temperature fluctuations in the plasma, induce velocity Doppler shifts in the photons, and gravitational Doppler shifts in photons climbing out of over dense regions.

These acoustic oscillations are well described by standard fluid dynamics in the linear regime. The presence of a magnetic field allows plasma dynamics to be radically altered as Magneto-Hydro-Dynamics (MHD) has to be taken into account.

The simplest situation is to consider a single component plasma, and neglect any dissipative effect (for example, heat conductivity, or viscosity). If one assumes the magnetic field $\mathbf{B}_0$ is homogeneous on scales larger than the plasma oscillation wavelength, one may treat the background field as a uniform field in the equations. Performing this analysis one sees that in addition to the ordinary sound waves involving density fluctuations, the magnetic field allows three new kinds of solutions ([1, 2, 45]):

- *Fast Magnetosonic Waves*
  These approach ordinary sound waves in the limit of small magnetic field, and involve fluctuations in the velocity, density, magnetic, and gravitational field. The velocity and density fluctuations are out of phase by $\pi/2$.

They waves travel at a velocity

$$c_+^2 \sim c_s^2 + v_A^2 \sin^2\theta, \tag{3.15}$$

where θ is the angle between the wave propagation direction and the magnetic field,

$$v_A^2 \sim \frac{B_0^2}{\rho} \tag{3.16}$$

is the Alfvén velocity, and c_s is the ordinary sound speed (in the absence of the magnetic field). This is only valid for $v_A \ll c_s$, and for such fields, the waves are approximately longitudinal.

- *Slow Magnetosonic Waves*
  These waves also involve fluctuations in the velocity and density. In contrast to the fast magnetosonic waves, these waves fluctuate both transversally and longitudinally even for small fields. Their velocity is approximately
  $$c_-^2 \sim v_A^2 \cos^2\theta. \tag{3.17}$$

- *Alfvén Waves*
  These waves contrast to the magnetosonic waves, in that they are purely rotational, involving no density fluctuations. They are linearly polarised, and propagate at
  $$c_A^2 = v_A^2 \cos^2\theta. \tag{3.18}$$

Adams et al. [1] were the first to investigate the possible effects of MHD waves on the temperature anisotropies. In the simple case of magnetosonic waves, they found that in the tight-coupling limit the effect of the field could be somewhat mimicked by a variation of the baryon density. However, the amplitude of the fast waves depends on the angle between the wave-vector and the magnetic field. As the magnetic field is assumed to change at scales larger than the scale of the fluctuations, different patches of the sky might show different fluctuation spectra depending on the angle. By performing all sky averaging, summing also over the angle of the field and the line of sight, the authors were able to determine the effect on the temperature power spectrum. They found that a magnetic field had a tendency to reduce the amplitude of the first peak with respect to the free field case, as the magnetic field pressure opposes the in-fall of the photon-baryon fluid into the potential well of the fluctuations. The magnetic field also yielded a subtle shift of the position of the peaks. These effects together allowed them to conclude that magnetic fields with a strength today $> 5 \times 10^{-8}$ should be detectable by the upcoming PLANCK satellite.

While it is difficult to disentangle the signature of the magnetosonic waves on the CMBR, the signature that Alfvén waves may leave is quite peculiar, due to the fact that they involve only rotational fluctuations, without fluctuations in density. Indeed, as the density does not change, the velocity Doppler shift would not be cancelled by the gravitational redshift, which could provide a clear signature of magnetic fields at last scattering [1].

Alfvén waves are interesting for a further reason in that they are vector perturbations. Whereas vector perturbations are suppressed by expansion and do not arise from small deviations from FLRW, this is not true for magnetic fields.

Thus Alfvén waves are well suited to probe more unusual initial conditions, such as those generated from primordial phase transitions.

As will be discussed in the next section, Alfvén waves also suffer less from dissipation than magnetosonic waves do. Subramanian and Barrow [75] and Durrer et al. [17] both did a detailed investigation of the effects Alfvén waves leave on the CMB. They found that these waves produce Doppler peaks with a period determined by the Alfvén velocity. However, for reasonable values of the magnetic field strength the Alfvén velocity is very small, these would be quite difficult to detect.

However, Durrer et al. argued that the presence of Alfvén modes would lead to a phenomenologically interesting effect on the statistical properties of the CMB anisotropies. If one decomposes the temperature anisotropies using the usual spherical harmonic decomposition, the C_l's are just $C_l = \langle a_{lm} a^*_{lm} \rangle$. However, the spin-1 nature of vorticity perturbations introduces phase transitions $l \to l \pm 1$ introducing a corelation between the $a_{l+1,m}$ and $a_{l-1,m}$ harmonics, which would be measured by

$$D_l(m) = \langle a_{l-1,m} a^*_{l+1,m} \rangle = \langle a_{l+1,m} a^*_{l-1,m} \rangle. \tag{3.19}$$

Durrer et al. determined the form of the C_l and D_l coefficients for the case of a homogeneous magnetic field with a spectral index in the range $(-7, -1)$, and, on comparing their results with the COBE data, determined a limit on the magnetic field amplitude of the order $(2 - 7) \times 10^{-9}$ Gauss.

MHD modes in the presence of dissipation

In the previous section dissipative effects were assumed negligible. Jedamzik et al. [42] were the first to study the effects of dissipation of MHD perturbation modes. It was shown [42, 76] that the dissipation of MHD modes produce an effective damping of inhomogeneous magnetic fields.

In the absence of a magnetic field acoustic density fluctuations are effectively damped in the diffusive regime due to viscosity and heat conductivity (Silk damping). At recombination, this dissipation occurs for modes smaller than the approximate photon diffusion length, $d_\gamma \sim (l_\gamma t_H)^{1/2}$, with l_γ the photon mean free path. Fast magnetosonic waves are damped in a very similar manner, with the dissipation scale coinciding with the Silk length scale. However, Alfvén and slow magnetosonic waves are damped quite differently. Indeed, the Alfvén waves may become overdamped when the photon mean free path becomes large enough for dissipative effects to overcome oscillation. The strong viscosity prevents fluid acceleration by magnetic forces, and thus damping is quite inefficient for non-oscillating Alfvén modes with

$$\lambda \leq \lambda_{od} \simeq \frac{2\pi l_\gamma(T)}{v_A \cos\theta}. \tag{3.20}$$

The damping scale for Alfvén modes is thus much smaller than that for sound and fast magnetosonic modes, by a factor $L_A \sim v_A \cos\theta d_\gamma$. It follows that for the discussion in the previous section to be valid, the magnetic field must have a coherence length less than the co-moving Silk damping scale ($L_S \sim 10$ Mpc) for fast magnetosonic waves, and greater than L_A for Alfvén waves.

Further interesting work was done by Jedamzik et al. [43]. They reasoned that the dissipation of tangled magnetic fields before recombination would lead

to a nonthermal injection of energy into the heat-bath distorting the CMB power spectrum. With this reasoning, and using the COBE/FIRAS data, they were able to exclude primordial magnetic fields with strength $\gtrsim 3 \times 10^{-8}$ G and co-moving coherence length ~ 400 pc. On scales of ~ 0.6 Mpc, the COBE data disallows magnetic fields of strength $\gtrsim 3 \times 10^{-8}$ Gauss, by similar reasoning.

Polarisation effects

As noted in Ch. 2, Thomson scattering naturally creates CMB polarisation. All that is required is for the photon distribution function to have a quadrupole anisotropy, as seen by the electrons. This can not occur in the tight coupling regime, wherein the development of anisotropy in the baryon rest frame is prevented, however, near decoupling, where the photons begin to free-stream, quadrupole anisotropies may develop in the photon distribution function, sourcing a space dependent polarisation. Thus temperature and polarisation anisotropies are expected to be coupled.

Kosowsky and Loeb [50] noticed that a magnetic field could induce a sizeable Faraday rotation in the CMB. The rotation depends both on the magnetic field strength and on the free electron density, and although the former is expected to be larger at early times, the latter drops to negligible values as recombination ends. Thus rotation may only be generated in the brief time where photons and electrons have started to decouple, but have not yet done so to the point where Faraday rotation ceases. Kosowsky and Loeb found that under the assumption of a uniform magnetic field at the co-moving scale of ~ 5 Mpc, a primordial field of $B_0 \sim 10^{-9}$ Gauss would result in rotation of the order of 280 rad m^{-2}, which would in principal be detectable by the PLANCK experiment.

Scannapieco and Ferreira [67] examined how a magnetic field would affect the correlation of temperature and polarisation anisotropies. It is usual to separate the polarisation patterns on the sky into "electric" (E) and "magnetic" (B) parities, the E-mode having $(-1)^l$ parity on the sphere, and the B-mode $(-1)^{l+1}$. Isotropy forbids cross correlation between E and B modes, as this would imply parity violation. However, the magnetic field is maximally parity violating, and therefore may produce cross correlation, revealing their presence. The authors concluded that this cross-correlation would render fields with strengths as low as 10^{-9} detectable by the PLANCK satellite. Only the case of a uniform field was considered, but many of the key ideas should carry through to fields with finite coherence length.

Faraday rotation may also affect the temperature anisotropy via a back-reaction of the radiation depolarisation inducing a larger photon diffusion length, and thus reducing viscous damping of temperature anisotropies. Harari, Hayward, and Zaldarriaga [36] considered this effect, and showed that on small angular scales ($l \simeq 1000$) the magnetic field tends to increase the temperature anisotropy. They calculate that both MAP and PLANCK should be sensitive to magnetic fields at a level of about $B_0 = 10^{-7}$ Gauss, which is comparable to the BBN limit.

Stochastic magnetic fields

Recently various authors have considered primordial magnetic fields that are stochastic in nature [18, 44, 48, 75, 77, 62]. These are argued to be more realistic

as any causal mechanism results in such fields. In this approach the magnetic field is modelled as a statistically homogeneous and isotropic magnetic field, so that in Fourier space

$$\langle B_i(\mathbf{k}) B_j^*(\mathbf{q}) \rangle = \delta^3(\mathbf{k}-\mathbf{q})(\delta_{ij} - \hat{k}_i \hat{k}_j) B^2(k), \tag{3.21}$$

where $\mathbf{k}$ is the mode vector. The magnetic spectrum $B(k)$ is assumed to be approximated by a simple power law $B(k) \propto k^n$ up to some cut-off frequency k_c, the scale at which modes are exponentially damped. Durrer et al. [18] argue that for causally generated magnetic fields, n must be a strictly positive even number. At any rate, $n > -3$ in order to avoid over-production of long-range coherent magnetic fields.

Koh and Lee [48] examine scalar stochastic perturbations. They are not overly concerned with the mechanisms whereby the field is generated, and simply assume it appears instantaneously at some time. They assume the usual power-law form, with spectral index larger than -3, and

cut-off k_c. They calculated power spectra for both temperature and polarisation, finding that the presence of a magnetic field tended to shift the peaks up. They found that the spectrum curves depended strongly on the cut-off frequency – larger cut-off frequencies having greater effect. Increasing the spectral index was found to decrease the impact of the magnetic fields on the spectrum. The authors ignore the effect of Faraday rotation on the polarisation spectrum. They conclude that fields needed be at least of the order of 10^{-8} Gauss to have an appreciable effect on the spectra.

Subramanian and Barrow [75, 77] explore how stochastic fields create vorticial, or vector, perturbations that may survive Silk damping. These modes would then presumably have an important contribution to the CMB spectrum at small angular scales, where other modes would be damped out. As is usual, they assume a power-law spectrum in their calculations. They find that a scale-invariant spectrum which red-shifts to $B_0 = 3 \times 10^{-9}$ at present should yield temperature anisotropies of the order of 10μK between $l \sim 1000 - 3000$. Λ-dominated universes, and steeper spectra, or universes with a larger baryon density all produce larger signals.

In a series of papers Durrer and co-workers [18, 44, 62] explore the effects of stochastic magnetic fields on the tensor and vector contributions to the CMB power spectrum. Assuming that the field has a power-law spectrum with a cut-off, they are able to derive analytic expressions for the power spectra. For the tensors, they found that the field induces a scale invariant spectrum as the index approaches -3. For such spectra, they deduce a constraint of order 10^{-9} Gauss. For initial spectra with index n, they found that the field averaged over the the co-moving length scale $10h^{-1}$ Mpc, B_λ is constrained by $B_\lambda < 7.9 \times 10^{-6} e^{3n}$ Gauss for $n < -3/2$, and $B_\lambda < 9.5 \times 10^{-8} e^{0.36n}$ Gauss for $n > -3/2$. Taking into account vector perturbations, and calculating the effect both on temperature and polarisation spectra, Mack et al. [62] expect the MAP satellite to be able to constrain fields to be no greater than $\sim \times 10^{-9}$ G, and strengthen the constraint to 4×10^{-13} G if the fields are generated causally.

In [77], Subramanian and Barrow compare their estimates to those of Durrer et al. [18, 44, 62] if magnetic effects are detected at high l, then the expressions for the tensor power spectra derived in [18, 62] show that the magnetic field would lead to perturbations of the order of 10% for $l < 100$, and thus their effects at large angular scales would need to be taken seriously.

Chapter 4

Scalar perturbations in the presence of a magnetic field

In this chapter we are going to present analytic results on the nature of scalar perturbations in the presence of a magnetic field. In order for this to be possible we will use a simple two-fluid model, the fluids being radiation and magnetised dust[1]. Our analysis will follow that of Padmanabhan [64], who performs this analysis for non-magnetised dust.

For our analysis it is convenient to adopt the energy frame. This is defined as the frame in which the total flux is zero. We follow the approximation scheme outlined in Sec. 2.4.2. This leads to the equation for conservation of total momentum:

$$\rho\left(1+w+\frac{2B^2}{3\rho}\right) = -\frac{\rho^{(\gamma)}}{S}\mathcal{D}_a + \frac{2}{S}\mathcal{B}_{[ab]}B^b, \tag{4.1}$$

where

$$\mathcal{B}_{ab} = S\tilde{\nabla}_b B_a. \tag{4.2}$$

This allows us to write the evolution equation for the gradient of the expansion as

$$\begin{aligned}\dot{\mathcal{Z}}_a &= -2H\mathcal{Z}_a - \frac{1}{2}\rho\mathcal{D}_a - \frac{1}{2}B^2\mathcal{B}_a - 3\mathcal{B}_{[ab]}B^b - \frac{1}{3}\frac{\rho^{(\gamma)}}{\rho}\frac{1}{\left(1+w+\frac{2B^2}{3\rho}\right)}\tilde{\nabla}^2\mathcal{D}_a^{(\gamma)} \\ &\quad -\frac{1}{2}\frac{B^2}{\rho}\frac{1}{\left(1+w+\frac{2B^2}{3\rho}\right)}\tilde{\nabla}^2\mathcal{B}_a + \frac{2}{3}\frac{B^2}{\rho}\frac{1}{\left(1+w+\frac{2B^2}{3\rho}\right)}\rho\mathcal{D}_a \\ &\quad -\left[\frac{6c_s^2(1+w)}{\left(1+w+\frac{2B^2}{3\rho}\right)} + 4\frac{B^2}{\rho}\frac{1}{\left(1+w+\frac{2B^2}{3\rho}\right)}\right]SH\tilde{\nabla}^b\omega_{ab} \\ &\quad -\frac{4}{3}\frac{B^2}{\rho}\frac{1}{\left(1+w+\frac{2B^2}{3\rho}\right)}H\mathcal{Z}_a,\end{aligned} \tag{4.3}$$

[1] In this section, the superscript "(γ)" refers to the radiation fluid, and "(b)" to the dust. Total variables, like ρ, w, $\mathcal{D}_a$ refer to the total contribution of the dust and radiation fluid, and exclude the contribution of the magnetic fluid. Each fluid is considered to be perfect.

and that for the co-moving spatial gradient of the total energy density as

$$\rho\dot{\mathcal{D}}_a + \rho(1+w)\mathcal{Z}_a - 3Hw\mathcal{D}_a + \frac{6H}{\rho}\mathcal{B}_{[ab]}B^b - 2aH\frac{B^2}{\rho}a_a = 0. \tag{4.4}$$

The individual fluid components will in general move relative to the energy frame, and have their own peculiar velocities. The magnetic field is frozen into the dust, and only the total (magnetised dust) energy-momentum is conserved. However, as magnetic energy densities are identically conserved, the dust energy density is conserved. Thus, the equations for the co-moving gradients of the individual energy densities are, for the dust:

$$\dot{\mathcal{D}}_a^{(b)} + \mathcal{Z}_a + 3SHa_a + S\tilde{\nabla}_a \mathrm{div}v^{(b)} = 0, \tag{4.5}$$

and for the radiation

$$\dot{\mathcal{D}}_a^{(\gamma)} + \frac{4}{3}\mathcal{Z}_a + 4SHa_a + \frac{4}{3}S\tilde{\nabla}_a \mathrm{div}v^{(\gamma)} = 0. \tag{4.6}$$

The momentum conservation equation for the magnetised dust is:

$$\dot{v}_a^{(b)} = \left(3c_{s(T)}^2 - 1\right)Hv_a^{(b)} - a_a + \frac{2}{S}\frac{1}{\rho^{(b)}\left(1+\frac{2B^2}{3\rho^{(b)}}\right)}\mathcal{B}_{[ab]}B^b, \tag{4.7}$$

and for the radiation:

$$\dot{v}_a^{(\gamma)} = \left(3c_{s(\gamma)}^2 - 1\right)Hv_a^{(\gamma)} - a_a + \frac{4}{S}\mathcal{D}_a^{(\gamma)}. \tag{4.8}$$

Here $c_{s(\gamma)}^2 = 1/3$ is the sound speed of the radiation, and

$$c_{s(T)}^2 = \frac{1}{3}\frac{B^2}{B^2 + \frac{3}{2}\rho^{(b)}} \tag{4.9}$$

is the sound speed of the magnetised dust.

We follow Dunsby et al. [15] in defining the difference variables

$$\mathcal{S}_a^{(b\gamma)} = \frac{1}{1+w^{(b)}}\mathcal{D}_a^{(b)} - \frac{1}{1+w^{(\gamma)}}\mathcal{D}_a^{(\gamma)} = \mathcal{D}_a^{(b)} - \frac{3}{4}\mathcal{D}_a^{(\gamma)}, \tag{4.10}$$

$$v_a^{(b\gamma)} = v^{(b)} - v^{(\gamma)}. \tag{4.11}$$

The propagation equation for $\mathcal{S}_a^{(b\gamma)}$ can be derived from Eqs 4.5 and 4.6, giving:

$$\dot{\mathcal{S}}_a^{(b\gamma)} = -S\tilde{\nabla}_a \mathrm{div}v^{(b\gamma)}, \tag{4.12}$$

and that for $v_a^{(b\gamma)}$ from Eqs 4.7 and 4.8, giving

$$\dot{v}_a^{(b\gamma)} = (3c_z^2 - 1)Hv_a^{(b\gamma)} + \frac{4}{S}\mathcal{D}_a^{(\gamma)} + \frac{2}{S}\frac{1}{\rho^{(b)}\left(1+\frac{2B^2}{3\rho^{(b)}}\right)}\mathcal{B}_{[ab]}B^b, \tag{4.13}$$

where

$$c_z^2 = \frac{1}{3}\frac{\rho^{(b)}\left(1+\frac{2B^2}{3\rho^{(b)}}\right)}{\rho\left(1+w+\frac{2B^2}{3\rho}\right)}. \tag{4.14}$$

The propagation equation for the co-moving spatial gradient of the magnetic energy density is given by:

$$\dot{\mathcal{B}}_a + \frac{4}{3}\mathcal{Z}_a + 4SHa_a + \frac{4}{3}S\tilde{\nabla}_a \mathrm{div}v^{(b)} = 0. \tag{4.15}$$

4.1 Scalar equations

In contrast to Sec. 2.6, where scalar harmonics are used to explicitly separate out the scalar contribution to the propagation equations, we will in this section be constructing explicit scalar variables. These are defined as

$$\mathcal{D} = S\tilde{\nabla}^a\mathcal{D}_a, \tag{4.16}$$
$$\mathcal{Z} = S\tilde{\nabla}^a\mathcal{Z}_a, \tag{4.17}$$
$$\mathcal{S}^{(b\gamma)} = S\tilde{\nabla}^a\mathcal{S}_a^{(b\gamma)}, \tag{4.18}$$
$$V^{(b\gamma)} = S\tilde{\nabla}^a V_a^{(b\gamma)}, \tag{4.19}$$
$$\mathcal{B} = S\tilde{\nabla}^a\mathcal{B}_a. \tag{4.20}$$

By taking the divergence of the equation for the conservation of momentum one obtains the useful relation:

$$A = \frac{1}{\rho\left(1+w+\frac{2B^2}{3\rho}\right)}\left(\frac{1}{3}\frac{B^2}{S^2}\mathcal{K} - \frac{1}{2}\frac{B^2}{S^2}\mathcal{B} - \frac{1}{3}\frac{\rho^{(\gamma)}}{S^2}\mathcal{D}^{(\gamma)}\right), \tag{4.21}$$

where $\mathcal{K}$ is defined in terms of the 3-Ricci scalar $\mathcal{R}$ by:

$$\mathcal{K} = S^2\tilde{\nabla}^2\mathcal{R}. \tag{4.22}$$

In order for $\mathcal{K}$ to be $O(\epsilon_1)$ we require the background to be flat.

One may now obtain a closed set of propagation equations:

$$\begin{aligned}\dot{\mathcal{D}} &= -(1+w)\dot{\mathcal{Z}} + 3Hw\mathcal{D} + \frac{3}{2}\frac{B^2}{\rho}H\mathcal{B} - \frac{B^2}{\rho}H\mathcal{K} \\ &\quad -\frac{2}{3}\frac{1}{\left(1+w+\frac{2B^2}{3\rho}\right)}\frac{B^2}{\rho}\frac{\rho^{(\gamma)}}{\rho}\mathcal{D}^{(\gamma)},\end{aligned} \tag{4.23}$$

$$\begin{aligned}\dot{\mathcal{Z}} &= -2H\mathcal{Z} - \frac{\rho}{2}\mathcal{D} - \frac{B^2}{2}\mathcal{K} + \frac{B^2}{4}\mathcal{B} - \frac{1}{3}\frac{1}{\left(1+w+\frac{2B^2}{3\rho}\right)}\frac{\rho^{(\gamma)}}{\rho}\tilde{\nabla}^2\mathcal{D}^{(\gamma)} \\ &\quad -\frac{1}{2}\frac{1}{\left(1+w+\frac{2B^2}{3\rho}\right)}\frac{B^2}{\rho}\tilde{\nabla}^2\mathcal{B} + \frac{2}{3}\frac{1}{\left(1+w+\frac{2B^2}{3\rho}\right)}\frac{B^2}{\rho}\rho\mathcal{D} \\ &\quad -\frac{4}{3}\frac{1}{\left(1+w+\frac{2B^2}{3\rho}\right)}H\mathcal{Z},\end{aligned} \tag{4.24}$$

$$\dot{\mathcal{S}}^{(b\gamma)} = -S\tilde{\nabla}^2 v^{(b\gamma)}, \tag{4.25}$$

$$\begin{aligned}\dot{v}^{(b\gamma)} &= \left(3c_s^2 - 1\right)Hv^{(b\gamma)} + \frac{4}{S}\mathcal{D}^{(\gamma)} - \frac{1}{2S}\frac{1}{\left(1+\frac{2B^2}{3\rho^{(b)}}\right)}\frac{B^2}{\rho^{(b)}}\mathcal{B} \\ &\quad +\frac{1}{3S}\frac{1}{\left(1+\frac{2B^2}{3\rho^{(b)}}\right)}\frac{B^2}{\rho^{(b)}}\mathcal{K},\end{aligned} \tag{4.26}$$

$$\begin{aligned}\dot{\mathcal{B}} &= -\frac{4}{3}\mathcal{Z} - \frac{4}{3}\frac{1}{\left(1+w+\frac{2B^2}{3\rho}\right)}\frac{B^2}{\rho}H\mathcal{K} + 2\frac{1}{\left(1+w+\frac{2B^2}{3\rho}\right)}\frac{B^2}{\rho}H\mathcal{B} \\ &\quad +\frac{4}{3}\frac{1}{\left(1+w+\frac{2B^2}{3\rho}\right)}\frac{\rho^{(\gamma)}}{\rho}H\mathcal{D} - \frac{4}{3}S\tilde{\nabla}^2 v^{(b\gamma)},\end{aligned} \tag{4.27}$$

$$\dot{\mathcal{K}} = -\frac{4}{3}\frac{1}{\left(1+w+\frac{2B^2}{3\rho}\right)}\frac{B^2}{\rho}H\mathcal{K} + 2\frac{1}{\left(1+w+\frac{2B^2}{3\rho}\right)}\frac{B^2}{\rho}H\mathcal{B} - \frac{4}{3}\frac{1}{\left(1+w+\frac{2B^2}{3\rho}\right)}\frac{\rho^{(\gamma)}}{\rho}H\mathcal{D}, \tag{4.28}$$

where the propagation equation for $\mathcal{K}$ is obtained from the Gauss-Codazzi equations. $\mathcal{D}^{(\gamma)}$ may be written in terms of $\mathcal{D}$ and $\mathcal{S}$ via

$$\mathcal{D}^{(\gamma)} = \frac{\rho\mathcal{D} - \rho^{(b)}\mathcal{S}}{\rho^{(\gamma)} + \frac{3}{4}\rho^{(b)}}. \tag{4.29}$$

4.2 Harmonic decomposition

In order to do the analyse these equations, it is desirable to harmonically decompose them in terms of the Helmholtz functions introduced in Sec. 2.6, via the decomposition:

$$\mathcal{D} = \sum_k \mathcal{D}_k Q^{(k)}, \tag{4.30}$$

$$\mathcal{Z} = \sum_k \mathcal{Z}_k Q^{(k)}, \tag{4.31}$$

$$\mathcal{S}^{(b\gamma)} = \sum_k \mathcal{S}_k^{(b\gamma)} Q^{(k)}, \tag{4.32}$$

$$v^{(b\gamma)} = \sum_k v_k^{(b\gamma)} Q^{(k)}, \tag{4.33}$$

$$\mathcal{B} = \sum_k \mathcal{B}_k Q^{(k)}, \tag{4.34}$$

$$\mathcal{K} = \sum_k \mathcal{K}_k Q^{(k)}. \tag{4.35}$$

Padmanabhan introduces the convenient time variable x defined by

$$x = \frac{S}{S_{\rm eq}}, \tag{4.36}$$

where $S_{\rm eq}$ is the scale factor at radiation-matter equality. To zeroth order in ϵ_1 the radiation and magnetic energy densities scale like S^{-4}, and the matter energy density like S^{-3}. One may thus write the various energy densities in terms of x as:

$$\frac{\rho^{(\gamma)}}{\rho_{\rm eq}} = \frac{1}{2x^4}, \quad \frac{\rho^{(b)}}{\rho_{\rm eq}} = \frac{1}{2x^3}, \quad \frac{\rho}{\rho_{\rm eq}} = \frac{1+x}{2x^4}, \quad \frac{B^2}{\rho_{\rm eq}} = \frac{\beta}{x^4}. \tag{4.37}$$

We can now see that

$$w = \frac{1}{3(1+x)}. \tag{4.38}$$

The zero-order Friedmann equation allows us to determine the Hubble parameter as a function of x:

$$H^2(x) = H_{\rm eq}^2 \frac{1}{2x^4}(1+x). \tag{4.39}$$

The perturbations are expressed in terms of a wave number k. It is convenient, however, to use the ratio $2\pi\omega = [d_H(t_{\rm eq})/\lambda(S_{\rm eq})]$ between the Hubble radius at $S = Sc_{\rm eq}$ and the wavelength of the perturbation at $S = S_{\rm eq}$. The two are related via:

$$\frac{k^2}{H^2S^2} = \frac{2x^2}{1+x}\omega^2. \tag{4.40}$$

We may convert the propagation equations from differential equations in t to differential equations in x via

$$\frac{d}{dt} = HS\frac{d}{dS} = H(x)x\frac{d}{dx} \equiv H\widehat{D}, \tag{4.41}$$

$$\frac{d^2}{dt^2} = H^2S\frac{d}{dS}\left(S\frac{d}{dS}\right) - \frac{3}{2}H^2(1+w)S\frac{d}{dS} \equiv H^2\hat{D}^2 - \frac{3}{2}H^2(1+w)\widehat{D}, \tag{4.42}$$

where $\widehat{D} = x\frac{d}{dS}$.

One may now write the harmonic equations:

$$\begin{aligned}\widehat{D}\mathcal{D}_k &= -\frac{3x+4}{3(1+x)}\mathcal{Z}_k + \frac{1}{1+x}H(x)\mathcal{D}_k + \frac{3\beta}{2(1+x)}H(x)\mathcal{B}_k \\ &\quad -\frac{\beta}{1+x}H(x)\mathcal{K}_k - \frac{2\beta}{(3x+4)(1+x)}H(x)\mathcal{D}_k^{(\gamma)},\end{aligned} \tag{4.43}$$

$$\begin{aligned}\widehat{D}\mathcal{Z}_k &= -2H(x)\mathcal{Z}_k - \frac{1+x}{4x^4}\rho_{\rm eq}\mathcal{D}_k + \frac{2H^2(x)x^2}{(3x+4)(1+x)}\omega^2\mathcal{D}_k^{(\gamma)} \\ &\quad -\frac{\beta}{4x^4}\rho_{\rm eq}\mathcal{K}_k + \frac{\beta}{8x^4}\rho_{\rm eq}\mathcal{B}_k + \frac{3\beta H^2(x)x^2}{(3x+4)(1+x)}\omega^2\mathcal{B}_k \\ &\quad +\frac{2\beta(1+x)}{x^4(3x+4)}\rho_{\rm eq}\mathcal{D}_k - \frac{4\beta}{3x+4}H(x)\mathcal{Z}_k,\end{aligned} \tag{4.44}$$

$$\widehat{D}\mathcal{S}_k^{(b\gamma)} = \frac{2S_{\rm eq}H^2(x)x^3}{1+x}\omega^2 v_k^{(b\gamma)}, \tag{4.45}$$

$$\widehat{D}v_k^{(b\gamma)} = \frac{-4}{3x+4}H(x)v_k^{(b\gamma)} + \frac{4}{S_{\rm eq}x}\mathcal{D}_k^{(\gamma)} - \frac{\beta}{2S_{\rm eq}x^2}\mathcal{B}_k + \frac{\beta}{3S_{\rm eq}x^2}\mathcal{K}_k, \tag{4.46}$$

$$\begin{aligned}\widehat{D}\mathcal{B}_k &= -\frac{4}{3}\mathcal{Z}_k - \frac{4\beta}{3x+4}H(x)\mathcal{K}_k + \frac{6\beta}{3x+4}H(x)\mathcal{B}_k \\ &\quad +\frac{4}{3x+4}H(x)\mathcal{D}_k^{(\gamma)} - \frac{8S_{\rm eq}H^2(x)x^3}{3(1+x)}\omega^2 v_k^{(b\gamma)},\end{aligned} \tag{4.47}$$

$$\widehat{D}\mathcal{K}_k = -\frac{4\beta}{3x+4}H(x)\mathcal{K}_k + \frac{6\beta}{3x+4}H(x)\mathcal{B}_k + \frac{4}{3x+4}H(x)\mathcal{D}_k^{(\gamma)}. \tag{4.48}$$

In order to facilitate comparison with Padmanabhan's analysis, we now eliminate for $v_k^{(b\gamma)}$ and $\mathcal{Z}_k$, making the differential equations for $\mathcal{D}_k$ and $\mathcal{S}_k^{(b\gamma)}$ second

order:

$$\begin{aligned}\left[\widehat{D}^2 \right. &+ \left(\frac{5}{2}\frac{x}{1+x} - \frac{x}{x+4/3} - 1 - \beta\frac{2}{9}\frac{15x+16}{(x+4/3)^2}\right)\widehat{D} \\ &+ \left(\frac{x^2}{2(1+x)^2} + \frac{3x}{4} + \frac{9}{4}\frac{x^2}{x+4/3} - 3\frac{x^2}{1+x} - 2\right. \\ &\left.\left. + \beta\frac{2}{9}\frac{9x^3+43x^2+80x+48}{(1+x)(x+4/3)^3}\right)\right]\mathcal{D} \\ &= \left(\frac{8}{9}\frac{\omega^2x^2}{(1+x)(x+4/3)} - \beta\frac{4}{27}\frac{3x^2+8x+8}{(1+x)^2(x+4/3)^3}\right)(x\mathcal{S} - (1+x)\mathcal{D}) \\ &\quad -\beta\frac{\omega^2x^2}{(1+x)^2}\mathcal{B} - \beta\frac{1}{6}\frac{9x^2+15x+8}{(x+4/3)(1+x)^2}\mathcal{B} + \frac{\beta}{3}\frac{6x^2+13x+8}{(x+4/3)(1+x)^2}\mathcal{K},\end{aligned} \tag{4.49}$$

$$\begin{aligned}\left[\widehat{D}^2 \right. &+ \left.\left(\frac{1}{2}\frac{x}{1+x} - \frac{x}{x+4/3}\right)\widehat{D} + \frac{2}{3}\frac{\omega^2x^3}{(1+x)(x+4/3)}\right]\mathcal{S} \\ &= \frac{2}{3}\frac{\omega^2x^2}{x+4/3}\mathcal{D} - \beta\frac{\omega^2x}{1+x}\mathcal{B} + \beta\frac{4}{3}\frac{\omega^2x}{1+x}\mathcal{K},\end{aligned} \tag{4.50}$$

$$\widehat{D}\mathcal{B} = \frac{4}{3}\left(\frac{1+x}{x+4/3}\widehat{D} + \frac{1}{3(x+4/3)^2}\right)\mathcal{D} \tag{4.51}$$

$$-\frac{4}{3}\left[\widehat{D} + \frac{4}{3}\left(\frac{x}{(x+4/3)^2} + \beta\frac{2}{3}\frac{x}{(x+4/3)^3}\right)\right]\mathcal{S}, \tag{4.52}$$

$$\widehat{D}\mathcal{K} = 2\beta\frac{1}{x+4/3}\mathcal{B} - \beta\frac{4}{3}\frac{1}{x+4/3}\mathcal{K} + \frac{16}{9}\frac{1+x}{(x+4/3)^2}\mathcal{D} - \frac{16}{9}\frac{x}{(x+4/3)^2}\mathcal{S}. \tag{4.53}$$

Given $\mathcal{D}$ and $\mathcal{S}$, one may solve for $\mathcal{D}^{(\gamma)}$ and $\mathcal{D}^{(b)}$ and find

$$\Delta_R \equiv \frac{4}{3}\mathcal{D}^{(\gamma)} = \frac{\mathcal{D}^{(\gamma)}}{1+w^{(\gamma)}} = \frac{(x+1)\mathcal{D} - x\mathcal{S}}{x+4/3}, \tag{4.54}$$

$$\Delta_C \equiv \mathcal{D}^{(c)} = \frac{\mathcal{D}^{(c)}}{1+w^{(c)}} = \frac{(x+1)\mathcal{D} + \frac{4}{3}\mathcal{S}}{x+4/3}. \tag{4.55}$$

In terms of these variables we obtain:

$$\widehat{D}\mathcal{B} = \frac{4}{3}\left(1 - \frac{4}{3}\frac{1}{x+4/3}\right)\widehat{D}\Delta_R + \beta\frac{32}{27}\frac{1}{(x+4/3)^2}\Delta_R - \frac{16}{9}\frac{1}{x+4/3}\Delta_C, \tag{4.56}$$

$$\widehat{D}\mathcal{K} = 2\beta\frac{1}{x+4/3}\mathcal{B} + \frac{16}{9}\frac{1}{x+4/3}\Delta_R - \beta\frac{4}{3}\frac{1}{x+4/3}\mathcal{K}, \tag{4.57}$$

$$\left\{\widehat{D}^2 + \left(\frac{x}{2(1+x)} - 1 - \beta\frac{2}{9}\frac{9x+28}{(x+4/3)^2}\right)\widehat{D} + \left[\frac{2}{3}\frac{\omega^2x^2}{1+x} + \frac{4}{3}\frac{1}{x+4/3}\left(\frac{x}{x+4/3} - 2\right)\right.\right.$$
$$\left.\left. + 4\beta\left(-\frac{1}{1+x} + \frac{16}{27}\frac{1}{(x+4/3)^3} + \frac{8}{9}\frac{1}{(x+4/3)^2} - \frac{1}{x+4/3}\right)\right]\right\}\Delta_R$$
$$= \left(\frac{-x}{x+4/3} + \beta\frac{4}{3}\frac{x-2}{(x+4/3)^2}\right)\widehat{D}\Delta_C + \left(\frac{3}{2}\frac{x}{1+x} - 2\beta\frac{x}{(1+x)(x+4/3)}\right)\Delta_C$$
$$-3\beta\left(\frac{1}{1+x} - \frac{2}{3}\frac{1}{(x+4/3)^2} - \frac{1}{2}\frac{1}{x+4/3}\right)\mathcal{B}$$
$$+\beta\left(-\frac{3}{1+x} - \frac{4}{3}\frac{1}{(x+4/3)^2} - \frac{1}{x+4/3} - \frac{2}{3}\frac{\omega^2x^2}{(1+x)(x+4/3)}\right)\mathcal{K}, \qquad (4.58)$$

$$\left[\widehat{D}^2 + \left(\frac{1}{2}\frac{x}{1+x} - \beta\frac{4}{3}\frac{x-2}{(x+4/3)^2}\right)\widehat{D} - \left(\frac{3}{2}\frac{x}{1+x} + 2\beta\frac{x}{(1+x)(x+4/3)}\right)\right]\Delta_C$$
$$= \left(\frac{4}{3}\frac{1}{x+4/3} + \beta\frac{2}{9}\frac{9x+28}{(x+4/3)^2}\right)\widehat{D}\Delta_R + \left[\frac{4}{3}\frac{1}{x+4/3}\left(2 - \frac{x}{x+4/3}\right)\right.$$
$$\left. -4\beta\left(\frac{1}{1+x} + \frac{16}{27}\frac{1}{(x+4/3)^3} + \frac{8}{9}\frac{1}{(x+4/3)^2} - \frac{1}{x+4/3}\right)\right]\Delta_R$$
$$+3\beta\left(\frac{-1}{1+x} + \frac{2}{3}\frac{1}{(x+4/3)^2} + \frac{1}{2}\frac{1}{x+4/3} - \frac{\omega^2x}{3(1+x)}\right)\mathcal{B}$$
$$+\beta\left(\frac{3}{1+x} - \frac{4}{3}\frac{1}{(x+4/3)^2} - \frac{1}{x+4/3} - \frac{8}{9}\frac{\omega^2x}{(1+x)(x+4/3)}\right)\mathcal{K}. \qquad (4.59)$$

4.3 Analysis of equations

These equations cannot be solved exactly, but their most important properties may be derived by suitable approximation.

Modes are labelled by the parameter ω. If $\omega > 1$, the mode enters the Hubble radius in the radiation dominated era, and if $\omega <$, it enters in the matter dominated era. We thus have $x_{\rm enter} \approx \omega^{-2}$ if $\omega \ll 1$, and $x_{\rm enter} \approx \omega^{-1}$ if $\omega \gg 1$. We will thus consider the modes $\omega \ll 1$ and $\omega \gg 1$ separately.

4.3.1 The case $\omega \ll 1$

When $\omega \ll 1$, we have $x_{\rm enter} \approx \omega^{-2}$. It is convenient to deal with the ranges $x \ll 1 \ll x_{\rm enter}$ and $x > x_{\rm enter} \gg 1$ separately. For the former, one may obtain the lowest order solutions to the variables $(\mathcal{D}, \mathcal{S}, \mathcal{B}, \mathcal{K})$ by a dual series expansion in the small parameters ω and β, using Eqs 4.49 – 4.53. One obtains four principal modes (two other modes exist, but are unimportant) which, by convention, are labelled the adiabatic or isothermal growing or decaying modes.

The adiabatic growing mode is given by:

$$\begin{aligned}
\mathcal{D}_{\rm ga} &= x^2\,(1+\cdots) - \frac{\omega^2 x^4}{15}\,(1+\cdots) + \frac{11}{24}\beta x^2\log(x)\,(1+\cdots)\,,\\
\mathcal{S}_{\rm ga} &= \frac{\omega^2 x^4}{32}\,(1+\cdots) + O(\beta\omega^2),\\
\mathcal{B}_{\rm ga} &= \frac{9}{8}x^2\,(1+\cdots) - \frac{9}{80}\omega^2 x^4\,(1+\cdots) + \frac{33}{64}\beta x^2\log(x)\,(1+\cdots)\,,\\
\mathcal{K}_{\rm ga} &= \frac{x^2}{2}\,(1+\cdots) - \frac{\omega^2 x^4}{60}\,(1+\cdots) + \frac{11}{48}\beta x^2\,(1+\cdots)\,,
\end{aligned}$$

the adiabatic decaying mode by:

$$\begin{aligned}
\mathcal{D}_{\rm da} &= x^{-1}\,(1+\cdots) + \frac{1}{3}\omega^2 x\,(1+\cdots) + \frac{29}{12}\beta x^{-1}\log(x)\,(1+\cdots)\,,\\
\mathcal{S}_{\rm da} &= \frac{1}{2}\omega^2 x\,(1+\cdots) + O(\omega^2\beta),\\
\mathcal{B}_{\rm da} &= \frac{3}{4}x^{-1}\,(1+\cdots) - \frac{13}{12}\omega^2 x\,(1+\cdots) - \frac{29}{16}\beta x^{-1}\,(\log(x)+\cdots)\,,\\
\mathcal{K}_{\rm da} &= -x^{-1}\,(1+\cdots) - \frac{1}{3}\omega^2 x^2\,(1+\cdots) - \frac{29}{12}\beta x^{-1}\,(1+\cdots)\,,
\end{aligned}$$

the isothermal decaying mode by:

$$\begin{aligned}
\mathcal{D}_{\rm di} &= \frac{1}{6}\omega^2 x^3\,(1+\cdots) + \frac{3}{4}\beta x\,(1+\cdots)\,,\\
\mathcal{S}_{\rm di} &= 1 - \frac{\omega^2 x^3}{18}\,(1+\cdots) + O(\omega^2\beta),\\
\mathcal{B}_{\rm di} &= -x\,(1+\cdots) + \frac{55}{216}\omega^2 x^3\,(1+\cdots) + \frac{15}{16}\beta x\,(1+\cdots)\,,\\
\mathcal{K}_{\rm di} &= -x\,(1+\cdots) + \frac{1}{18}\omega^2 x^3\,(1+\cdots) + \frac{1}{4}\beta x\,(1+\cdots)\,,
\end{aligned}$$

and the isothermal growing mode by:

$$\begin{aligned}
\mathcal{D}_{\rm gi} &= \frac{1}{6}\omega^2 x^3\,(\log(x)+\cdots) - \frac{2}{3}\beta\,(\log(x)+\cdots)\,,\\
\mathcal{S}_{\rm gi} &= \log(x) + \cdots - \frac{1}{18}\omega^2 x^3\,(\log(x)+\cdots) + O(\omega^2\beta),\\
\mathcal{B}_{\rm gi} &= -\frac{4}{3}\,(\log(x)+\cdots) + \frac{55}{72}\omega^2 x^3\,(\log(x)+\cdots) - \frac{1}{12}\beta\,(\log(x)+\cdots)\,,\\
\mathcal{K}_{\rm gi} &= -x\,(\log(x)+\cdots) + \frac{1}{18}\omega^2 x^3\,(\log(x)+\cdots) - 2\beta\,(\log(x)+\cdots)\,.
\end{aligned}$$

The "adiabatic" modes are labelled such, because, for these, $\mathcal{S}$ is very small. For the isothermal modes, the labels "decaying" and "growing" are somewhat arbitrary.

The coupling between $\mathcal{D}$ and $\mathcal{S}$ is $O(\omega^2 x^n)$ or $O(\beta x^n)$, so in this limit is rather weak. Thus the distinction between adiabatic and isothermal modes is well defined, and evolution will not mix the two while the modes are larger than the Hubble radius

If one neglects terms $O(\omega^2 x^2)$ and higher, one sees from Eq. 4.60 that $\mathcal{S} = 1$ is a valid solution. In other words, there are solutions where $\mathcal{S}$ is approximately conserved.

As noted earlier, the modes labelled "growing" and "decaying" in the adiabatic case truly deserve their labels. We see that for adiabatic initial conditions, the variables $\mathcal{B}$ and $\mathcal{K}$ follow $\mathcal{D}$. The back-reaction of these variables onto $\mathcal{D}$ is very small, and does not change the over-all behaviour of the solutions.

In the isothermal case, $\mathcal{D} \ll \mathcal{S}$. This causes the variables $\mathcal{B}$ and $\mathcal{K}$ to follow $\mathcal{S}$. However, the back-reaction is still negligible. There is only a small perturbation of energy density, so spacetime geometry does note change significantly. Thus the isothermal modes correspond to a re-distribution of energy densities between the radiation and dust fluids. As a matter of convention, the dominant isothermal mode is called "growing".

We now consider the case when $x \ll 1$ (i.e. $x^2\omega^2 \ll 1$). This is when the modes have entered the Hubble radius, and is matter dominated. The strong coupling between $\mathcal{S}$ and $\mathcal{D}$ leads to only two important modes being present:

$$\mathcal{D}_{\rm g} = \mathcal{S}_{\rm g} = x, \qquad \mathcal{D}_{\rm d} = \mathcal{S}_{\rm d} = x^{-\frac{3}{2}},$$

with the variable $\mathcal{K}$ and $\mathcal{B}$ constant in both regimes. We see that the presence of a magnetic field does not significantly affect this situation. It also makes no sense to distinguish adiabatic and isothermal modes here, as $\mathcal{D}$ and $\mathcal{S}$ are equal.

4.3.2 The case $\omega \gg 1$

We now consider the case $\omega^2 \gg 1$. This is more complicated, there being three regimes: the mode is bigger than the Hubble radius ($x\omega \ll 1$, which means $x \ll 1$), the mode is smaller than the Hubble radius, but the universe is still radiation dominated ($\omega^{-1} \ll x \ll 1$), and finally, the mode has entered the universe and it is matter dominated ($x \gg 1$, so that $\omega x \gg 1$). We work now with the equations in terms of Δ_R and Δ_C (Eqs 4.56 – 4.59).

In the case $\omega x \ll 1$, i.e. the mode has yet to enter the Hubble radius the equations may be approximated as:

$$\left[\widehat{D}^2 - \left(1+\frac{7}{2}\beta\right)\widehat{D} - 2(1-2\beta)\right]\Delta_R \approx -\frac{3}{2}\beta\widehat{D}\Delta_C - \frac{3}{4}\beta\mathcal{B} + \frac{3}{2}\beta\mathcal{K}, \tag{4.60}$$

$$\widehat{D}^2\Delta_C \approx \widehat{D}^2\Delta_R, \tag{4.61}$$

$$\widehat{D}\mathcal{B} \approx \frac{2}{3}[4\widehat{D}+\beta]\Delta_R - \frac{4}{3}\Delta_C, \tag{4.62}$$

$$\widehat{D}\mathcal{K} \approx \frac{4}{3}\Delta_R + \frac{3}{2}\beta\mathcal{B} - \beta\mathcal{K}. \tag{4.63}$$

We see that the Δ_C perturbations are driven by the Δ_R perturbations – the universe being radiation dominated. The back-reaction is negligible, though.

The dominant mode is given by:

$$\begin{aligned}
\Delta_R &= x^2 + \frac{5}{6}\beta x^2 \log(x), \\
\Delta_C &= x^2 + \frac{5}{6}\beta x^2 \log(x), \\
\mathcal{B} &= 2x^2 + \frac{35}{18}\beta x^2 \log(x) + \frac{17}{36}\beta x^2, \\
\mathcal{K} &= \frac{2}{3}x^2 + \frac{10}{9}\beta x^2 \log(x) + \frac{8}{9}\beta x^2,
\end{aligned}$$

which is clearly adiabatic. We see that the back-reaction of the magnetic variables on the radiation perturbations is small.

For the case $x \ll 1$, $\omega x \gg 1$, the equations may be approximated by:

$$\left[\widehat{D}^2 - \left(1 + \frac{7}{2}\beta\right)\widehat{D} + \frac{2}{3}\omega^2 x^2\right]\Delta_R \approx -\frac{3}{2}\beta\widehat{D}\Delta_C - \frac{3}{4}\beta\mathcal{B} - \frac{2}{3}\beta\omega^2 x^2 \mathcal{K}, \quad (4.64)$$

$$\widehat{D}^2\Delta_C \approx \widehat{D}\Delta_R - \beta\omega^2 x^2\left(\mathcal{B} + \frac{2}{3}\mathcal{K}\right), \quad (4.65)$$

$$\widehat{D}\mathcal{B} \approx \frac{2}{3}[4\widehat{D} + \beta]\Delta_R - \frac{4}{3}\Delta_C, \quad (4.66)$$

$$\widehat{D}\mathcal{K} \approx \frac{4}{3}\Delta_R + \frac{3}{2}\beta\mathcal{B} - \beta\mathcal{K}. \quad (4.67)$$

To zero order in β, the equation for Δ_R is then the oscillator equation, giving:

$$\begin{aligned}
\Delta_R &= A\exp(\pm i\nu x) - \frac{3}{2}\beta D, \quad \nu^2 = \frac{2}{3}\omega^2 \gg 1, \\
\Delta_C &= B\log(x) + C \\
&\quad + \frac{2}{3}B\beta\omega^2 x(\log)^2(x), \\
\mathcal{B} &= -\frac{2}{3}B(\log)^2(x) - \frac{4}{3}C\log(x) + A\exp(\pm i\nu x) \\
&\quad - \frac{8}{9}B\beta\omega^2 x(\log)^2(x), \\
\mathcal{K} &= D - \frac{1}{3}B\beta(\log(x))^3.
\end{aligned}$$

One sees that the perturbations in the radiation now oscillate rapidly. The dark matter and magnetic perturbations do not grow at a significant rate in this era, increasing only logarithmically. We see that, although there is a back-reaction due to the magnetic field, it does not alter the behaviour of the system – although the oscillations of the radiation fluid are shifted, it is only by a small amount.

Finally, we consider the range $x \gg 1$. The universe is now matter dominated,

and the equations may be approximated by

$$\left[\widehat{D}^2 + \frac{1}{2}\widehat{D} - \frac{3}{2}\right]\Delta_C \approx -\beta\omega^2\mathcal{B}, \tag{4.68}$$

$$\left[\widehat{D}^2 + \frac{1}{2}\widehat{D} + \frac{2}{3}\omega^2 x\right]\Delta_R \approx -\left(\widehat{D} - \frac{2}{3}\right)\Delta_C - \frac{2}{3}\beta\omega^2\mathcal{K}, \tag{4.69}$$

$$\widehat{D}\mathcal{B} \approx \frac{4}{3}\widehat{D}\Delta_R - \frac{16}{9x}\Delta_C, \tag{4.70}$$

$$\widehat{D}\mathcal{K} \approx 0. \tag{4.71}$$

We see that the perturbations are now driven by the dark matter. To zero order in β, the dark matter perturbations are given by

$$\Delta_C \approx Ax + Bx^{-3/2} \approx Ax. \tag{4.72}$$

Following Padmanabhan [64], we may then compute Δ_R (to zero order in β) using the WKB approximation:

$$\Delta_R \approx \frac{3A}{4\omega^2} + \frac{B}{\sqrt{\omega x}}\exp\left(\pm i\sqrt{\frac{8}{3}}\omega x^{1/2}\right). \tag{4.73}$$

Computing $\mathcal{B}$ and $\mathcal{K}$ (to zero order in β) then gives:

$$\mathcal{B} \approx \frac{16}{9}A\log(x) + C + \frac{4B}{3\sqrt{\omega x}}\exp\left(\pm i\sqrt{\frac{8}{3}}\omega x^{1/2}\right), \tag{4.74}$$

$$\mathcal{K} \approx D. \tag{4.75}$$

Thus the Δ_R continues to oscillate rapidly, the oscillations dominating over the driving by the dark matter term. The magnetic perturbations grow slowly in this era, while oscillating. While the back-reaction on the radiation perturbations is negligible, it does have an effect on the CDM perturbations. To first order in β, and highest order in x, this back-reaction is given by:

$$\Delta_C^B = -\frac{16}{9}A\beta\omega^2\log(x), \tag{4.76}$$

where Δ_C^B represents the back-reaction of the magnetic perturbations onto the CDM perturbations.

4.3.3 Numerical analysis

Figures 4.1 and 4.2 are show the evolution of the scalar variables under the system 4.56 – 4.59. These were generated by numerical integration. It must be noted that the model presented does not include the effect of Silk damping. Inspecting the graphs, one may clearly see the behaviour predicted by the analytic approximations derived in the previous section. One can clearly see how in late times the CDM perturbations grow faster in the presence of a stronger magnetic field. As noted in the previous chapter, the presence of a magnetic field changes the frequency of the late-time oscillations. This effect is not seen here, however, as this change of frequency depends on the interaction of photons and electrons

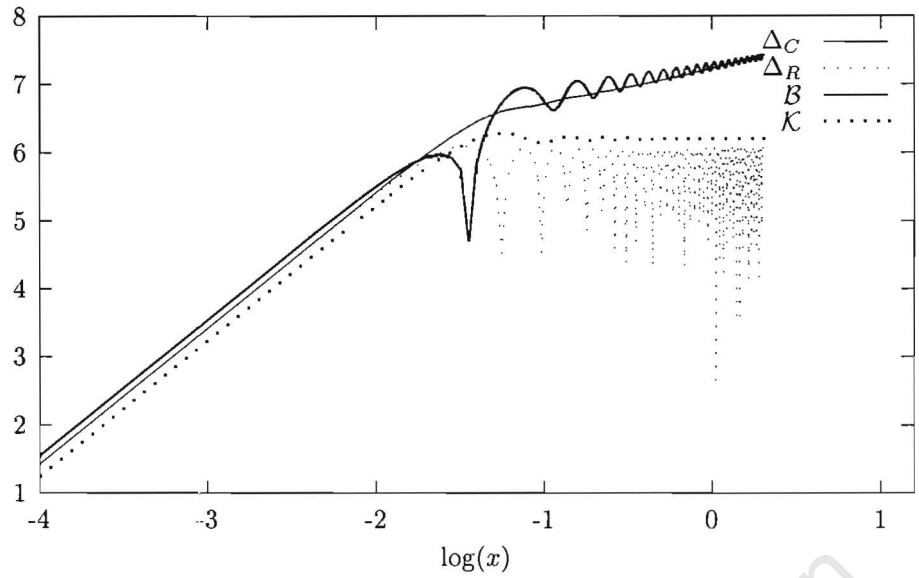

Figure 4.1: Numerical integration showing the evolution of the perturbation variables with adiabatic initial conditions in the presence of a very weak magnetic field ($\beta = 10^{-10}$, $\omega = 100$). Here the magnetic variables and the matter variables effectively decouple.

before decoupling. Naturally, the CDM does not share this coupling with the photons. In the next chapter the "tight coupling" approximation of the full set of equations (given in Sec. 2.6) will be derived. This will show how coupled photons and baryons oscillations change frequency in the presence of a weak magnetic field.

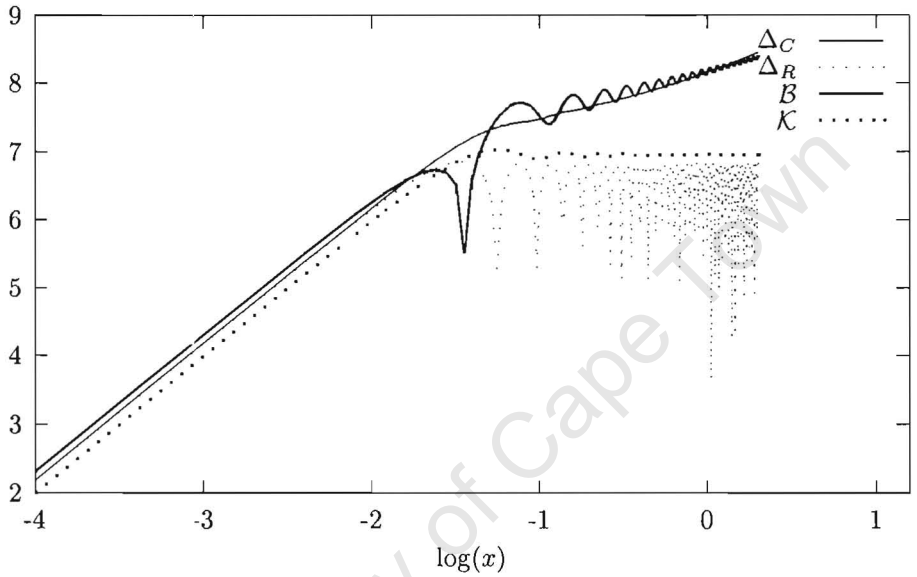

Figure 4.2: Numerical integration showing the evolution of the perturbation variables with adiabatic initial conditions in the presence of a stronger magnetic field ($\beta = 10^{-4}$, $\omega = 100$). One may see how weak coupling affects the evolution of the variables.

Chapter 5

Calculating the CMBR power spectrum

As we have seen in the previous chapter, the CMB power spectrum is the cleanest cosmological observable. It is vital then to have an efficient technique to predict the CMB power spectrum. The CAMB code, a covariant modification of the CMBFAST code [68] does this using the symbolic "integral solution" for the radiation [11, 56]. This next section presents the code, followed by sections showing how the code has be modified to predict the power spectrum with a primordial magnetic field.

5.1 The CAMB code

The CAMB code (`http://camb.info`) [56], a modification of the CMBFAST code [68], provides a fast and accurate means of calculating the predicted CMB power spectrum for given initial conditions. This chapter will describe the function and the design of the code in order to facilitate future modification.

5.1.1 Running CAMB

Assuming FORTRAN 90 is correctly installed, one may easily run the CAMB code. Before running it, however, it must be compiled. This is done by running the make utility (which should be installed) which will then compile the program. After the program is correctly compiled, one runs it by typing

```
./camb inifile
```

at the command-line, where *`inifile`* is the name of the initialisation file containing the initialisation parameters. The default file, `params.ini`, is shipped with the code. Any modifications should be based on this file. The parameters are self-explanatory.

5.1.2 The organisation of the CAMB code

The CAMB code code is organised into several files:

- `bessels.f90` – Contains a module to calculate the spherical Bessel functions. This is based on Arthur Kosowsky's "`hyperjl.c`".

- `camb.f90` – Main wrapper routines for running CAMB as part of another program. By adding "`use camb`" to the program one may call the routines in the file, which include

  - `CAMB_GetResults` generates output from a set of model parameters (specified in `CAMBparams` type – which is defined at the top of `modules.f90`).
  - `CAMB_ValidateParams` checks that the parameter set is valid.
  - `CAMB_SetDefaultParams` sets the parameter set to the defaults.
  - `CAMB_GetAge` computes the age of a model in gigayears.
  - `CAMB_GetCls` to retrieve the computed Cls.

  The results can also be accessed directly using the arrays in the `ModelData` module (defined in `modules.f90`).

- `cmbmain.f90` – This file contains the `CAMBmain` module which contains the main subroutine (`cmbmain`) that does integrations, etc. It encompasses CMBFAST's `cmbflat` and `cmbopen`.

- `equations.f90` – This file contains the `GaugeInterface` module which contains the background and perturbation evolution equations. These calculation routines are then used by the `cmbmain` function to do the numerical integration. Amongst the important subroutines in the module are:

  - `GetNumEqns` – This calculates the number of equations to propagate.
  - `output` and `outputt` – These compute the scalar and tensor sources at a given time for a given wavenumber.
  - `outtransf` writes out the matter transfer functions. These depend on which variable set is used.
  - `initial` and `initialt` – These compute the scalar and tensor initial conditions.
  - `(f)derivs` and `(f)derivst` – These compute the (conformal time) derivatives for the scalar and tensor variables. The functions prefixed by "f" do so in the flat case.

  The majority of modifications to the code will be done here, so a later section will discuss the file in detail.

- `inidriver.f90` – Driver for the command-line `camb` program.

- `inifile.f90` – Reads in parameters from a file of name/value pairs and calls CAMB. Modify this file to generate grids of models, change the parameterisation, etc.

- `lensing.f90` – Lensing module for computing the lensed CMB power spectra from the unlensed spectra and a lensing power spectrum. Adapted from code written by Gayoung Chon (`gchon@mrao.cam.ac.uk`).

- `modules.f90` – This file defines the modules:
  - `ModelParams` – This contains definitions of various model parameter data types as well as code to set the values of these parameters.
  - `ModelData` – This contains the computed output power spectra data.
  - `TimeSteps`
  - `Transfer` – Various routines involved in the calculation of transfer functions.
  - `lvalues`
  - `MassiveNu` – Routines involved in massive neutrino calculations.
  - `ThermoData` – Routines for calculating thermodynamic data, like the sound speed.

  which are used in other parts of the program.
- `power_tilt.f90` – This file defines a module called `InitialPower` that returns the initial power spectra.
- `recfast.f90` – RECFAST integrator for Cosmic Recombination of Hydrogen and Helium by Douglas Scott (with minor modifications for CMBFAST and the CAMB).
- `sigma8.f90` – Sample tester program showing how one might use the CAMB code in ones own program. This prints out σ_8 as a function of CDM density.
- `subroutines.f90` – This contains useful subroutines involved in interpolation, and and the modified Runga-Kutta integrator `dverk` for parallelised evolution.
- `tester.f90` – Sample tester program showing how one might use the CAMB code in ones own program. This gets the scalar and tensor C_ls as well as their sum.
- `writefits.f90` – This file contains routines to output power spectrum in FITS format.

5.1.3 Modifying the CAMB code

Many modifications will involve modifying only the propagation equations, with the possible addition of new first-order variables. The CAMB code uses conformal time, and the signature convention of [11], so, before any changes may be made, the propagation equations must be made to conform with the signature choice and transformed to conformal time. All the changes needed for such a modification will take place in the `equations.f90` file.

An overview of the `equations.f90` file

The `equations.f90` file contains the propagation equations that get numerically integrated in order to generate the CMB power spectrum. It also contains the code that sets the initial conditions for the variables to be propagated, as well as code to calculate the scalar and tensor sources and the output transfer functions.

The variables are propagated via Runga-Kutta integration. Crudely speaking, this may be seen as a very sophisticated version of the Euler integration technique taught in elementary calculus courses. In order to integrate the DE

$$\frac{dx}{dt} = f(x,t), \tag{5.1}$$

from t_0 to t_1, the Euler method would proceed as follows:

1. The initial value x_0 is given. The time variable is set to $t = t_0$.
2. The derivative is calculated at the known point (x_{old}). This is then used to estimate the next point via

$$x_{new} = x_n + f(x_{old}, t)\Delta t, \tag{5.2}$$

   where Δt is a small, fixed time increment.
3. The t variable is incremented by Δt. If it is less than t_1, then loop back to step 2, else stop.

In the CAMB code, the initial values are calculated in the `initial(t)` functions, with the `(f)derivs(t)` functions calculating the derivatives[1]. For numerical stability, the spatial gradient of the 3-curvature, η_k is propagated instead of propagating the gradient of the expansion, $\mathcal{Z}_k$, and the shear, σ_k, for the scalars. The latter may be recovered via the constraints[2]:

$$\left(\frac{k}{S}\right)^2 \eta_k = -\frac{\kappa^2\rho}{2}\mathcal{D}_k + \frac{k\mathcal{H}}{S^2}\mathcal{Z}_k, \tag{5.3}$$

$$\kappa^2\rho q_k = \frac{2}{3}\left(\frac{k}{S}\right)^2 (\mathcal{Z}_k - \sigma_k). \tag{5.4}$$

The propagation equation for η_k is

$$\frac{k}{S^2}\eta_k = -\frac{\kappa^2\rho}{2}\mathcal{D}_k. \tag{5.5}$$

The variables are propagated as a single array (or vector) of length `nvar(t)` which is a field of the `EvolutionVars` type. The length of these arrays naturally depend on what variables are to be propagated, and are calculated by the `GetNumEqns` function. The `EvolutionVars` type contains further state information that is needed during the integration. This state information is set at the beginning of the integration and is not changed during the integration.

[1] The addition of a "t" to the end of a variable name usually indicates that it is involved in the tensor calculations. The "f" in front of `fderivs(t)` indicate that these are for the purely flat case.

[2] The equations in this section are in the signature of [11]. "$\cdot$" refers to $d/d\tau$ in this section (τ is conformal time). $\mathcal{H} = SH$ is the conformal time Hubble parameter. Obviously the equations in this section need to be changed to reflect any changes to the model used.

The background matter variables $\rho^{(i)}$ are not propagated using the Runga-Kutta integrator. Instead, the values of $\kappa\rho S^2$ are determined when $S = 1$, and then at any other time, the zero-order relations:

$$\rho^{(\gamma)} \propto \frac{1}{S^4}, \tag{5.6}$$

$$\rho^{(\nu)} \propto \frac{1}{S^4}, \tag{5.7}$$

$$\rho^{(c)} \propto \frac{1}{S^3}, \tag{5.8}$$

$$\rho^{(b)} \propto \frac{1}{S^3}, \tag{5.9}$$

are used. The baryon fluid is treated as dust with a sound speed.

The scalar and tensor sources are calculated in `output(t)` using the symbolic integral solution for those sources. The output transfer functions are calculated in `outtransf`.

We are now at a point where a simple recipe may be given to effect basic changes to the propagation equations.

A simple recipe to change the CAMB code

1. Write down the propagation and constraint equations in conformal time using the signature in [11].

2. Change `GetNumEqns` so as to include any extra variables. This is done as follows:

   - For scalar variables it is best to place the entries in the array directly before the photon variables. This is to avoid accidental overwriting of the new variables. Only one line in the `GetNumEqns` function need then be modified, line 188:

     ```
     EV%nvar=5+ (EV%lmaxg+1) + EV%lmaxgpol-1 +(EV%lmaxnr+1).
     ```

     If one is adding n variables, then the change will be as follows:

     ```
     EV%nvar=5+n+ (EV%lmaxg+1) + EV%lmaxgpol-1 +(EV%lmaxnr+1).
     ```

   - One may add the new tensor variables before the photon variables or after all the existing variables. The latter gives less work in the remaining functions that need changing, but the former gives consistency to the procedure of adding new variables. Only one line in the `GetNumEqns` function need be modified, line 215:

     ```
     EV%nvart=(EV%lmaxt-1)+(EV%lmaxpolt-1)*2+3.
     ```

     If one is adding n variables, then the change will be as follows:

     ```
     EV%nvart=(EV%lmaxt-1)+(EV%lmaxpolt-1)*2+3+n.
     ```

3. Change `initial(t)` to set the initial conditions for the new variables and reflect any changes to the initial conditions. The procedure for deriving these initial conditions is described in [11] as well as in Sec. 5.2 in this document. The variable `x` in the subroutines is the time variable

$$x = \frac{k}{HS}. \tag{5.10}$$

The `y(t)` array is the array of variables that need to be given their initial value. The arrangement of the variables in the array is as follows:

- For scalars (`y`):

$$\begin{aligned}
\texttt{y(1)} &= S, \\
\texttt{y(2)} &= k\eta_k, \\
\texttt{y(3)} &= \mathcal{D}_k^{(c)}, \\
\texttt{y(4)} &= \mathcal{D}_k^{(b)}, \\
\texttt{y(5)} &= v_k^{(b)}, \\
\texttt{y(6)} &= \mathcal{D}_k^{(\gamma)}, \\
\texttt{y(7)} &= q_k^{(\gamma)}, \\
\texttt{y(8)} &= \pi_k^{(\gamma)}, \\
\texttt{y(6+l)} &= I_k^{(l)},\ 3 \le \texttt{l} \le \texttt{EV\%lmaxg}, \\
\texttt{y(7+EV\%lmaxg)} &= \mathcal{D}_k^{(\nu)}, \\
\texttt{y(8+EV\%lmaxg)} &= q_k^{(\nu)}, \\
\texttt{y(9+EV\%lmaxg)} &= \pi_k^{(\nu)}, \\
\texttt{y(7+EV\%lmaxg+l)} &= G_k^{(l)},\ 3 \le \texttt{l} \le \texttt{EV\%lmaxnr}, \\
\texttt{y(EV\%polind+l)} &= \mathcal{E}_k^{(l)},\ 0 \le \texttt{l} \le \texttt{EV\%lmaxgpol}, \\
\texttt{y(k), k} > \texttt{EV\%polind+EV\%lmaxgpol} &= \text{Massive neutrino variables.}
\end{aligned}$$

- For tensors (`yt`):

$$\begin{aligned}
\texttt{y(1)} &= S, \\
\texttt{y(2)} &= H\chi_k, \\
\texttt{y(3)} &= \sigma_k, \\
\texttt{y(4)} &= \pi_k^{(\gamma)}, \\
\texttt{y(2+l)} &= I_k^{(l)},\ 3 \le \texttt{l} \le \texttt{EV\%lmaxt}, \\
\texttt{E(l)} &= \mathcal{E}_k^{(l)},\ 2 \le \texttt{l} \le \texttt{EV\%lmaxpolt}, \\
\texttt{B(l)} &= \mathcal{B}_k^{(l)},\ 2 \le \texttt{l} \le \texttt{EV\%lmaxpolt}, \\
\texttt{neut(2)} &= \pi_k^{(\nu)}, \\
\texttt{neut(l)} &= G_k^{(l)},\ 3 \le \texttt{l} \le \texttt{EV\%lmaxnrt},
\end{aligned}$$

  The remaining `yt` elements are massive neutrino variables. The array `E` starts at the `EV%lmaxt+2`'th element of `yt`, the `B` array starts at the `EV%lmaxt+EV%maxpolt+2`'th element and the `neut` array starts at the `2*EV%lmaxt+EV%maxpolt+2`'th element.

For this simple recipe it is assumed that the changes will not include new perturbation modes (apart from the usual adiabatic and baryon/CDM isocurvature modes). If one is not adding the new variables at the end,

one must remember to increment the subsequent variables indices by the number of new variables. This need only be done for the radiation and massless neutrinos for the scalars, as the other variables' increments are precalculated in the `GetNumEqns` function. Similarly, for the tensors, this manual increment need only be done for the radiation fluid.

4. One may now modify the `(f)derivs(t)` subroutines. The `ay(t)` array contains the current state of the variables to be propagated, and the subroutine calculates the `ay(t)prime` array of derivatives of these variables at that point.

   The matter variables at the current conformal time are given by `grho(i)_t` $= \kappa^2 \rho^{(i)} S^2$, with `i` taking on the following values:

   `g` – radiation,

   `r` – massless neutrinos,

   `b` – baryons,

   `c` – cold dark matter,

   `nu` – massive neutrinos.

   The `E%Kf(t)` array contains useful constants relating to the curvature:

$$\begin{aligned} \texttt{EV\%Kf(1)} &= 1 - l(l+2)\frac{K}{k^2}, \\ \texttt{EV\%Kft(1)} &= 1 - \left[(l+1)^2 - 3\right]\frac{K}{k^2}, \end{aligned}$$

   allowing one to write the equations for the higher moments easily.

   In adding one's own equations, it is best to follow the example of the equations already there. One must again be careful to increment the indices if all the subsequent elements of the array by the number of variables one is adding.

   For efficient calculation the tight coupling approximation is used to calculate the baryon relative velocity, and the photon moments with $l \geq 1$ at sufficiently early times.

5. If the integral solution changes, then one must modify the `output(t)` functions to reflect this change. The `scal_eqns.map`, which comes with the CAMB code, allows one to easily calculate the new output code for the scalars.

6. It is important to make sure that the indices of the old variables are changed to reflect the insertion of the new variables. This needs to be done in the `initial(t)`, `output(t)`, `outtransf`, and `(f)derivs(t)` subroutines.

This recipe only covers changes where new variables are introduced and propagated. If the Friedmann equation changes, then one must also change the `dtauda` function. If this change involves the introduction of new matter species, then one must also do the following:

1. Find a zero-order relation between this matter and the scale factor.

2. Add the matter species to the list on line 122 of `modules.f90` and give its initial value (at $S = 1$) at line 238. If necessary add an `omega` variable at line 68.

3. In `equations.f90` modify the `GetOmegak` function. If any additional initialisation needs to take place, modify the `init_background` subroutine.

4. Modify the Friedmann equation wherever it appears (`dtauda`, `output(t)`, and `(f)derivs(t)`).

5. Modify the initial conditions and the propagation equations as before.

Other changes

This gives a brief review of other possible changes:

Changing the initial power spectrum The initial power spectrum is specified in the `InitialPower` module in `power_tilt.f90`. The file comments provide detailed descriptions as to how to make the changes.

Adding fields to the initialisation file The `inidriver.f90` is a simple driver program that reads initialisation parameters from an initialisation file. It uses the ini-file reading subroutines defined in `inifile.f90`. By modifying the `inidriver.f90` file, following the example of the code already there, one may easily add new fields to the initialisation file.

5.2 Initial conditions

Initial conditions for the CAMB code may be obtained by solving the propagation and constraint equations for the dynamical and kinetic variables, decomposed into covariant harmonic modes (Ch. 2), when appropriate simplifying assumptions are imposed [11].

5.2.1 Initial conditions for scalars

The CAMB code uses the CDM frame; this causes the acceleration a_a and the CDM relative velocity to vanish identically. At early times the universe is radiation dominated, leading to an equation of state $p = \frac{1}{3}\rho$. We only consider the modes where the baryon and CDM density perturbations make a negligible contribution to the total matter contribution, so that:

$$\rho\mathcal{D}_k = \rho^{(\gamma)}\mathcal{D}_k^{(\gamma)} + \rho^{(\nu)}\mathcal{D}_k^{(\nu)}, \quad \rho q_k = \rho^{(\gamma)}q_k^{(\gamma)} + \rho^{(\nu)}q_k^{(\nu)}. \tag{5.11}$$

This effectively removes two possible perturbation modes: the baryon and CDM isocurvature modes. However, the decoupling of baryon and photon perturbations leads to considerable simplification of the equations.

Sufficiently before decoupling the photons and baryons are tightly coupled. The high opacity of the Thomson scattering leads to a damping of the photon moments for $l \geq 2$. We thus, to a good approximation, may set $I_k^{(l)} = 0$ for $l \geq 2$, and set $q_k^{(\gamma)} = 4v_k^{(b)}/3$, so that the radiation is isotropic in the rest frame of the baryons. For simplicity, we also set the neutrino moments with $l \geq 2$ zero, even

though the free-streaming of neutrinos causes the neutrino anisotropic stress to be non-zero in general.

Furthermore, we only consider modes $|K|/k^2 \ll 1$, so that terms involving K in the scalar equations may be ignored. Equivalently, we assume that the characteristic length scale associated with each mode, S/k, is small compared to the curvature radius of the universe, so that k is effectively the co-moving wavenumber. We also require that the mode be well outside the horizon scale $1/H$ (it is frozen in). Thus only modes satisfying

$$1 \ll \mathcal{H}_k \ll \frac{H^2 S^2}{|K|} \tag{5.12}$$

are considered, where $\mathcal{H}_k \equiv SH/k$ is the ratio of the characteristic length to the horizon scale.

It is convenient to change to the time variable

$$x \equiv \mathcal{H}_k^{-1}, \tag{5.13}$$

so that (under the assumptions) the propagation equations become[3]:

$$\begin{aligned}
x^2 \mathcal{Z}_k' + x\mathcal{Z}_k + 3[(1-R)\mathcal{D}_k^{(\gamma)} + R\mathcal{D}_k^{(\nu)}] &= 0, && (5.14)\\
x^2 \Phi_k' + x\Phi_k + 2\sigma_k + \frac{3}{2}[(1-R)q_k^{(\gamma)} + Rq_k^{(\nu)}] &= 0, && (5.15)\\
x\sigma_k' + \sigma_k + x\Phi_k &= 0, && (5.16)\\
\mathcal{D}_k^{(\gamma)\prime} + \frac{4}{3}\mathcal{Z}_k + q_k^{(\gamma)} &= 0, && (5.17)\\
\mathcal{D}_k^{(\nu)\prime} + \frac{4}{3}\mathcal{Z}_k + q_k^{(\nu)} &= 0, && (5.18)\\
q_k^{(\gamma)\prime} - \frac{1}{3}\mathcal{D}_k^{(\gamma)} &= 0, && (5.19)\\
q_k^{(\nu)\prime} - \frac{1}{3}\mathcal{D}_k^{(\nu)} &= 0. && (5.20)
\end{aligned}$$

Here " $'$ " denotes differentiation w.r.t x, we have used the zero-order Friedmann equation

$$H^2 = \frac{\rho}{3}, \tag{5.21}$$

and defined

$$R \equiv \frac{\rho^{(\nu)}}{\rho^{(\nu)} + \rho^{(\gamma)}}. \tag{5.22}$$

The constraint equations become

$$\begin{aligned}
2x^3\Phi_k - 3x[(1-R)\mathcal{D}_k^{(\gamma)} + R\mathcal{D}_k^{(\nu)}] & \\
-9[(1-R)q_k^{(\gamma)} + Rq_k^{(\nu)}] &= 0, && (5.23)\\
2x^2(\mathcal{Z}_k - \sigma_k) + 9[(1-R)q_k^{(\gamma)} + Rq_k^{(\nu)}] &= 0. && (5.24)
\end{aligned}$$

These may be combined to give a single, closed, second-order equation for Φ_k,

$$3x\Phi_k'' + 12\Phi_k' + x\Phi_k = 0, \tag{5.25}$$

[3]For this chapter, unless otherwise noted, equations follow the signature of [11] to facilitate comparison with the CAMB code.

giving the solutions ($y \equiv x/\sqrt{3}$):

$$\Phi_k = -3y^{-3}[(Cy - D)\cos y - (C + Dy)\sin y], \tag{5.26}$$

$$\mathcal{Z}_k = 3\sqrt{3}y^{-3}[2(C + Dy)\cos y + 2(Cy - D) \times \sin y - C(2 + y^2)], \tag{5.27}$$

$$\sigma_k = 3\sqrt{3}y^{-2}[D\cos y + C\sin y - C], \tag{5.28}$$

$$q_k^{(\gamma)} = -4\sqrt{3}y^{-1}[C\cos y - D\sin y - C], \tag{5.29}$$

$$q_k^{(\nu)} = -\frac{2\sqrt{3}}{R}y^{-1}[(2RC + Dy)\cos y + (Cy + 2RD)\sin y) - 2RC], \tag{5.30}$$

$$\mathcal{D}_k^{(\gamma)} = 12y^{-2}[(C + Dy)\cos y + (Cy - D)\sin y - C], \tag{5.31}$$

$$\mathcal{D}_k^{(\nu)} = \frac{6}{R}y^{-2}[(2RC - Cy^2 + 2RDy)\cos y + (2RCy - 2RD + Dy^2)\sin y - 2RC], \tag{5.32}$$

where C and D are constants, for non-vanishing Φ_k. There are also three solutions with vanishing Weyl tensor:

$$\mathcal{Z}_k = \frac{\sqrt{3}}{4}A_3 y^{-3}(2 + y^2), \tag{5.33}$$

$$\sigma_k = \frac{\sqrt{3}}{4}A_3 y^{-1}, \tag{5.34}$$

$$q_k^{(\gamma)} = -\frac{1}{\sqrt{3}}(A_1\cos y - A_2\sin y + A_3 y^{-1}), \tag{5.35}$$

$$q_k^{(\nu)} = -\frac{R-1}{\sqrt{3}R}(A_1\cos y - A_2\sin y) + A_3 y^{-1}, \tag{5.36}$$

$$\mathcal{D}_k^{(\gamma)} = A_1\sin y + A_2\cos y + A_3 y^{-2}, \tag{5.37}$$

$$\mathcal{D}_k^{(\nu)} = \frac{R-1}{R}(A_1\sin y + A_2\cos y) + A_3 y^{-2}, \tag{5.38}$$

where A_1, A_2 and A_3 are constants. All of the constants naturally depend on the mode label k.

The solution labelled by A_3 (in other words, all other constants are zero), describes an exact, radiation dominated, FLRW universe, except that the CDM peculiar velocity is non-zero (in this case it is $v_a^{(c)} = v_a^{(0)}/S$, where $v_a^{(0)}$ is a first order vector orthogonal to the fundamental velocity u_a, parallel transported along flow lines). In order to see this clearly, it is best to adopt the energy frame[4]. If one chooses this frame and ignores anisotropic stresses, the CDM relative velocity evolves according to

$$\dot{v}_a^{(c)} + \frac{1}{3}\Theta v_a^{(c)} - \frac{1}{4S}[(1 - R)\mathcal{D}_a^{(\gamma)} + R\mathcal{D}_a^{(\nu)}] = 0 \tag{5.39}$$

in the radiation dominated era. The CDM interacts with other matter components through gravitation alone. Furthermore the gravitational influence of

[4]The energy frame, defined by the condition $q_a = 0$, is arguably a better frame to adopt in the early universe as then u^a is defined in terms of the dominant matter components as opposed to in terms of the CDM, which is a minority component in this epoch.

the CDM on the other matter components during the epoch of interest may be ignored (it is a minority component in a radiation dominated universe), so then Eq. 5.39 is the only equation governing the evolution of perturbations making reference to the CDM. But then any solution of Eq. 5.39 defines a valid solution of the linearised perturbation variable. The solution corresponding to A_3 is the solution with $v_a^{(c)} = v_a^{(0)}/S$. This solution decays, so we may ignore this mode, and set $A_3 = 0$. One may similarly ignore the mode labelled D in Eq. 5.26 to Eq. 5.32.

The remaining modes describe adiabatic perturbations and neutrino isocurvature modes. We will now isolate adiabatic perturbations, demanding that the he adiabatic condition,

$$\frac{\tilde{\nabla}_a \rho^{(i)}}{\rho^{(i)} + p^{(i)}} = \frac{\tilde{\nabla}_a \rho^{(j)}}{\rho^{(j)} + p^{(j)}}, \tag{5.40}$$

where i and j are matter species [9], be true between photons and neutrinos. This leaves only one free constant of integration, which without loss of generality may be taken to be C. Then the remaining constants are $A_1 = A_3 = D = 0$, and $A_2 = -6C$.

As stated earlier, the higher neutrino moments may not necessarily vanish. If one includes the higher moments into the set of equations, one may no longer find an analytic solution. However, one may then find a series expansion (about $x = 0$) of the system in terms of x (including terms up to x^3):

$$\Phi_k = C\left[1 - \frac{389R + 700}{168(2R + 25)}x^2\right], \tag{5.41}$$

$$\mathcal{D}_k^{(\gamma)} = \frac{(4R + 15)C}{6(R + 5)}x^2, \tag{5.42}$$

$$\mathcal{D}_k^{(\nu)} = \frac{(4R + 15)C}{6(R + 5)}x^2, \tag{5.43}$$

$$\mathcal{Z}_k = -\frac{(4R + 15)C}{4(R + 5)}\left[x - \frac{4R + 5}{18(4R + 15)}x^3\right], \tag{5.44}$$

$$\sigma_k = -\frac{5C}{2(R + 5)}\left[x + \frac{112R^2 - 16R - 1050}{2520(2R + 25)}x^3\right], \tag{5.45}$$

$$q_k^{(\gamma)} = \frac{(4R + 15)C}{54(R + 5)}x^3, \quad \pi_k^{(\gamma)} = -\frac{2C}{3(R + 5)}x^2, \tag{5.46}$$

$$q_k^{(\nu)} = \frac{(4R + 23)C}{54(R + 5)}x^3, \quad G_k^{(3)} = -\frac{5C}{63(R + 5)}x^3, \tag{5.47}$$

$$G_k^{(l)} = 0 + O(x^l) \text{ for } l > 3. \tag{5.48}$$

We may obtain the baryon and CDM variables perturbations from the adiabaticity condition:

$$\mathcal{D}_a^{(b)} = \mathcal{D}_a^{(c)} = \frac{3}{4}\mathcal{D}_a^{(\gamma)} = \frac{3}{4}\mathcal{D}_a^{(\nu)} \tag{5.49}$$

for the spatial gradients of the CDM and baryon densities. As noted earlier, isotropy allows us to write the baryon peculiar velocity as

$$v_a^{(b)} = \frac{4}{3}q_a^{(\gamma)}. \tag{5.50}$$

5.2.2 Initial conditions for tensors

In order to find initial conditions for the tensor modes, we use a somewhat different technique. We follow Bardeen's notation and write the metric with tensor perturbations in the form [3]:

$$ds^2 = S^2(\eta)\left[-d\eta^2 + \left(\gamma_{ij} + 2h^T_{ij}\right)dx^i dx^j\right]. \tag{5.51}$$

Here η is conformal time, the spatial coordinates are arbitrary,and h^T_{ij} is the tensor perturbation to the metric, satisfying [9]:

$$h^{T\,\prime\prime}_{ij} + 2\frac{a'}{a}h^{T\,\prime}_{ij} + (2K - \nabla^2)h^T_{ij} = -\kappa\pi_{ij}, \tag{5.52}$$

where " $'$ " denotes differentiation w.r.t. conformal time.

The shear is related to the metric perturbations via:

$$\sigma_{ij} = Sh^{T\,\prime}_{ij}, \tag{5.53}$$

and the electric part of the Weyl tensor via:

$$E_{ij} = -\frac{1}{2}\left[h^{T\,\prime\prime}_{ij} + \left(\nabla^2 - 2K\right)h^T_{ij}\right]. \tag{5.54}$$

For our purposes we will assume flatness ($K = 0$), radiation dominance, and that the anisotropic stress of the photons and neutrinos is negligible.

One may decompose these equations into harmonics[5] , using

$$h^T_{ij} = h_k(\eta)Y_{ij}, \tag{5.55}$$

and, changing the time variable to $x = k/HS$, obtain

$$x^2\frac{d^2h_k}{dx^2} + 2x\frac{dh_k}{dx} + x^2h_k = 0, \tag{5.56}$$

and

$$\sigma_k = \frac{dh_k}{dx}, \tag{5.57}$$

$$E_k = -\frac{1}{2}\left(\frac{d^2h_k}{dx^2} - h_k\right). \tag{5.58}$$

The CAMB code uses the variable χ, which is the Wronskian of E_k and σ_k. It is related to these two variables via:

$$\chi_k = \frac{\sigma_k}{x} - E_k. \tag{5.59}$$

[5]Bardeen's metric perturbation variables are defined on the foliation that arises locally as the level surfaces of constant time, and are treated as 3-tensors propagating on the background 3-geometry. The appropriate harmonics to use are thus not the Q_{ab}, but the Y_{ij}, which do not depend on coordinate time. If one works in co-moving coordinates, these are related via:

$$Q_{ab} = S^2\delta^i_a\delta^j_b Y_{ij}, \quad Q^a{}_b = \delta^a_i\delta^j_b Y^i_j, \quad Q^{ab} = S^{-2}\delta^a_i\delta^b_j Y^{ij}.$$

Thus

$$\dot{Q}_{ab} = 0 \Leftrightarrow u^0\partial_0 Y_{ij} = 0.$$

Further details of the relation between Bardeen's formalism and the covariant formalism may be found in [9].

The solution to Eq. 5.56 can be written in terms of Bessel functions:

$$h_k = C_1 x^{-\frac{1}{2}} J_{\frac{1}{2}}(x) + C_2 x^{-\frac{1}{2}} Y_{\frac{1}{2}}(x). \tag{5.60}$$

However, we are only interested in the growing mode. Furthermore, it is computationally more convenient to express the solutions in terms of a power series for x. Then we have

$$h_k(x) \propto 1 - \frac{x^2}{6} + O(x^4). \tag{5.61}$$

For the shear

$$\sigma_k \propto -\frac{x}{3} + \frac{x^3}{30} + O(x^5), \tag{5.62}$$

and for the electric part of the Weyl tensor,

$$E_k \propto -\frac{1}{3} + \frac{x^2}{15} + O(x^4). \tag{5.63}$$

5.3 Magnetic Fields

As described in Sec. 2.4, a magnetic field acts like an additional fluid in the universe model. The equations generated may be decomposed into scalar and tensor modes (as described in Sec. 2.6) which may then be integrated. In order to be able to integrate these equations using the CAMB code, two things still need to be done:

- The equations need to be transformed to conformal time, and their signature needs to be changed to that used in the code.
- Initial conditions need to be derived.

The first of these is trivial, if rather tedious. It should also be said, as noted in the previous sections, that the CAMB code integrates two new variables, $k\eta_k$ for scalars, and $H\chi_k$ for tensors, which are simple transformations of existing variables, and result in more stable numerics. It was also convenient to introduce the dimensionless parameter

$$\beta = \frac{\rho_{\text{mag}}}{\rho_{(\gamma)}} = \frac{B^2}{2\rho_{(\gamma)}}, \tag{5.64}$$

which is constant to zero-order. The transformation of the equations to these variables is trivial.

Less trivial is understanding what to do about the initial conditions. In principal, we should modify the equations obtained in the previous discussion on initial conditions, including new equations for the evolution of the magnetic field, and solve them. The expressions obtained when doing this, however, prove to be somewhat complicated, involving slowly converging power series which take into account the in-homogeneity that the magnetic fields add to the equations. However, numerical testing of these functions showed that, in the range of interest for the initial magnetic field strength, and initial x, these solutions differed only by a very small amount (usually by less than was discernible to floating point precision) from the solutions obtained using the non-magnetised original set of equations. Thus, for efficiency and simplicity, it was decided to use the

old initial conditions in the CAMB code, simply adjoining appropriate initial values for the new (magnetic) variables.

The results of the numerical simulations are presented below, with a separate discussion for scalar and tensor modes. For tensor modes the formal derivation of the initial conditions will also be discussed, and it will be shown that they do indeed differ by a negligible amount from those which do not take the initial magnetic field into account.

5.3.1 Scalar modes

The tight-coupling approximation

The tight-coupling approximation allows us to see analytically how the photon-baryon fluid oscillates in the era before decoupling. The time-scales of importance in this era are: $t_c \equiv (n_e \sigma_T)^{-1}$, the photon mean free time, $t_H \equiv H^{-1}$, the expansion time scale, and $t_k \equiv S/k$, the time for light to travel across a wavelength of the current mode. Defining the perturbation variable $\epsilon = \max(t_c/t_k, t_c/t_H)$, one obtains the tight-coupling approximation to the perturbation equations by expanding them in terms of this variable, and retaining only first-order terms. This is well described in [11]. Assuming adiabatic initial conditions allows a wave equation for the photon fluid to be found, which to zero order is given by:

$$\ddot{\mathcal{D}}_k^{(\gamma)} + \frac{2}{3}\Theta\dot{\mathcal{D}}_k^{(\gamma)} + \frac{R + 3c_{s(T)}^2}{3(1+R)}\frac{k^2}{S^2}\mathcal{D}_k^{(\gamma)} \tag{5.65}$$

$$= \frac{2}{3}\kappa\sum_i(\rho^{(i)} + 2p^{(i)})\mathcal{D}_k^{(i)} + \frac{4R}{9(1+R)}\frac{k}{S}\Theta v_k^{(b)}, \tag{5.66}$$

where $R = 4\rho^{(\gamma)}/3\rho^{(b)}$, and

$$c_{s(T)}^2 = \frac{\dot{p}_T}{\dot{\rho}_T} \approx c_{s(b)}^2 + \frac{4}{9}\frac{\rho^{(m)}}{\rho^{(\gamma)}}. \tag{5.67}$$

It is immediately apparent that the magnetic field has an influence on the frequency of the oscillations. This is due to the modification the sound speed by the field. One may also observe the usual way expansion damps oscillation, whereas gravitation drives it through the gradient $\bar{\nabla}_a(\rho + 3p)$. This leads to almost constant amplitude oscillation in the radiation dominated era. Silk-damping is not taken into account at zero order in the tight-coupling variable ϵ.

Numerical results

As discussed in the introduction of this section, the initial conditions derived in [11] were used without modification in the numerical integration of the scalar variables, even when including the effects of a magnetic field. Of course, initial conditions for the new variables had to be set. This was done in the simplest way possible, by assuming that they are scale-invariant.

The tight-coupling approximation is used in the original code at sufficiently early times for efficiency reasons. It was thus necessary to derive tight-coupling approximations to the modified scalar equations for the baryon velocity, and photon flux. Furthermore, the variable $k\eta_k$ is used in the code for stability

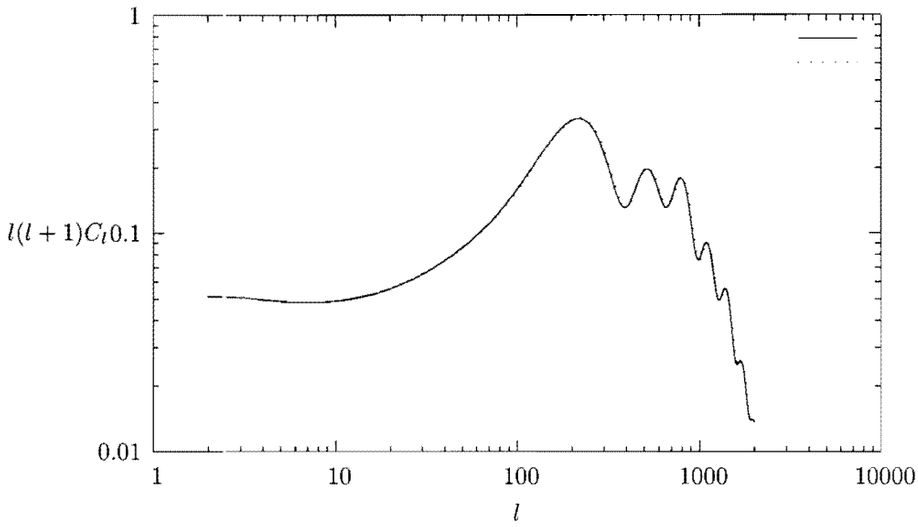

Figure 5.1: The effects of a magnetic field on the scalar power spectrum. The solid spectrum represents the reference with $B_0 = 0$. The dotted spectrum is calculated with a background field strength of 10^{-5} Gauss, $\mathcal{B}_k = \Pi_k = 1$.

reasons, and thus a change of variables had to be made. Apart from these minor deviations, and the change to the sign conventions of [11] and conformal time, the scalar equations derived in Ch. 2 are used essentially as derived.

Numerical integrations were done over an array of initial values for the magnetic variables. The magnetic field strength was varied between $B_0 = 10^{-9}$ and $B_0 = 10^{-5}$, with the perturbation variables $\mathcal{B}_k$ and Π_k having an initial scale-invariant spectrum, $\mathcal{B}_k = \alpha$, $\Pi_k = \beta$, where α and β dimensionless normalisation constants ranging between 10^{-3} and 10^3. Fig. 5.1 shows the general effects of such initial conditions on the scalar power-spectrum. As is just discernible, the magnetic field does move the position of the peaks. However, the overall effect of the magnetic field is very small. One needs unrealistically large fields to generate an appreciable effect. Perhaps a less naive choice of initial conditions for the magnetic field would lead to a more obvious signature of the magnetic field.

5.3.2 Tensor modes

Initial conditions

Following the procedure outlined in 5.2.2, but including the effect of the magnetic anisotropic stress, we obtain an equation for the metric perturbation

$$x^2 h_k'' + 2x h_k + x^2 h_k = \frac{1}{3}\kappa\beta(1-R)\Pi_k. \tag{5.68}$$

where $\beta = B^2/\rho^{(\cdot)}$, which is constant to zero order. This couples with the propagation equation for Π_k:

$$\Pi_k' = -\frac{4}{3}k\sigma_k. \tag{5.69}$$

But we have

$$h_k' = k\sigma_k, \tag{5.70}$$

so that we obtain the closed equation for h_k:

$$x^2 h_k'' + 2x h_k + \left[x^2 + \frac{4}{9}\kappa\beta(1-R)\right] h_k = K, \tag{5.71}$$

where K is a constant. Setting K to zero gives us a Bessel equation with the regular (growing mode) solution:

$$h_k(x) = \frac{1}{\sqrt{x}} J_\nu(x), \quad \nu = \frac{1}{6}\sqrt{9 - 16\beta(1-R)}, \tag{5.72}$$

where $J_\nu(x)$ is the regular fractional Bessel function of order ν.

With this one may now find expressions for σ_k and χ_k:

$$\sigma_k(x) = \frac{1}{6x^{3/2}} J_\nu(x)\,(\nu - 6x)\,, \tag{5.73}$$

$$\chi_k(x) = \frac{1}{9x^{5/2}} J_\nu(x)\left[2\beta(1-R) - 9x^2\right]. \tag{5.74}$$

One may now explicitly check the difference between these derived initial conditions, and the ICs derived ignoring the initial magnetic field, and find that for all reasonable values of β, in the range of x used to set up the initial conditions, the difference between the two is negligible.

Numerical results

As in the scalar case, the tensor equations need to be transformed to conformal time, and the signature of [11]. One also has to change variables from E_k to χ_k, the conserved Wronskian between E_k and σ_k. These changes are trivial. Apart from these, one may implement the equations derived in Chapter 2 as given. For simplicity, a scale-invariant initial spectrum was assumed for the magnetic perturbations.

The tensor equations were integrated for a variety of initial conditions, with B_0 ranging initially from 10^{-9} Gauss through 10^{-1} Gauss. The initial magnetic stress energy (Π_k) was chosen to have a scale-invariant spectrum, $\Pi_k = \alpha$, with the dimensionless normalisation constant α ranging from 10^{-3} to 1. Separate calculations where done including, and ignoring, the effect of the gravitational back-reaction on the field. Fig. 5.2 shows the tensor power spectrum calculated in the presence of a weak magnetic field ignoring the effect of the gravitational back-reaction, contrasted with the tensor power spectrum in the absence of a magnetic field. One may see that the effect of increasing the initial anisotropic stress is to cause an overall (scale-invariant) increase in the power. As one would expect, this increase was found to be approximately proportional to the product of the the magnetic field strength and the initial anisotropic stress. It

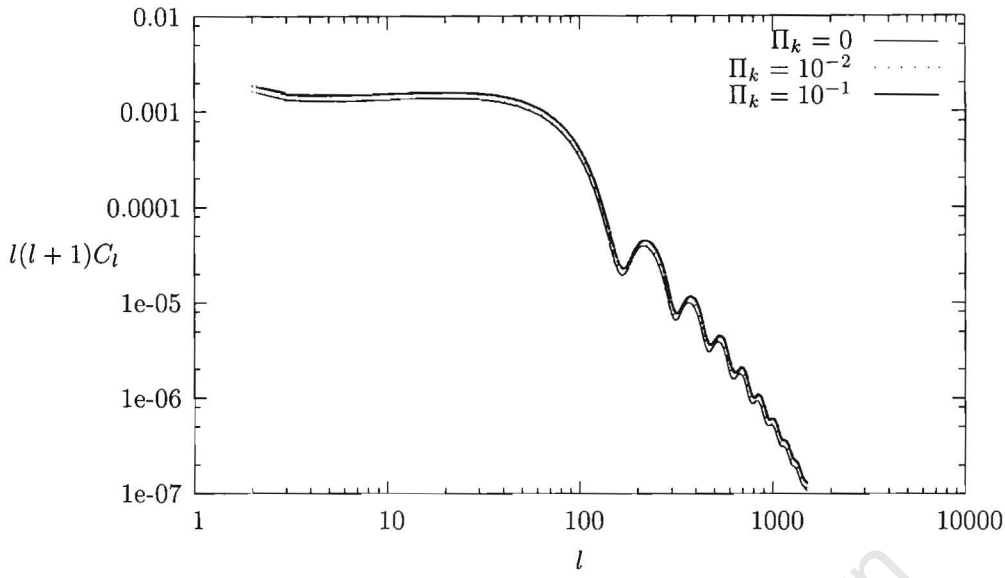

Figure 5.2: The effects of a magnetic field on the tensor power spectrum, ignoring the back-reaction of gravitation on the field. The $\Pi_k = 0$ spectrum is the reference with $B_0 = 0$. The other two spectra are calculated with a background field strength of 10^{-5} Gauss.

was also found that an increase in the magnetic field strength had the effect of shifting the peaks of the spectrum slightly. This corresponds with the tight-coupling prediction (as discussed in the scalar case). However, this shifting was very slight. At physically reasonable levels, with $B_0 \sim 10^{-9}$ Gauss, the initial anisotropic stress had to be rather large for the magnetic field to have any effect on the spectrum. Fig. 5.3 shows a calculation of the power-spectrum showing how the back-reaction affects the spectrum. While there is little effect for low l, at higher l the back-reaction damps out the effect of the magnetic field, causing the spectrum overall effect at higher l to be very small.

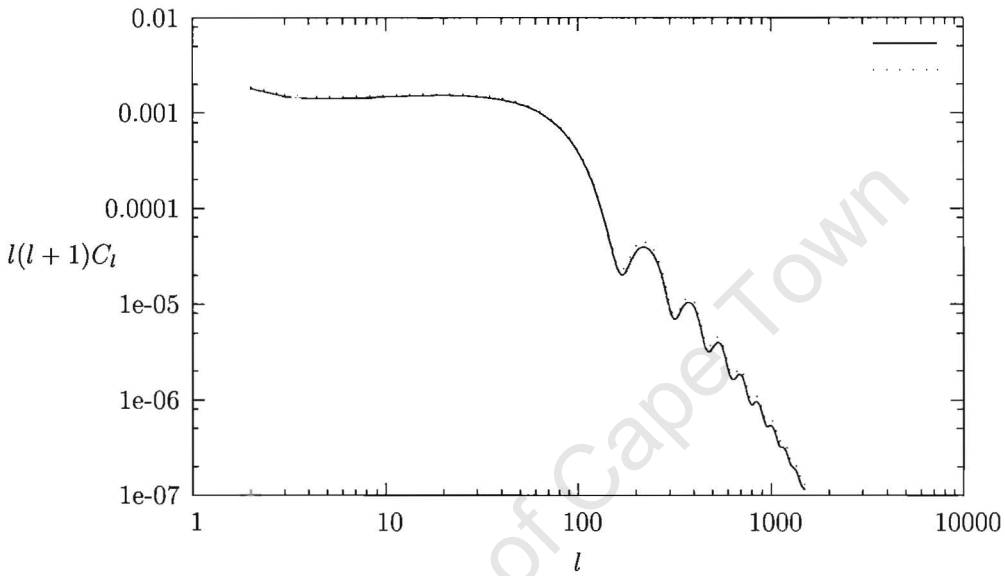

Figure 5.3: Tensor power spectra showing the effect of the gravitational back-reaction on the magnetic field. The solid line represents the power-spectrum calculation including the effect of the back-reaction on the field, whereas the dotted represents the calculation without the effects of the back-reaction. Both are calculated with a field strength of 10^{-5} Gauss, and anisotropic stress $\Pi_k = 10^{-1}$.

Chapter 6

Discussion

With the prospect of increasingly precise measurements of microwave background anisotropies, the calculation of possible signatures of magnetic fields on the CMB power spectrum has become an important way to help settle the question as to the origin of magnetic fields in the universe. This thesis has attempted to do exactly that, first examining the general theory surrounding the calculation of the microwave background power spectrum, and then deriving the set of equations required in order to do the calculation in the presence of a magnetic field. Under the simplifying two-fluid assumption, explicit analytic calculation was done to show how the magnetic field affects the evolution of density perturbations. This allowed us to see that the magnetic field would serve to amplify oscillations in the radiation dominated era. The CAMB code, used to calculate the CMB power spectrum under the covariant approach, was discussed in detail in order to help make it easier for people to modify it in future. The code was modified to include the effects of a magnetic field, both for scalar and tensor perturbations. For scalar perturbations, the tight-coupling approximation allowed us to see how the magnetic field might theoretically alter the frequency of the photon-baryon plasma oscillations in that regime. However, numerical results were disappointing. In the scalar case, only unrealistically large magnetic fields could be seen to have any effect on the spectrum. For tensor perturbations, the presence of a magnetic field was seen to have some effect. However, this also proved to be small.

As pointed out in work by other authors, vector perturbations play an unusually important role in searching for effects of magnetic fields on the CMB spectrum. In contrast to the standard FLRW universe, where vector perturbations are seen to decay, these modes do not decay greatly in the presence of a magnetic field. A further area where magnetic effects are quite different from those of the standard isotropic models is polarisation anisotropies. While it would be impossible for E- and B-polarisation modes to mix in the standard models, as this would imply a violation of parity, the presence of a magnetic field necessitates such mixing, as it is maximally parity violating. This should leave a unique signature on polarisation anisotropies. It would thus be worthwhile to extend this work to the calculation of these spectra. In the case of vector perturbations this would imply a major addition to the CAMB code, which at present has no facility to calculate vector anisotropies.

The covariant formalism seems to be well suited to study stochastic magnetic

fields. These may be imagined to be more realistic than large scale homogeneous fields, as stochastic fields are generated by standard causal physical processes. It would be interesting to duplicate the work of Durrer, Mack, and coworkers [18, 44, 48, 62] in the covariant formalism. This would allow the rather simplistic approach to initial conditions that is used in this paper to be remedied. One might also expect to be able to include effects such as the gravitational back-reaction on the magnetic field into the analysis without too much difficulty.

In conclusion, this thesis may be seen as laying the foundation for the calculation of CMB anisotropies resulting from early magnetic fields using the covariant approach. Although the final numerical results showed little that would encourage the detection of early magnetic fields using the CMB, the work on the most important observables for magnetic effects, the vector and polarisation spectra, has yet to be done. One may reasonably hope that this would yield interesting results. Furthermore, the initial conditions used for these numerical calculations were simplistic. Perhaps a more sophisticated of initial conditions would lead to the observation of effects in scalar and tensor power spectra. All of this new work would in the end rely on the framework laid down here. Thus, even if the numeric results were inconclusive, the analysis done in the paper will hopefully be useful to others wishing to extend this work.

The author would like to thank the NRF, and University of Cape Town for the financial support that made this work possible. He is grateful to Christos Tsagas, Matthias Marklund and especially Peter Dunsby for all their helpful comments.

Appendix A

First order covariant identities

This section presents a table of first-order covariant identities that simplify computation in the covariant approach to gauge invariant perturbations. These may also be found in [83]. They all follow from basic commutation rule for any scalar ψ:

$$\tilde{\nabla}_{[a}\tilde{\nabla}_{b]}\psi = -\omega_{ab}\dot{\psi}, \tag{A.1}$$

The identities are:

$$\begin{aligned}
\operatorname{curl}\tilde{\nabla}_a\phi &= 2\dot{\phi}\omega_a, && \text{(A.2)}\\
(S\tilde{\nabla}_a\phi)^{\cdot} &= S\tilde{\nabla}_a\dot{\phi} + S\dot{\phi}a_a, && \text{(A.3)}\\
\tilde{\nabla}^2(\tilde{\nabla}_a\phi) &= \tilde{\nabla}_a(\tilde{\nabla}^2\phi) + 2\dot{\phi}\operatorname{curl}\omega_a, && \text{(A.4)}\\
(S\tilde{\nabla}_a T_{b\ldots c})^{\cdot} &= S\tilde{\nabla}_a\dot{T}_{b\ldots c}, && \text{(A.5)}\\
\tilde{\nabla}_{[a}\tilde{\nabla}_{b]}V_c &= 0, && \text{(A.6)}\\
\tilde{\nabla}_{[a}\tilde{\nabla}_{b]}T_{cd} &= 0, && \text{(A.7)}\\
\operatorname{div}\operatorname{curl}V &= 0, && \text{(A.8)}\\
(\operatorname{div}\operatorname{curl}T)_a &= \frac{1}{2}\operatorname{curl}(\operatorname{div}T)_a, && \text{(A.9)}\\
\operatorname{curl}\operatorname{curl}V_a &= \tilde{\nabla}_a(\operatorname{div}V) - \tilde{\nabla}^2 V_a, && \text{(A.10)}\\
\operatorname{curl}\operatorname{curl}T_{ab} &= \frac{3}{2}\tilde{\nabla}_{\langle a}(\operatorname{div}T)_{b\rangle} - \tilde{\nabla}^2 T_{ab}. && \text{(A.11)}
\end{aligned}$$

Note that these are only valid to first order.

The commutation relation

$$\tilde{\nabla}_{[a}\tilde{\nabla}_{b]}B_c = \frac{1}{2}{}^3R_{dcba}B^d - \varepsilon_{abc}\omega^d\dot{B}_d, \tag{A.12}$$

arises because the magnetic field vector is not considered first order in the primary perturbation variable. Here ${}^3R_{abcd}$ is the 3-curvature tensor defined by

$${}^3R_{abcd}V^d = -2\tilde{\nabla}_{[a}\tilde{\nabla}_{b]}V_c \tag{A.13}$$

for any space-like vector V^a.

Bibliography

[1] Adams, J. *et al.* 1996, Phys. Lett. B **388**, 253.

[2] Akhiezer, A. I. *et al.* 1975, Plasma Electrodynamics, vol. 1 (Pergamon Press).

[3] Bardeen, J. M. 1980, Phys. Rev. D **22**, 1882.

[4] Barrow, J. D 1997, Phys. Rev. D **55**, 7451.

[5] Barrow, J. D , Ferreira, P. G., & Silk J. 1997, Phys. Rev. Lett. **78**, 3610.

[6] Battaner, E., & Lesch, H. 2000, `astro-ph/0003370`.

[7] Bennett, C. L. *et. al.* 2003, `astro-ph/0302207`.

[8] Biermann, L. 1950, Z. Naturf. **A5**, 65.

[9] Bruni, M., Dunsby, P. K. S., & Ellis, G. F. R. 1992, Ap.J. **395**, 34.

[10] Challinor, A. D., & Lasenby, A. N. 1998, Phys. Rev. D **58**, 023001.

[11] Challinor, A. D., & Lasenby, A. N. 1998, Ap.J. **513**, 1.

[12] Challinor, A. D. 2000, Class. Quantum Grav. **17** 871.

[13] Challinor, A. D. 1999, `astro-ph/9911481`.

[14] Dunsby, P. K. S., Bassett, B. A. C. C., & Ellis. G. F. R. 1997, Class. Quantum Grav. **14**, 1215.

[15] Dunsby, P. K. S., Bruni, M., & Ellis. G. F. R. 1992, Ap.J. **395**, 54.

[16] Dunsby, P. K. S., & Ellis, G. F. R. 1999, Perturbations of Cosmological Backgrounds, In Black Holes, Gravitational Radiation and the Universe; Essays in Honor of C. V. Vishveshwara, ed. B. R. Iyer and B. Bhawal, 493 (Kluwer Academic Publishers, 1999).

[17] Durrer, R., Kahniashvili, T. & Yates, A. 1998, Phys. Rev. D **58**, 123004.

[18] Durrer, R., Ferreira, P. G., & Kahniashvili, T. 2000, Phys. Rev. D **61**, 043001.

[19] Ehlers, J. 1993, Gen. Rel. Grav. **25**, 1225.

[20] Ehlers, J., Geren, P. & Sachs, R. K. 1968, J. Math. Phys. **9**, 1344.

[21] Eilik, J., astro-ph/9906485.

[22] Ellis, G. F. R. 1971, in General Relativity and Cosmology, Proceedings of the International School of Physics, "Enrico Fermi", Course XLVII, ed. R. K. Sachs (New York: Academic Press), 104.

[23] Ellis, G. F. R 1973, in Cargese Lectures in Physics, Volume 6, Ed. Schatzmann, R. (Gordon and Breach)

[24] Ellis, G. F. R. 1996, in Current Topics in Astrofundamental Physics, ed. N. Sánchez & A. Zicichi (Singapore: World Scientific), 3.

[25] Ellis, G. F. R., & Bruni, M. 1989, Phys. Rev. D **40**, 1804.

[26] Ellis, G. F. R., & Dunsby, P. K. S. 1997, Ap.J. **479**, 97.

[27] Ellis, G. F. R, & Dunsby, P. K. S. 1998, Covariant Analysis of Dynamics and of the CBR Anisotropy, In Current Topics in Astrofundamental Physics: Primordial Cosmology, ed N. Sánchez and A. Zichichi, 3-33 (Kluwer Academic Publishers, 1998).

[28] Ellis, G. F. R, & Dunsby, P. K. S. 2001 The 1+3 Covariant Approach to CMB Anisotropies, In Current Topics in Astrofundamental Physics: Primordial Cosmology, ed N. Sánchez and A. Zichichi, 3-33 (Kluwer Academic Publishers, 2001).

[29] Ellis, G. F. R , Hwang, J., & Bruni, M. 1989, Phys. Rev. D **40**, 1819.

[30] Ellis, G. F. R , Lecture notes on Cosmology (UCT, 1997).

[31] Ellis, G. F. R. & van Elst, H. 1998, Cosmological Models. Theoretical and Observational Cosmology. Cargèse Lectures. Kluwer Academic Publishers.

[32] Ellis, G. F. R., Matravers, D. R., & Treciokas, R. 1983, Annals of Physics, **150**, 455.

[33] Feretti, L. *et al.* 1995, Astron. Astroph. **302**, 554.

[34] Gebbie, T., & Ellis, G. F. R. 1998, Covariant cosmic microwave background anisotropies. I: Algebraic relations for mode and multipole. representations, submitted.

[35] Grasso, D. & Rubenstein, H. 2001, Phys.Rept. **348** 163.

[36] Harari, D. D., Hayward, J. D. & Zaldarriaga, M. 1997, Phys. Rev. D **55**, 1841.

[37] Harrison, E. R. 1967, Rep. Mod. Phys. **39**, 862.

[38] Hawking, S. W. 1966, Ap.J. **145**, 544.

[39] Hobbs, S. W. & Dunsby, P. K. S. 2000, Phys. Rev. D **62**, 124007.

[40] Hu, W., Scott, D., Sugiyama, N., & White, M. 1995, Phys. Rev. D **52**, 5498.

[41] Jackson, J. D. 1975, Classical Electrodynamics (New York: Wiley).

[42] Jedamzik, K., Katalinic, & Olinto, A. V. 1998, Phys. Rev. D **57**, 3264.

[43] Jedamzik, K., Katalinic, & Olinto, A. V. 2000, Phys. Rev. Lett. **85**, 700.

[44] Kahniashvili, T., Kosowski, A., Mack, A. & Durrer, R. 2000, `astro-ph/0011095`.

[45] Kaplan, S. A & Tsytovich, V. N., 1973, Plasma Astrophysics (Pergamon Press).

[46] Kim, E., Kronberg, P. P., & Tribble, P. C. 1991, Ap.J. **379**, 80.

[47] Kim, E., Olinto, A., & Rosner, R. 1996, Ap.J. **468**, 28.

[48] Koh, S., & Lee, C. H. 2000, Phys. Rev. D **62**, 083509.

[49] Kolatt, T., 1998, Ap.J. **495**, 564.

[50] Kosowsky, A. & Loeb, A. (1996) Ap.J. **469**, 1.

[51] Kronberg, P. P. 1994, Rec. Prog. Phys. **57**, 325.

[52] Kulsrud, R., Cowley, S. C., Guzinov, A. V., & Sudan, R. N. 1997, Phys. Rep. **283**, 213.

[53] Leong, B., Dunsby, P. K. S., Challinor, A., & Lasenby, A. 2002, Phys. Rev. D **65**, 104012.

[54] Lesch, H. & Chiba, M. 1995, Astron. Astroph. **297**, 305.

[55] Lasenby, A. N. 2001, Observations and theory of the cosmic microwave background, *Current Topics in Astrofundamental Physics: The Cosmic Microwave Background* (Kluwer Academic Publishers), 151.

[56] Lewis, A., Challinor, A. D., & Lasenby, A. N. 2000, Ap.J. **538** 473-476.

[57] Loeb, A., & Mao, S. 1994, Ap.J. **435**, L109.

[58] Ma, C. P., & Bertschinger, E. 1995, Ap.J. **455**, 7.

[59] Maartens, R., & Basset, B. A. 1998, Class. Quantum Grav. **15**.

[60] Maartens, R., Gebbie, T., & Ellis, G.F.R. 1999, Phys. Rev. D **59**.

[61] Maartens, R , Wands, D., Basset, B. & Heard, I. 2000, Phys. Rev. D **62**, 041301.

[62] Mack, A., Kahniashvili, T., & Kosowsky, A. 2002, Phys. Rev. D**65**, 123004.

[63] Misner, C. W., Thorne, K. S., & Wheeler, J. A. 1973, Gravitation (San Francisco: W. H. Freeman and Company).

[64] Padmanabhan, T., 1993, Structure formation in the universe (Cambridge University Press).

[65] Plaga, R. 1995, Nature **374**, 430.

[66] Randall, L., & Sundrum R. 1999, Phys. Rev. Lett. **83**, 4680.

[67] Scannapieco, E. S., & Ferreira, P. G. 1997, Phys. Rev. D **56**, R7493.

[68] Seljak, U., & Zaldarriaga, M. 1996, Ap.J. **469**, 437.

[69] Shiromizu, T., Maeda, K., & Sasaki, M. 2000, Phys. Rev. D **62**, 024012.

[70] Stewart, J. M., & Walker, M. 1974, Proc. R. Soc. London A **341**, 49.

[71] Stoeger, W. R., Ellis, G. F. R., & Schmidt, B. G. 1991, Class. Quantum Grav. **23**, 1169.

[72] Stoeger, W. R., Ellis, G. F. R., & Xu, C. M. 1994, Phys. Rev. D **49**, 1845.

[73] Stoeger, W. R., Maartens, R., & Ellis, G. F. R. 1995, Ap.J. **443**, 1.

[74] Stoeger, W. R., Xu, C. M., Ellis, G. F. R., & Katz, M. 1995, Ap.J. **445**, 17.

[75] Subramanian, K., & Barrow, J., D., 1998, Phys. Rev. Lett. **81**, 3575.

[76] Subramanian, K., & Barrow, J., D., 1998, Phys. Rev. D **5808**, 3502.

[77] Subramanian, K., & Barrow, J., D., 2002, MNRAS **335** L57.

[78] Taylor, G. B., & Perley, R. A. 1993, Ap.J. **416**, 554.

[79] Thorne, K. S. 1981, MNRAS **194**, 439.

[80] Tsagas, C. G.. & Barrow, J. D. 1997, Class. Quantum Grav. **14**, 2539.

[81] Tsagas, C. G.. & Barrow, J. D. 1998, Class. Quantum Grav. **15**, 3523.

[82] Tsagas, C. G.. 1998, PhD thesis, Sussex University.

[83] Tsagas, C. G.. & Maartens, R. 2000, Phys. Rev. D **61**, 083519.

[84] Zel'dovich, Ya. B. 1970, Astron. Zh. **46**, 775 [Sov. Astron. **13**, 608].

[85] Zel'dovich, Ya. B. & Novikov, I. D., The Structure and Evolution of the Universe (The University of Chicago Press), 1983.

[86] Zweibel, E. G., Heiles, C. 1997, Nature **384**, 131.